February, 2013

Master THESIS

A Study on Nonlinear Inelastic Buckling and Response Behavior of Steel Members Under Axial Loading

Graduate School of Chosun University

Architectural Engineering (Architecture and Architectural Engineering)

Daniel Yeshewawork Abebe

축하중을 받는 철골부재의 비탄성좌굴 및 응답거동에 관한 연구

A Study on Nonlinear Inelastic Buckling and Response Behavior of Steel Members Under Axial Loading

February 25, 2013

Graduate School of Chosun University

Architectural Engineering (Architecture and Architectural Engineering)

Daniel Yeshewawork Abebe

A Study on Nonlinear Inelastic Buckling and Response Behavior of Steel Members Under Axial Loading

Advisor: Pro. Jae-hyouk Choi

A Thesis Submitted for Partial Fulfillment of the Requirements for the degree of Masters of Engineering Applied in

October, 2012

Graduate School of Chosun University

Architectural Engineering (Architecture and Architectural Engineering)

Daniel Yeshewawork Abebe

Evaluating Committee of the Thesis

Chairman (Prof. Chosun Univ.) Kim, Eui-Sik

Member (Prof. Chosun Univ.) Cho, Chang-Geun

Member (Prof. Chosun Univ.) Choi, Jae-Hyouk

November, 2012

Graduate School of Chosun University

Table of Contents

ABSTRACT

CHAPTER 1 INTRODUCTION

1.1 General Over view ····· 1
1.1.1 Causes of Progressive Collapse ····· 3
1.1.2 Conditions of Progressive Collapse of Building Structures ····· 3
1.2 Elastic and Inelastic Buckling Characteristics of Steel ····· 5
1.3 Objectives and Scope ····· 6
1.4 Reading Directions ····· 6

CHAPTER 2 INELASTIC BUCKLING EVALUATION OF H-SHAPE PINNED-PINNED STEEL COLUMN MEMBER UNDER AXIAL COMPRESSION LOADING

2.1 Introduction ····· 10
2.2 Theoretically Derived Equations ····· 11
2.2.1 Bazant's Hinge-ended Model ····· 11
2.2.2 AIJ Recommendation ····· 12
2.2.3 Paris's Analysis ····· 16
2.3 Finite Element Analysis Model ····· 18
2.3.1 Material Modeling ····· 18
2.3.2 Constraint and Loading Condition ····· 21
2.3.3 Analysis Process ····· 23
2.4 Finite Element Analysis Result ····· 23

2.4.1 Failure Mode ····· 23
2.4.2 Equivalent plastic strain and stresses of elements ····· 25
2.4.3 Load-deformation Curve of Analysis Result ····· 27
2.5 Compression Test Process ····· 29
2.6 Test Result ····· 31
2.6.1 Deformation Mode ····· 31
2.6.2 Load-deformation Relationships ····· 32
2.7 Comparison of Analysis and Test Results ····· 34
2.7.1 Deformation Mode ····· 34
2.7.2 Load-Deformation ····· 36
2.7.3 Energy Absorption ····· 38
2.8 Summary ····· 40

CHAPTER 3 INELASTIC BUCKLING EVALUATION OF H-SHAPE FIXED-FIXED STEEL COLUMN MEMBER
3.1 Theoretical Investigation Buckling Behavior ····· 41
3.2 Finite Element Analysis Model ····· 43
3.2.1 Material Modeling ····· 43
3.2.2 Constraint and Loading Condition ····· 45
3.3 Result and Discussion ····· 47
3.3.1 Failure Mode ····· 47
3.3.2 Equivalent Plastic Strain ····· 51
3.3.3 Load-displacement and Energy Absorption Curve Result ····· 55
3.4. Summary ····· 60

CHAPTER 4 INELASTIC RESPONSE OF H-SECTION AND CHS STEEL BRACING MEMBER UNDER CYCLIC LOADING
4.1 Introduction ····· 62

4.2 Literature Review on Bracing System ····· 63
4.3 Non-linear Inelastic Buckling ····· 68
4.3.1 Non-linear FE Analysis ····· 68
4.3.1.1 Material Model ····· 68
4.3.1.2 The Constraint and Loading Condition ····· 70
4.3.1.2.1 The Constraint ····· 70
4.3.1.2.2 Loading Condition ····· 70
4.3.2 Theoretical Investigations ····· 71
4.4 Analysis Result ····· 73
4.4.1 Buckling Mode of CHS Bracing Member ····· 73
4.4.2 Axial Load-Axial Displacement Relationship for CHS ····· 76
4.4.3 Buckling Mode of H-Section Bracing Member ····· 79
4.4.4 Axial Load-Axial Displacement Relationship for H-Section ····· 80
4.5 Lateral Brace Deformation ····· 82
4.6 Summary ····· 84

CHAPTER 5 CONCLUSION ····· 85

REFERENCES ····· 87

Appendix ····· 92

Appendix A INELASTIC RESPONSE OF SHEAR PANEL HYSTERESIS STEEL DAMPER

A.1 Introduction ····· 92
A.1.1 Material Properties of Specimen ····· 93
A.2 Finite Element Analysis Model ····· 94
A.2.1 Material Modeling ····· 94

A.2.2 Constraint and Loading Condition ····· 96
A.3 Verification and Validation of Analysis Model ····· 97
A.3.1 The Test Program and Process ····· 98
A.4 Comparison of the Results ····· 99
A.4.1 Failure Mode ····· 99
A.4.2 Comparison of Analysis and Test Result Hysteresis Curves ····· 105
A.5 Inelastic Response of Shear Panel Damper ····· 107
A.6 Cumulative Energy Dissipation ····· 110
A.7 Summary ····· 111

Appendix B INELASTIC RESPONSE OF CIRCULAR PIPE STEEL DAMPER
B.1 Introduction ····· 112
B.2 Properties of Specimen ····· 113
B.2.1 Chemical Composition ····· 113
B.2.2 Mechanical Properties ····· 113
B.3 Theoretical Equations ····· 114
B.4 Non-linear FEM Analysis ····· 120
B.4.1 Material Mode ····· 120
B.4.2 Loading and Constraint Condition ····· 121
B.5 Experimental Process ····· 122
B.6 Results and Discussions ····· 124
B.6.1 Deformation Shape ····· 124
B.6.2 Hysteresis Curve ····· 126
B.7 Summary ····· 128

Appendix C IMPERFECTION IN MODELLING STEEL MEMBERS
C.1 Introduction ····· 129
C.2 Imperfection in Column Member ····· 129
C.3. Nonlinearity in FEA ····· 131

List of Tables

Table 2.1 The Property of Material Used in the Analysis ····· 19
Table 2.2 Section Property of Specimen ····· 19

Table 3.1 The Property of Material Used in the Analysis ····· 44
Table 3.2 Section Property of Specimen, different cases considered ····· 45

Table A.1 Mechanical Properties of Specimen (Test Result) ····· 94
Table A.2 The Property of Material Used in the Analysis ····· 96
Table A.3 Specimen Detail ····· 97
Table A.4 Comparison of Analysis & Test results for yield and maximum forces..... 107

Table B.1 Chemical Composition of Steel used in this Study ····· 114
Table B.2 Mechanical Properties of Specimen (Coupon Test Result) ····· 115
Table B.3 Physical properties of specimen used ····· 122
Table B.4 The two cases of Experiment Considered ····· 124
Table B.5 Initial Stiffness and Plastic Displacement of Test Result Calculation Result of Type ····· 125

List of Figures

Fig. 1.1 The collapse of 2 World Trade Center ····· 1
Fig. 1.2 The massive collapse of 2 World Trade Center ····· 2
Fig. 1.3 Conditions of progressive collapse prevention for structures due to falling object ····· 4
Fig. 1.4 Reading Directives ····· 6

Fig. 2.1 (a) Hinge ended buckling of column member, (b) and free body diagram 11
Fig. 2.2 Interaction Diagram for H-section Steel column member..... 14
Fig. 2.3 Uniaxial stress-strain curve, biaxial stress-strain curve for kinematic hardening model ····· 19
Fig. 2.4 Uniaxial stress-strain curve, biaxial stress-strain curve for isotropic hardening model ····· 20
Fig. 2.5 Typical stress strain curve ····· 21
Fig. 2.6 (a) general layout of analysis model, (b) constraint and loading condition ····· 22
Fig. 2.7 deformation shape of analysis result on strong axis ····· 24
Fig. 2.8 deformation shape of analysis result on weak axis ····· 24
Fig. 2.9 Effective plastic strain for different element ····· 26
Fig. 2.10 Effective stress (von Mises's stress)for different element ····· 27
Fig. 2.11 Load-deformation curve of analysis result on strong axis ····· 28
Fig. 2.12 Comparison of load-deformation relationship for strong and weak axis 29
Fig. 2.13 (a) Test setup and (b) detail of specimen ····· 30
Fig. 2.14 Strong axis deformation shape of test specimen ····· 31
Fig. 2.15 Weak axis deformation shape of test specimen ····· 32
Fig. 2.16 Load-deformation curve of test result (Strong Axis) ····· 33
Fig. 2.17 Load-deformation curve of test result (Weak Axis) ····· 33
Fig. 2.18 Comparison of Test results ····· 34

Fig. 2.19 Comparison of deformed shape of test and analysis result on weak axis · ····· 35
Fig. 2.20 Comparison of deformed shape of test and analysis result on strong axis ····· 35
Fig. 2.21 Comparison of load-deformation curve for strong axis ····· 36
Fig. 2.22 Comparison of load-deformation result for weak axis ····· 37
Fig. 2.23 Comparison of Test and analysis results ····· 37
Fig. 2.24 Comparison of cumulative energy absorption capacity ····· 39
Fig. 2.25 Part total energy for strong axis ····· 39
Fig. 2.26 Part total energy for weak axis ····· 39

Fig. 3.1 (a), General layout (b), Bazant's plastic buckling mechanism model, (b) Free body diagram ····· 42
Fig. 3.2 Kinematic and Isotropic Hardening Model ····· 44
Fig. 3.3 (a) Analysis model, (b) Loading and constraint condition ····· 46
Fig. 3.4 The buckling mode of analysis result ····· 51
Fig. 3.5 Equivalent plastic strain of element for Type I ····· 52
Fig. 3.6 Equivalent plastic strain of element for Type II ····· 53
Fig. 3.7 Equivalent plastic strain of element for Type III ····· 54
Fig. 3.8 Equivalent plastic strain of element for Type IV ····· 55
Fig. 3.9 load-displacement relationship analysis result for Type I ····· 56
Fig. 3.10 load-displacement relationship analysis result for Type II ····· 57
Fig. 3.11 load-displacement relationship analysis result for Type III ····· 57
Fig. 3.12 load-displacement relationship analysis result for Type IV ····· 58
Fig. 3.13 Comparison of load-deformation curve ····· 58
Fig. 3.14 Comparison of cumulative energy absorption of analysis result ····· 59
Fig. 3.15 Comparison of Part total energy of analysis result ····· 60

Fig. 4.1 Test layout for Zayas et al. (1980) ····· 64

Fig. 4.2 Axial force-axial displacement relationship of Zayas et al. Experiment ··· 65
Fig. 4.3 Definition of different zones ····· 67
Fig. 4.4 Typical brace hysteretic response under symmetrical cyclic loading (Robert Tremblay 2002) ····· 69
Fig. 4.5 Different Constraint Condition Model Considered ····· 70
Fig. 4.6 Displacement Protocol ····· 71
Fig. 4.7 Theoretical Buckling mode of bracing member under compression loading ····· 72
Fig. 4.8 Buckling mode and von Mises's stress distribution for pinned-pined support condition of CHS ····· 74
Fig. 4.9 Fracturing and von Mises's stress distribution for pinned-pined support condition of CHS ····· 74
Fig. 4.10 Buckling mode and von Mises's stress distribution for fixed-pined support condition of CHS ····· 75
Fig. 4.11 Fracturing and von Mises's stress distribution for fixed-pined support condition of CHS ····· 76
Fig. 4.12 Hysteresis loops of analysis Result for CHS model ····· 78
Fig. 4.13 Buckling mode and von Mises's stress distribution for fixed-fixed support condition (H-Section) ····· 79
Fig. 4.14 Fracturing and von Mises's stress distribution for fixed-pined support condition (H-Section) ····· 80
Fig. 4.15 Hysteresis loops of analysis Result for H-Section model ····· 82
Fig. 4.16 Out-of-plane deformation of braces: (a) elastic with pinned ends; (b) inelastic with pinned ends; (c) elastic with fixed ends; (d) inelastic with fixed ends. ····· 83

Fig. A.1 Experiment result of tension strength. ····· 93
Fig. A.2 Detail of specimen ····· 94
Fig. A.3 Displacement Protocol ····· 96

Fig. A.4 Meshed 3-D Analysis Model ····· 97
Fig. A.5 Load experiment equipment ····· 98
Fig. A.6 Failure Type ····· 99
Fig. A.7 Failure mode of Analysis and Test Results ····· 104
Fig. A.8 Comparison of the hysteresis loops ····· 106
Fig. A.9 Inelastic response under loading ····· 108
Fig. A.10 Inelastic response under unloading ····· 109
Fig. A.11 Inelastic response under reloading ····· 110
Fig. A.12 One full CYCLE energy dissipation ····· 111

Fig. B.1 Stress-strain curve of test result. ····· 114
Fig. B.2 Loading condition under shear ····· 115
Fig. B.3 Stress distribution ····· 115
Fig. B.4 Loading Condition and Deformation mode ····· 117
Fig. B.5 Bilinear model with a kinematic hardening ····· 120
Fig. B.6 Detail dimension of specimen for K= (K= H/D) ····· 121
Fig. B.7 Schematic illustration of circular pipe steel damper tasting set up ····· 122
Fig. B.8 Displacement protocol ····· 123
Fig. B.9 Test result for monotonic loading ····· 125
Fig. B.10 Deformation Shape Results of Circular pipe damper ····· 126
Fig. B.11 Comparison of Test and Analysis (Explicit and Implicit) Hysteresis Loop Results ····· 127

Fig. C.1 Initial instability in column under compression loading ····· 130
Fig. C.2 Buckling of a simply supported beam of length L with a plastic hinge at mid length ····· 130
Fig. C.3 Geometric non linearities in a finite element: (a) large displacements, small strains; (b) large displacements, large strains ····· 133
Fig. C.4 Graphical representation of the Newton-Raphson method ····· 134

Abstract

A Study on Nonlinear Inelastic Buckling and Response Behavior of Steel Members Under Axial Loading

Daniel Yeshewawork Abebe
Advisor : Prof. Choi, Jae hyouk,
Department of Architectural Engineering,
Graduate School of Chosun University

A nonlinear analytical approach for evaluating the inelastic buckling and response behavior of steel members for different condition was carried out. The inelastic buckling behavior of H-section steel column member was studied in this thesis for two different cases: pinned-pinned constraint condition and fixed-fixed constraint condition.

A steel column member subjected to an axial compression load will shorten in the direction of load. If the load increased until the column buckles, the shortening will stop and the column will suddenly bend or deform laterally and may at the same time twist in a direction perpendicular to its longitudinal axis. But before final buckling or collapse, steel column member has a tendency of plastic deformation. The issue has been much discussed along with the evaluation of plastic deformation capacity and restoring force of column members in the large deformation range following post-buckling.

In order to predict the inelastic buckling behavior of the member, the load-deformation relationship needs to be identified in the whole process. The plastic deformation of column members and its loading energy absorption capacity through identifying inelastic buckling behavior will elucidate how to prevent progressive collapse of structures. In addition to nonlinear FE analysis, compression test on an H-shaped column member was carried out and both plastic deformation mode and load-deformation curve was compared for further verification of the analysis result.

Steel bracing members which are used to resist lateral loads (seismic load and wind loads) on the building structures are evaluated for CHS (circular hollow section) and

H-section in the same way. The inelastic response of bracing members under cyclic axial loading was tried to evaluate analytically. The hysteresis loop shape is compared with test result from available literatures. The cyclic behavior of bracing member is complex and accurately not yet investigated. Although this issue needs further study, it is tried to present both the buckling behavior and the cyclic characteristics of bracing members of CHS and H-section.

Furthermore, to mitigate damages caused by earthquake, energy absorbing devices have an important role. Here the inelastic seismic response of steel dampers called shear panel hysteresis damper and circular pipe damper have been studied analytically. The analysis result were verified by comparing with the loading test results.

초록

축하중을 받는 철골부재의 비탄성좌굴 및 응답거동에 관한 연구

아베베 다니엘 예쉬와웍
지도 교수: 최 재 혁
건축공학과,
조선 대학교 대학원

서로 다른 구속조건에 대한 철골부재의 비탄성좌굴과 비선형 응답거동을 평가하기 위해 유한요소해석을 수행하였다.

첫 번째, 서로 다른 구속조건(양단힌지, 양단고정)을 가지는 H형강 기둥부재의 비탄성 좌굴거동을 검토하기 위하여 세장비에 크기에 따라 기둥부재를 모델링하여 좌굴후 비탄성 거동특성, 최대내력의 변화, 잔존내력 및 에너지 흡수능력에 대해서 평가하였다. 더욱이, 실재하실험결과와 해석결과값을 비교하여 해석결과와의 정합성에 대해서도 검토하였다.

건축물에 가해지는 수평하중(지진하중과 풍하중)에 주로 저항하는 브레이스 시스템은 매우 복잡한 반복거동을 수행하고 있음에도 불구하고 거동특성은 아직 명확하게 제시되고 있지 못하다. 본 논문에서는 CHS(원형 중공형)강재와 H형 강재로 구성된 브레이스 부재의 비선형 응답특성을 검토하였다.

또한, 제진시스템에 사용되는 댐퍼는 지진으로 인한 피해를 완화시키기 위한 에너지 흡수장치는 최근 그 중요성이 더욱 강조되고 있다. 전단패널형 강재이력댐퍼와 원형파이프 강재애력댐퍼의 비탄성 지진응답 거동특성을 파악하기 위하여 유한요소해석을 실시하였다. 또한 해석결과를 실재하실험값과 비교하여 해석결과의 타당성을 검토하였다.

CHAPTER 1 INTRODUCTION

1.1 General Over View

Building structures are damaged due to many reasons. Factors such as construction errors, miscommunications, poor inspections, design flaws, explosions, unexpected loads; (that leads to progressive collapse), and natural disasters (like earthquake). In this study progressive collapse of building structures member due to unexpected loading and earthquake damage mitigating devices has been studied.

Progressive collapse is a failure mode of great concern for buildings structures, and is also typical of building demolitions. In Wikipedia progressive collapse of building is defined as: 'A building undergoes progressive collapse when a primary structural element fails, resulting in the failure of adjoining structural elements, which in turn causes further structural failure, similar to a house of cards.'

Fig. 1.1 The collapse of 2 World Trade Center (Taken from Wikipedia)

Numerous buildings were collapsed with different causes. Ronan Point was a building in Newham, east London, which suffered a partial collapse on 16 May

1968 when a gas explosion demolished a load-bearing wall, causing the collapse of one entire corner of the building. The other most infamous paradigm is the collapse of the twin towers of World Trade Center towers collapsed on September 11, 2001 by terrorists affiliated with al-Qaeda. After the aircraft hits the buildings as shown in Fig. 1.1 Massive damage and destruction on world trade center (WTC) Buildings propagates up to the base of the building as seen in fig 1.2.

Fig. 1.2 The massive collapse of 2 World Trade Center (Taken from Wikipedia)

The other building damage causes are earthquake. Earthquakes produce various damaging effects to the areas they act upon. This includes damage to buildings and in worst cases the loss of human life. The deadly earthquake areas of the 20th century are: Northern Peru(1970), Tangashan, China (1976), Northwest Armenia(1988), Kobe,Japan (1995), Northwest Iran(1997), Western Colombia(1999), Western Turkey, etc. In these hazard a number of properties damaged and so

many human life also loss. In order to mitigate the effect of earthquake energy dissipating device have an important role in the civil structures. Thus, in this study a simple and economical energy dissipating devices called shear panel hysteresis steel damper(SPD) and circular pipe steel amper (CPD) has resented. These dampers are simple easy to use and manufacturing and also installing.

1.1.1 Causes of Progressive Collapse

As mentioned on part 1.1 above the cause of progressive collapse are so many. For example the Federal Emergency Management Agency (FEMA) report on performance studies of the buildings in May 2002. It declared that the WTC design had been sound, and attributed the collapses wholly to extraordinary factors beyond the control of the builders. While calling for further study, FEMA suggested that the collapses were probably initiated by weakening of the floor joist by the fires that resulted from the aircraft impacts. According to FEMA′s report, the floors detached from the main structure of the building and fell onto each other, initiating a progressive collapse.

The other most commonly cause of progressive collapse is unexpected loading on the structures. When an expected object falls on structure, if the weight of the object is greater than the structure's design load then the structure will collapse. The condition will be clarified in the following section.

1.1.2. Conditions of Progressive Collapse of Building Structures

There is a great need to assess actual behavior of structural damage due to accidental loads. For doing this, it is necessary to identify the relationship of load-deformation of a column member in the entire process of a structure up to final collapse. Through the process, although a part of the column is accidentally damaged, it is possible to prevent progressive collapse. The condition is described in Fig. 1.3.

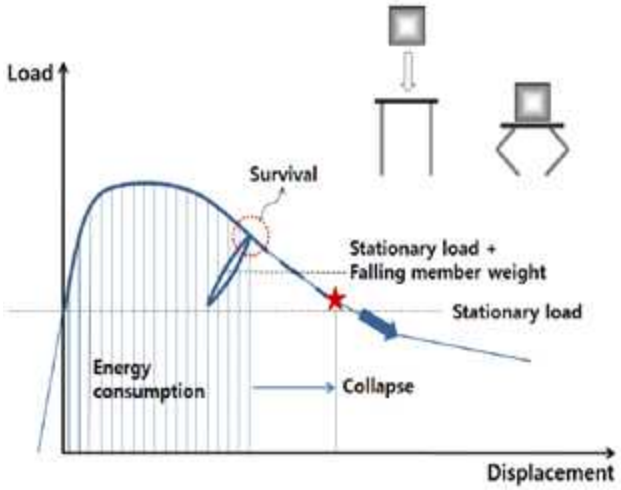

(a) Case that the weight of falling objects and the stationary load are considered separately

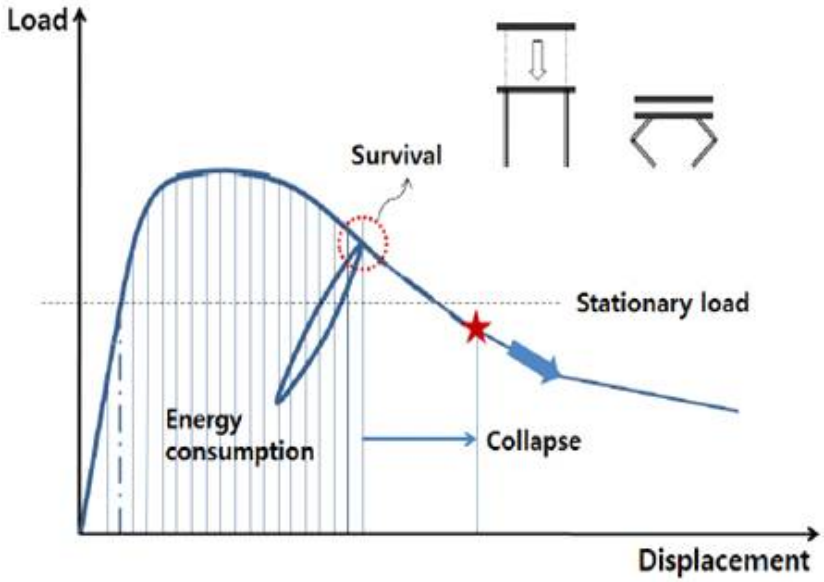

(b) Case that the weight of falling objects included in the stationary loads

Fig. 1.3. Conditions of progressive collapse prevention for structures due to falling object

It is possible to absorb the free potential energy of falling objects as plastic deformation energy as shown in Fig.1.(a) according to the relationship of load-deformation of a column member. The column is buckled when it failed to resist the applied load. However, as a result of energy absorption; if the residual strength is greater than the vertical load which is the sum of permanent vertical load and the weight of falling objects, progressive collapse is not caused. Meanwhile, the case that the weight of falling object is included in the permanent vertical load as shown in Fig.1.(b). In this case, it was assumed that uniform impact is exerted on all columns.

1.2 Elastic and Inelastic Buckling Characteristics of Steel

Elastic Buckling

Elastic buckling occurs in long columns that are simply supported. It is similar to inelastic buckling in that the basic properties of the column, strength and stiffness, are the same, but the end result is quite different. Elastic buckling causes the column or object to become malformed, but in a more severe way than inelastic buckling. While inelastic buckling appears to create a kneeling effect, elastic buckling creates an entirely bowed appearance of the object.
Elastic buckling of structure is also called temporary buckling because of the buckling mode will recover to its original shape up on unloading.

Inelastic Buckling

Inelastic buckling occurs in objects such as a column of intermediate length and made of a rigid material. Inelastic buckling happens when the stress load on an object exceeds the proportional limits of the material (i.e. the strength and stiffness.) Inelastic buckling can be identified by objects becoming misshapen due to excess force. A column, for example, goes through a process called kneeling, where the middle of the column bows outward away from the normal force.

Inelastic buckling unlike elastic buckling, the buckled structure will nor recover up on unloading (is also called irreversible buckling).

1.3 Objectives and Scope

The objective of this research was to produce a relatively simple yet reasonably accurate engineering analysis for predicting axial load as function of displacement for pinned-pinned, fixed-fixed H-shape column member and pinned-pined, fixed-pinned bracing member with an H-shape and tubular steel under cyclic loading. Furthermore, the hysteresis characteristics of steel structures (shear panel damper and circular pipe damper) have also been identified.

The accuracy of the analysis carried out in these study illustrated by comparison of the load-deformation relationships generated by test. Not only the load-displacement, but also the hysteresis curve result and deformation shape is also verified experimentally.

1.4 Reading Directions

To give the reader a short introduction to the different parts in this research the following section will explain the content in each chapter. The thesis report is divided into four phases, each including two chapters, see Figure 1.4.

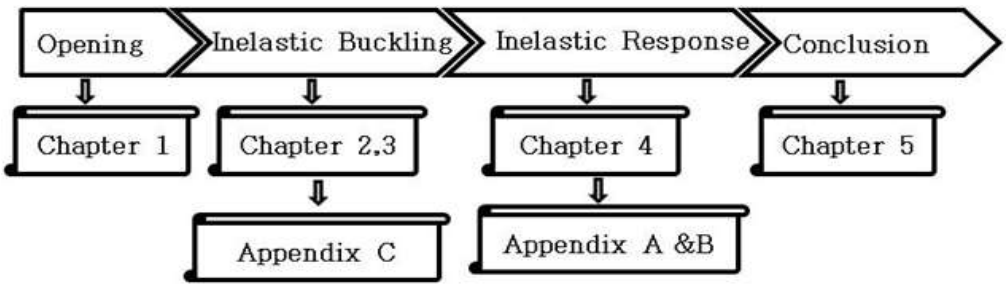

Fig. 1.4. Reading Directives

Chapter 1 - Introduction

To provide the reader with an understanding of the background and the approaches used for the study, this chapter will describe the general description of the problem background, the conditions considered, the objective and the scope. In the end the reading directives will be explained.

Chapter 2 - Inelastic Buckling Evaluation of Simply Supported H-section Column Member Under Axial Compression Loading

Both the inelastic buckling mode and load-deformation curve for pinned-pinned ended column model has been studied theoretically, Analytically, and verified by experiment. Furthermore, the energy absorbtion capacity of member from load-deformation curve was calculated for both analysis and loading test for comparison purpose.

Chapter 3 - Inelastic Buckling Evaluation of Fixed Ended H-section Column Member Under Axial Compression Loading

Both the inelastic buckling mode and load-deformation curve for both end fixed ended column model has been studied theoretically and Analytically for different slenderness ratios. In order to identify the effect of slenderness ratios on energy absorption capacity, it is calculated and compared for four members having different slenderness ratio.

Chapter 4 - Inelastic Buckling and Response of CHS and H-section Bracing Member Under Cyclic Loading

The inelastic buckling and response of circular hollow section and H-section steel

bracing member for different constraint condition was studied theoretically and analytically. This chapter first reviews the existing literatures. Though the analysis result were not verified by actual test; however, the shape of cyclic response from literature is quite match with the test result.

Chapter 5 - Conclusion

The summary of all above has been presented in this chapter. Since a conclusion of each chapter were presented, here the summary presented was a general conclusion.

Appendix A - Inelastic Seismic Response of Shear Panel Hysteresis Damper

The inelastic seismic response of shear panel damper with two different strength steel material has been studied in this chapter. Low yield point steel and conventional steel with different depth to thickness ratio used for study in both analysis and quasi static loading test. The failure mode, the hysteresis characteristics and cumulative energy absorption capacity curve of both results were compared.

Appendix B - Inelastic Seismic Response of Circular Pipe Hysteresis Damper

After deriving the effective size of circular pipe damper, the inelastic seismic response of CPD both analytically and experimentally investigated for two different strength steel material. By considering the effective size (having aspect ratio of K $=\sqrt{3}$) as a reference, a size less that and greater that $\sqrt{3}$ is studied in detail. The failure mode, the hysteresis characteristics and cumulative energy absorption capacity curve of both results were compared.

Appendix C - Imperfection in Modeling Steel Members

In structural engineering, structural elements are modeled as stable and perfect. However in the actual situation this condition is not the same so that in modeling structural elements it needs to consider some initial imperfection. This condition is dealt in this Appendix.

CHAPTER 2 INELASTIC BUCKLING EVALUATION OF H-SHAPE PINNED-PINNED STEEL COLUMN MEMBER UNDER AXIAL COMPRESSION LOADING

2.1 Introduction

Studies of structural stability, especially for column member, are mainly concerned with two problems - predicting buckling conditions and estimating inelastic behavior. Terminologically, the former is called buckling analysis and the latter is called inelastic analysis. Despite the fact that Euler's theory, which was presented in 1744 as a classic investigation of an axially compressed column, includes a complete inelastic analysis, the problem of the theory of stability has long been considered to be the determination of critical conditions. This is because the inelastic buckling region was, for a long time, of secondary practical interest and the governing differential equations in this region are nonlinear, posing fundamental analytical difficulties. The same situation is considered for column members subjected to unexpected compression load. These accidentally falling objects on the structure causes progressive collapse on the structure. In order to clearly predict the effect of progressive collapse it is crucial to identify the relationship between load-deformation. The column member will buckle when the applied load exceeds the critical load required to induce buckling. The steel column member exhibit a tendency of plastic deformation followed by large buckling before final collapse. Buckling characteristics and inelastic buckling strength of column member is dealt by many scholars to prevent progressive collapse of structure by plastic deformation capacity of steel members. In this chapter theoretical, experimental and analytical approaches are carried out to predict load - deformation curves and the failure mode of an H section column member with both end pined.

2.2 Theoretically Derived Equations

2.2.1 Bazant's Hinge-ended model

Many scholars had been investigated mainly for hinge ended column member both experimentally theoretically. Here further studies' including the existing has been presented. It is known that when both end hinged column members are subjected to axial compression force P and the applied axial force equals or exceeds the critical force that induces buckling; and displaces axial deformation (Δ), plastic hinge is formed at center of the member as shown in Fig 1(a).

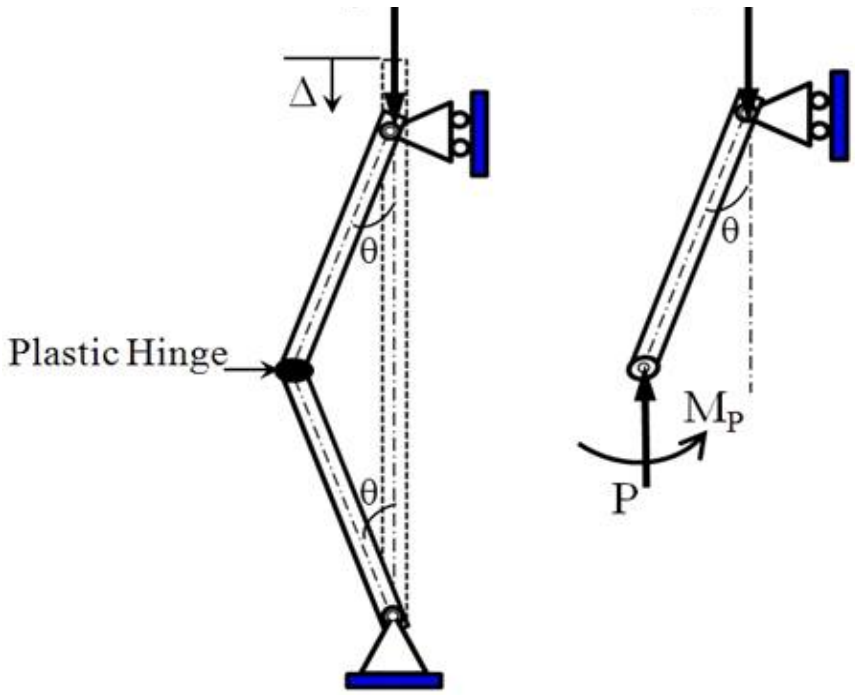

Fig. 2.1. (a) Hinge ended buckling of column member and (b) free body diagram

From the condition of moment equilibrium of the half column as a free body Fig. 1b, the axial load and from the buckling geometry, the axial shortening is given by equation (2.1) and (2.2) respectively.

$$P = \frac{2M_p}{Lsin\theta} \tag{2.1}$$

$$\Delta = L(1-\cos\theta) \tag{2.2}$$

where: L is distance between end hinges, M_p is the plastic moment and θ is the plastic rotation. Eliminating plastic rotation θ, it is found that the plastic load-shortening becomes:

$$P = \frac{2M_p}{L\sqrt{1-[1-(\triangle/L)]^2}} \tag{2.3}$$

From equation (2.1) and (2.3) the relationship between axial compression force and deformation can be expressed as:

$$\triangle = L - \sqrt{L^2-(2M_p/P)^2} \tag{2.4}$$

2.2.2 AIJ Recommendation

For H- shaped steel structure, as Architectural Institute of Japan of limit state design guidelines, in 1998, the relationship between the axial force and moment considering the tolerance is given by equation (2.3) and (2.4) for strongand weak axis respectively.

Interaction Diagram

Interaction diagrams are extensively used as a tool for designing prismatic members subjected to several combined stresses. For a long time, sets of these diagrams have been available in building technologies, such as reinforced concrete, steel and composite sections, under various stresses. For H-section steel column member of pin ended model have two interaction curve depending on the constraint condition on strong and weak axis.

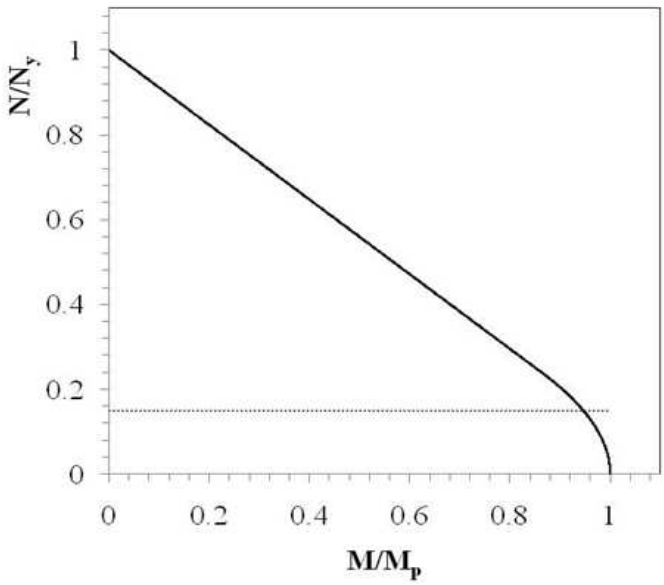

(a) Interaction diagram for H-section Strong axis

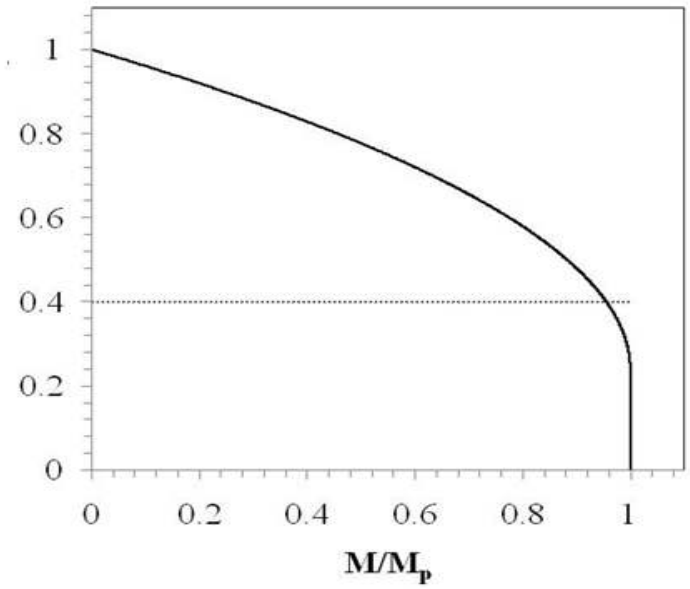

(b) Interaction diagram for H-section weak axis

Fig.2.2. Interaction surface diagram for H-section steel column member

$$\frac{M}{M_y} \le 1 \quad \text{for} \frac{N}{N_y} \le 0.15 \quad \text{and} \quad \frac{N}{N_y} + 0.85\frac{M}{M_y} \le 1 \qquad \text{for} \quad \frac{N}{N_y} > 0.15 \tag{2.5}$$

$$\frac{M}{M_y} \le 1 \quad \text{for} \frac{N}{N_y} \le 0.4 \quad \text{and} \quad \frac{N}{N_y} + 0.84\frac{M}{M_y} \le 1 \qquad \text{for} \quad \frac{N}{N_y} > 0.4 \tag{2.6}$$

The elastic section modulus is determined by I/y, where I is the second moment of area (or moment of inertia) and y is the distance from the neutral axis to any point or it is often reported that the distance from the neutral axis to the most extreme compression fibre. The section modulus at plastic state (Zp) is also often used to determine the plastic moment (Mp) such that:

$$M_p = Z_p * \sigma_y \tag{2.7}$$

where y is the yield strength of the material. So the plastic moment is also expressed as Py

$$M_p = \frac{Z_p * P_y}{A} \tag{2.8}$$

where A: is the cross sectional area.Z_p is the section modulus

1. From equation (2.4) , (2.5) and (2.7) the relation axial compression force and deformation for strong axis is derived as:

$$\frac{\triangle}{L} = 1 - \sqrt{1 - (\frac{2Z_p}{LA})^2 * (\frac{1}{P/P_y})^2} \qquad P/P_y < 0.15 \tag{2.9}$$

$$\frac{\triangle}{L} = 1 - \sqrt{1 - (\frac{2Z_p}{0.85LA})^2 * (1 - \frac{1}{P/P_y})^2} \qquad P/P_y \geq 0.15 \tag{2.10}$$

2. From equation (2.4), (2.6) and (2.7) the ratio of the deformation to the effective length of the column member for weak axis is:

$$\frac{\triangle}{L} = 1 - \sqrt{1 - (\frac{2Z_p}{LA})^2 * (\frac{1}{P/P_y})^2} \qquad P/P_y < 0.4 \tag{2.11}$$

$$\frac{\triangle}{L} = 1 - \sqrt{1 - (\frac{2Z_p}{0.84LA})^2 * (\frac{1}{P/P_y} - P/P_y)^2} \qquad P/P_y \geq 0.4 \tag{2.12}$$

2.2.3 Paris's Analysis

Paris reviews and introduces the relationships between vertical load on pin ended column model and the post-buckling deformation as equation (2.13).

The relationship between axial compression force and deformation proposed by Paris:

$$\frac{\triangle}{L} = \frac{P}{AE} + \frac{\pi^2}{4L^2}(\triangle_T)^2 \tag{2.13}$$

Where, $\triangle_T = \frac{M_p}{P}$, A is the cross-sectional area of the column, E young's modulus and L is the length between hinges.

From the stress-strain curve it the early (low strain) many materials including SS400 will obey Hooke's law; the stress is proportional to strain with the constant of proportionality being the modulus of elasticity or Young's modulus, denoted

$$\sigma = E\varepsilon \tag{2.14}$$

Though as the strain is increased, many materials eventually deviate from this linear proportionality, the point of departure being termed the proportional limit. By substituting $\sigma = \frac{P}{A}$ and rearranging and expressing the strain in terms of yield strength and strain

$$\varepsilon = \frac{P}{EA} \tag{2.15}$$

$$\varepsilon = \frac{P}{P_y}\varepsilon_y \tag{2.16}$$

From this equation and by substituting equation (2.12-16) into equation (2.5) and rearranging it is obtained for strong axis that:

$$\frac{\triangle}{L} = \frac{P}{AE} + \frac{\pi^2}{4L^2} * (\frac{M_p}{0.85})^2 (\frac{1}{P} - \frac{1}{P_y})$$

$$\frac{\triangle}{L} = \frac{P}{P_y}\varepsilon_y + \frac{\pi^2}{4L^2} * (\frac{Z_p}{A})^2 (\frac{1}{P/P_y}) \qquad P/P_y < 0.15 \tag{2.16}$$

$$\frac{\triangle}{L} = \frac{P}{P_y}\varepsilon_y + \frac{\pi^2}{4L^2} * (\frac{Z_p}{0.85A})^2 (\frac{1}{P/P_y} - 1) \qquad P/P_y \geq 0.15 \tag{2.17}$$

For Weak Axis

$$\frac{\triangle}{L} = \frac{P}{AE} + \frac{\pi^2}{4L^2} * (\frac{M_p}{0.84P})^2 (1 - \frac{P}{P_y})$$

$$\frac{\triangle}{L} = \frac{P}{P_y}\varepsilon_y + \frac{\pi^2}{4L^2} * (\frac{Z_p}{A})^2 (\frac{1}{P/P_y}) \qquad P/P_y < 0.4 \tag{2.17}$$

$$\frac{\triangle}{L} = \frac{P}{P_y}\varepsilon_y + \frac{\pi^2}{4L^2} * (\frac{Z_p}{0.84A})^2 (\frac{1}{P/P_y} - P/P_y) \qquad P/P_y \geq 0.4 \tag{2.18}$$

2.3 Finite Element Analysis Model

Non-linear finite element analysis was carried out to evaluation of plastic deformation capacity and restoring force of a member in a large deformation range following buckling for SS400 H-shaped steel column. The analysis specimen is modeled by H-100x100x6x8 cross sectional member as shell element.

2.3.1 Material Modeling

A nonlinear, inelastic, plastic kinematic characteristic of the material modeling was used with considering strain hardening. Generally, there are two types of hardening material model available; Kinematic hardening and Isotropic hardening.

Kinematic hardening is where the yield surface remains the same shape and size but merely translates in stress space, figure 3. In another words, kinematic hardening involves a shifting of the yield surface (primarily due to a reversal of loading).

Isotropic hardening model involves yielding the entire yield surface uniformly or it means expanding of the yield surface without translation. The kinematic hardening model is preferred for analyses involving cyclical loading (Bauschinger effect), but the stress-strain behavior of the actual material should be used to decide between isotropic and kinematic hardening.

The specimen's plastic kinematic characteristic analysis model's and sectional properties used in the analysis model with different cases considered are presented in the table 1and 2 respectively.

Table 2.1 The property of material used in the analysis

Property	Specimen	Upper and Lower Rigid body
Young's Modulus (GPa)	205	205
Poison's ratio	0.3	0.3
Density (kg/m^3)	7860	7700
Yield Strength (MPa)	345	
Tangent Modulus (MPa)	756	
Hardening Parameter	0.5	
Strain rate [C] (s^{-1})	40	
Strain rate [P]	5.0	
Failure Strain	0.75	

Table 2.2 Sectional property of specimen

Slenderness ratio		Area (mm^2)	Radius of Gyration (r_x)	Radius of Gyration (r_y)	Moment of area I_x(mm^4)	Moment of area I_y(mm^4)
λ_x	λ_y					
14	23	2190	41.8mm	24.7mm	3.83x10^6	1.34x10^6

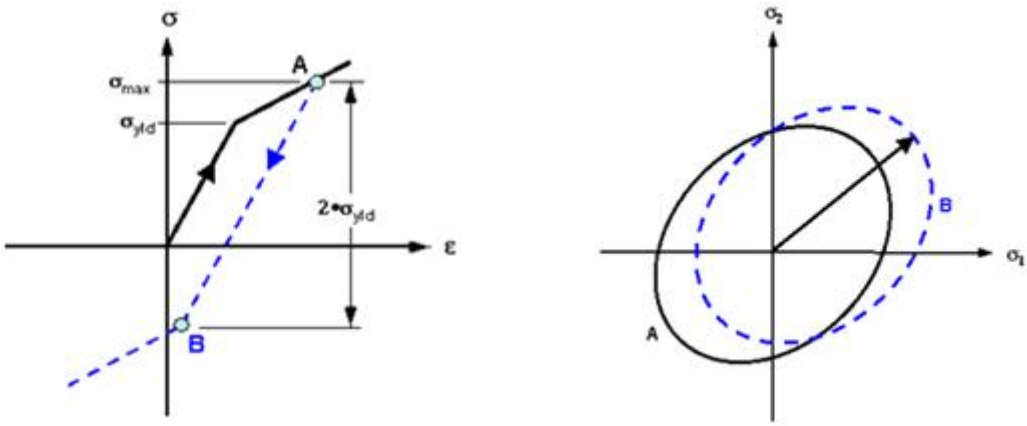

Fig. 2.3. Uniaxial stress-strain curve, biaxial stress-strain curve for kinematic hardening model

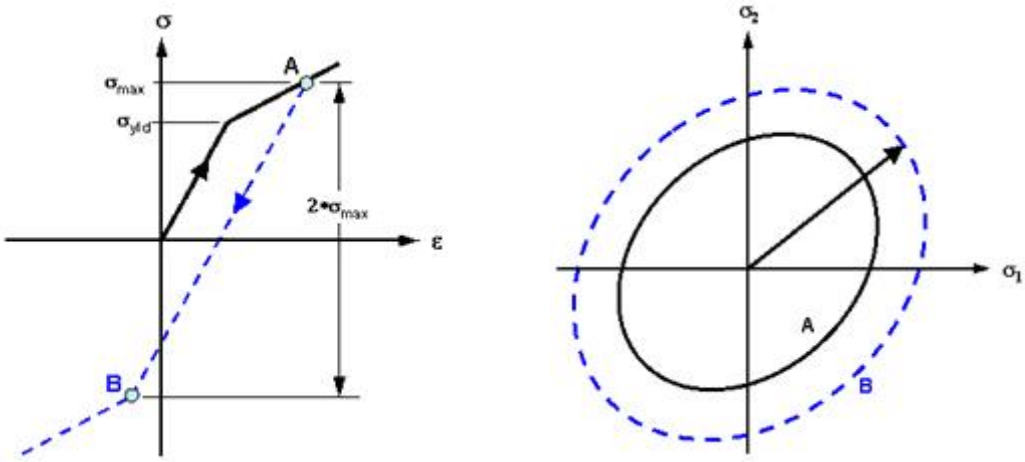

Fig. 2.4. Uniaxial stress-strain curve, biaxial stress-strain curve for isotropic hardening model

In the analysis of nonlinear finite element using ANSYS LS-Dyna the hardening characteristics is adjusting by the hardening parameter β. The parameter is adjusted between 0 (kinematic hardening) and 1 (isotropic hardening). For combined hardening where the initial yield surface shows both translation and expansion. Of course here combined hardening model has been used. The H-section steel columns were modeled with strain rate dependency and failure. Strain rate is accounted for using the Cowper-Symonds model which scales the yield stress by the stain rate dependent factor as shown below.

$$\sigma_y = [1 + (\frac{\dot{\varepsilon}}{C})^{\frac{1}{P}}](\sigma_o + \beta E_p \varepsilon_p^{eff}) \qquad (2.19)$$

Where: σ_o is the initial yield stress, $\dot{\varepsilon}$ is the strain rate, C and P are the Cowper-Symonds strain rate parameters, ε_p^{eff} is the effective plastic strain, and E_p is the plastic hardening modulus which is given by:

$$E_p = \frac{E_{\tan} E}{E - E_{\tan}} \tag{2.20}$$

$E_{\tan}$ is the tangent modulus or called strain hardening modulus and is given by:

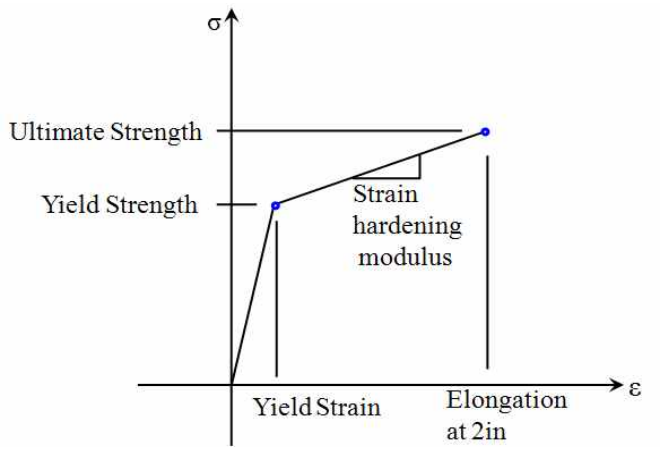

Fig. 2.5. Typical stress strain curve

$$Strain\ Hardening\ \mathrm{modulus} = \frac{Ultimate\ Strength - Yield\ Strength}{Elongation @ 2 \in / 100 - Yield\ Strain} \tag{2.21}$$

2.3.2 Constraint and Loading Condition

The way the axial compressive load is applied at the plate edges affects its buckling stress. There are basically two ways of applying that load: the constant stress loading and the constant strain loading. In the constant stress loading, a uniform load is prescribed at both rigid bodies while not constraining the displacements of these bodies to follow any pattern. On the other hand, the constant strain loading requires the rigid bodies to be constrained to have the same prescribed displacement. It has been proven that the case of constant strain loading

is more stable than the case of constant stress loading, for column member to have the maximum strain set. Therefore, the condition of constant stress loading has been applied in all the work presented herein.

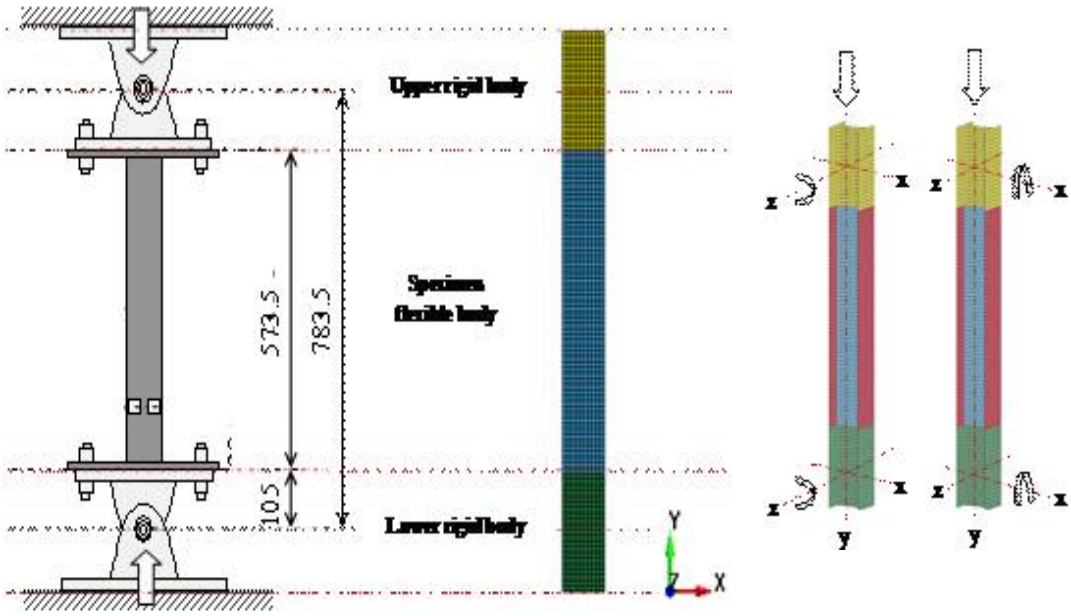

(a) (b)

Fig. 2.6 (a) general layout of analysis model, (b) the constraint and loading condition

The buckling load, of an axially loaded member is greatly affected by its boundary conditions. The member's are free rotation in two different options: free in strong axis and constraint in weak axis and constraint in strong axis and free in the weak axis. In both cases, the translation is also free in loading direction (vertical Y-axis).With the scribed loading and constraint condition, the load is applied only on the upper rigid body after setting strain.

2.3.3 Analysis Process

As it was mentioned so far, explicit nonlinear computer software called LS-Dyna is used in this study. The analysis starts by modeling the specimen between two rigid bodies as a shell element (Fig 2(a)). The thickness is specified in real constants. All material properties and constraint conditions of the system is controlled in material modeling command. The contacts between specimen and rigid bodies needs to be specified, and extra nodes was introduced to take account the explicit dynamic constraints. By controlling displacement with respect to time (array parameter command) the axial compression load is applied on the upper rigid body. To find the necessary outputs, it is specified the output file type and ASCII outputs by EDOPT and EDOUT command respectively.

2.4 Finite Element Analysis Result

2.4.1. Failure mode

The failure mode of hinge ended model for both constraints on strong and weak axis shows the column member buckles at the central part. Fig. 7 shows the deformed shape of large deformation non-linear FEM analysis for the specimen in strong axis and weak axis. The specimen buckles in the central part and local buckling of flanges around the centre, rotation at both ends.

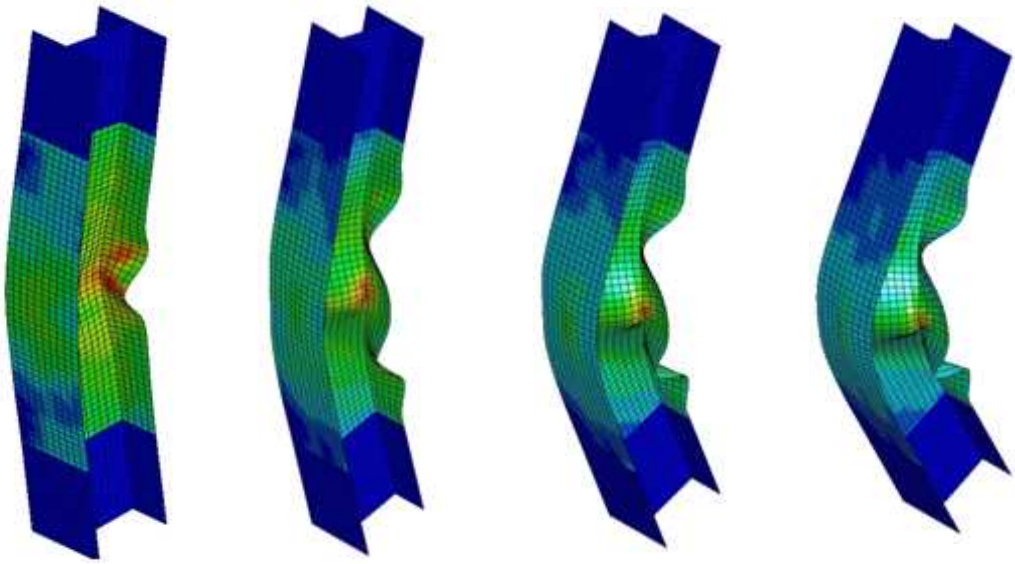

5% strain 10% strain 15% stain 20% strain

Fig. 2.7 deformation shape of analysis result on strong axis

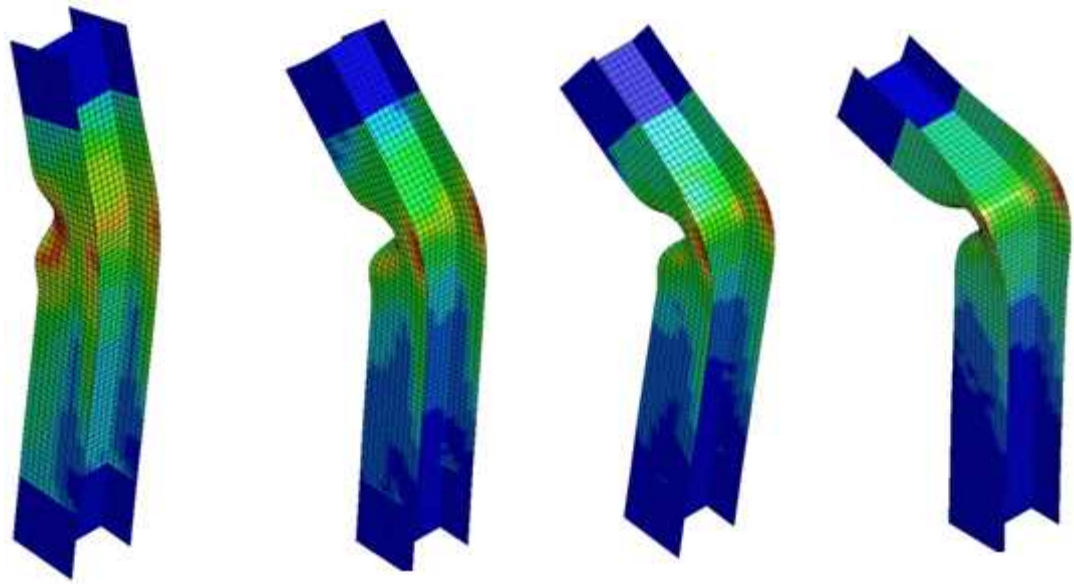

5% Strain 10% Strain 15% Strain 20% Strain

Fig.2.8 deformation shape of analysis result on weak axis

2.4.2. Equivalent plastic strain and effective stress of elements

The inelastic analysis model predicts the yielding, buckling and inelastic deformation modes, but it cannot directly predict the initiation of cracking, ductile tearing or fracture of the steel. Instead, the equivalent plastic strain ε_{eqv}^{pl}, resulting from the inelastic analysis is used as an indicator of initial cracking and fracture of the steel and weld by calibrating the computed value of ε_{eqv}^{pl} to the observed initiation of cracking and tearing in the experiments. In the analysis, ε_{eqv}^{pl} was based on the plastic strain components using the general von Mises equation:

$$\varepsilon_{eqv}^{pl} = \frac{1}{\sqrt{2}(1+\acute{\nu})}[(\varepsilon_x^{pl}-\varepsilon_y^{pl})^2+(\varepsilon_y^{pl}-\varepsilon_z^{pl})^2+(\varepsilon_z^{pl}-\varepsilon_x^{pl})^2+\frac{2}{3}(\gamma_{xy}^{pl^2}+\gamma_{yz}^{pl^2}+\gamma_{zx}^{pl^2})]^{\frac{1}{2}} \quad (2.22)$$

where,ε_x^{pl}, ε_y^{pl}, ε_z^{pl} γ_{xy}^{pl} etc are the appropriate components of plastic strain and υ' is the effective Poisson's ratio.

In the same way the equivalent stress is defined as

$$\sigma_{eqv} = (\frac{1}{2}[(\sigma_x-\sigma_y)^2+(\sigma_y-\sigma_z)^2+(\sigma_z-\sigma_x)^2+6(\sigma^{2_{xy}}+\sigma^{2_{zx}})])^{\frac{1}{2}} \quad (2.23)$$

and σ_x,σ_y , σ_z etc., are the appropriate component stresses.

It is possible to compute the effective plastic strain at any point throughout the member of the analysis model. The effective plastic strain with respect to axial strain for elements chosen from middle of the upper as well as lower part and form the center of the web is compared. The elements under considerations are indicated in fig.4. Fig. 8 presents the effective plastic strain-axial deformation relation of the element chosen from different part of the member. From the figure

we can say that the plastic strain at the bottom and top element increases up to axial strain of 2.5% then the plastic strain becomes constant. The plastic strain of the center element of the web increases throughout the process. Referring to fig. 9, the effective stress (von Mises's) at those points are drawn for both strong and weak axis. In both cases the stress concentration at the central part is higher. The effective stress for strong axis member is in all cases is relatively higher compared with weak axis.

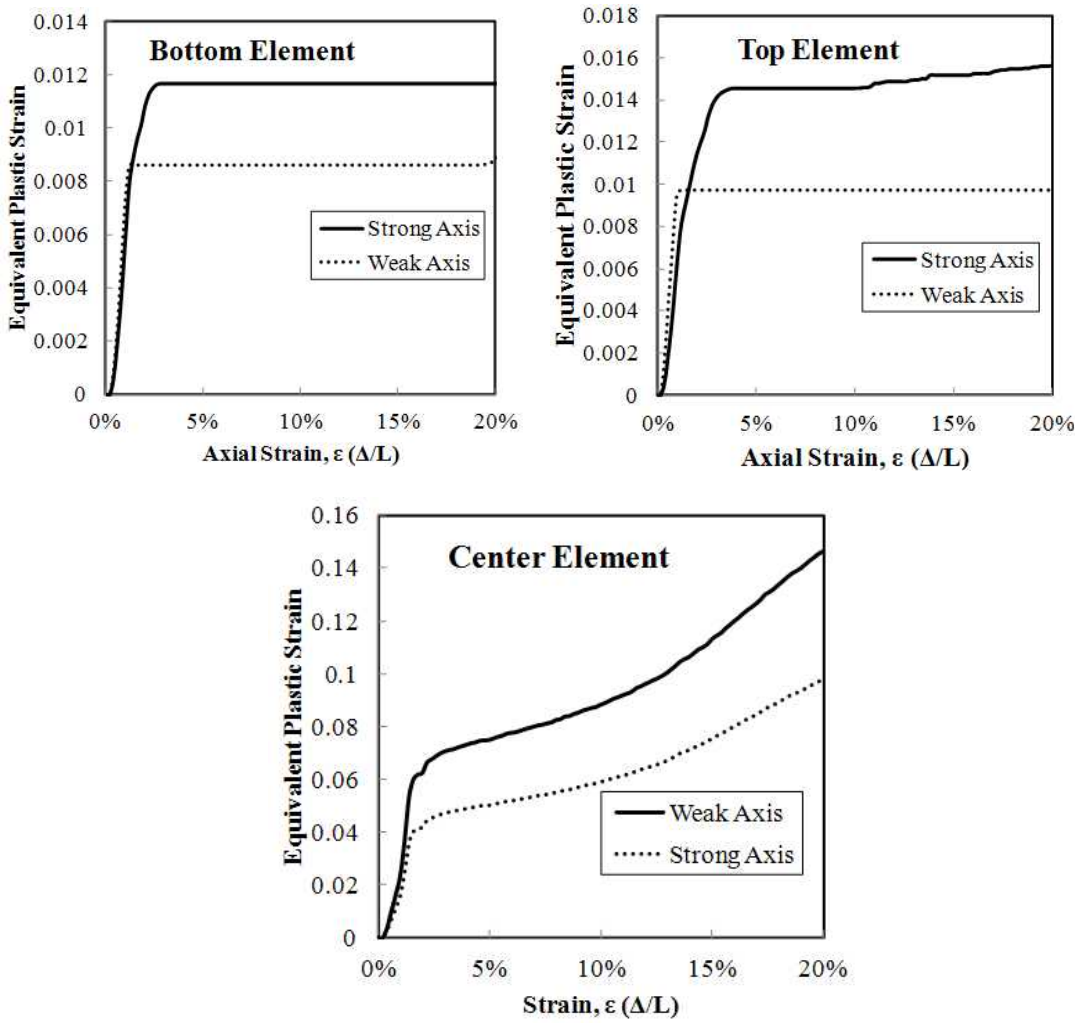

Fig. 2.9 Equivalent plastic strain for different element

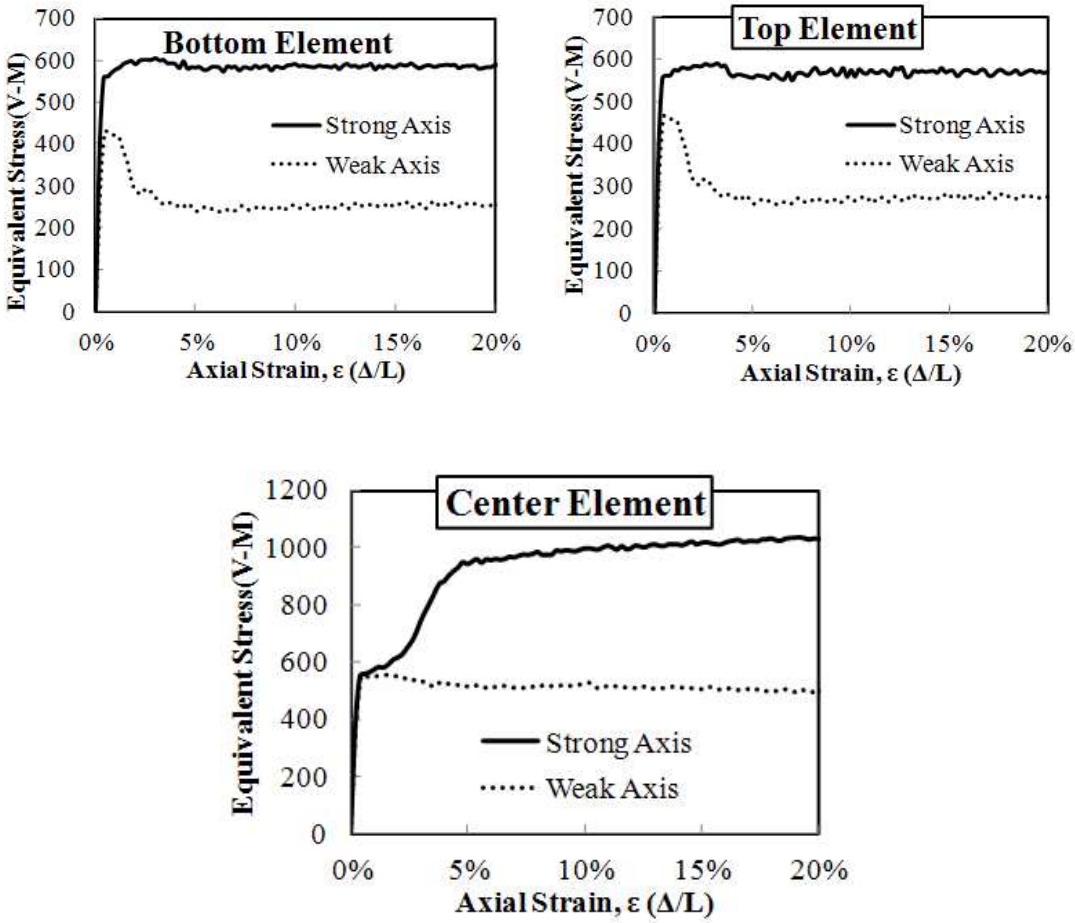

Fig. 2.10. Equivalent stress (von Mises's stress) for different element

2.4.3. Load-deformation Curve of Analysis Result

The relationship between vertical load and deformation at large deformation buckling analysis evaluated for pinned-pinned ended model result is presented in figure 10 and 11 for analysis and test result respectively. From fig. 10 of analysis result on strong and weak axis, the column member modeled on the strong axis have higher resisting capacity but in both cases after the load attains the

maximum point (critical point) the strength kept constant though for short period. For the test specimen the result shows unlike the analysis, after attains the critical load the strength declines automatically. When we compare the analysis and test result, except at the pick point all in the other the two results shows a great match especially in elastic range is quite match. In both cases for weak axis constraint specimen the strength declines rapidly after a critical point relative to strong axis constraint condition. After final collapse of the member the analysis and test result for both strong and weak axis the strength become equal. In general the inelastic buckling behavior and residual strength of column member evaluation carried out in this study was accurately evaluated as shown from the results.

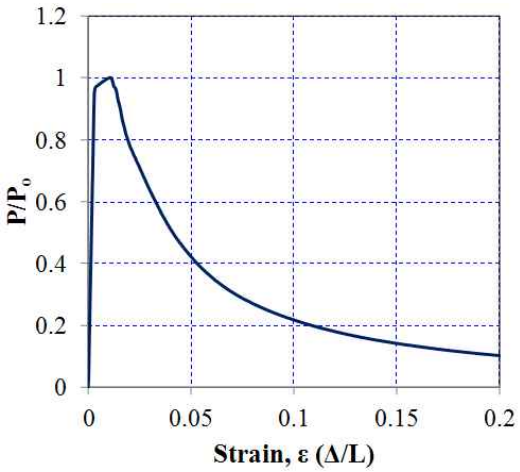

(a) load-deformation relationship for strong axis

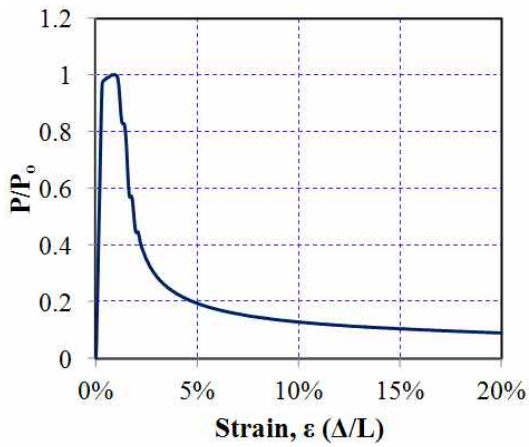

(b) load-deformation relationship for weak axis

Fig. 2.11 Load-deformation relationship of analysis result

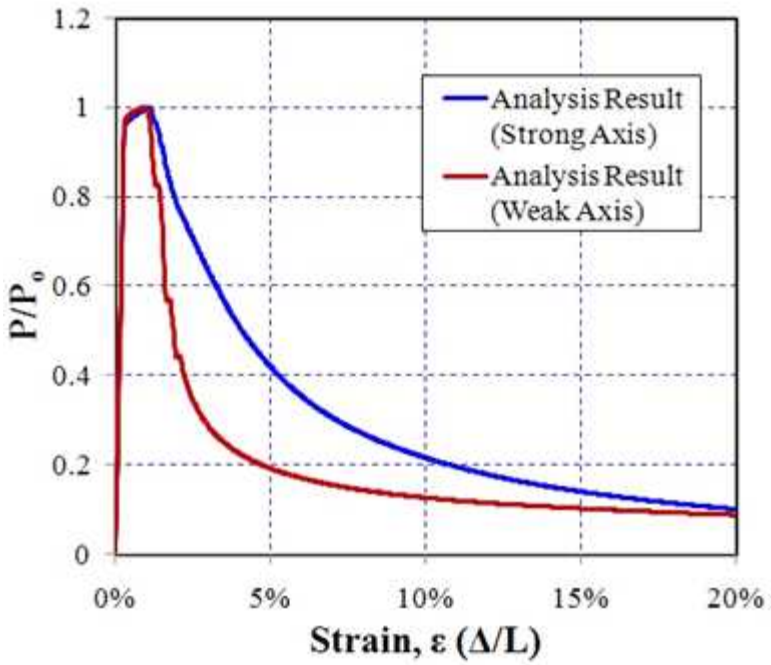

Fig. 2.12. Comparison of load-deformation relationship for strong and weak axis

2.5 Compression Test Process

The compression test on H-shaped steel column was carried out by Lee (2003) to review plastic deformation capacity and post-buckling strength in large-deformation range. The materials, configurations and conditions used in the experiment were the same as the material properties used in the analysis process. The column material was SS400 mild steel with cross sectional dimension of H-100x100x6x8. The test set up, loading condition and the overview of the specimen under consideration is shown in Fig. 6. As shown in the Figure, pin support condition was employed at both ends of the compression test on the column member.

(a)

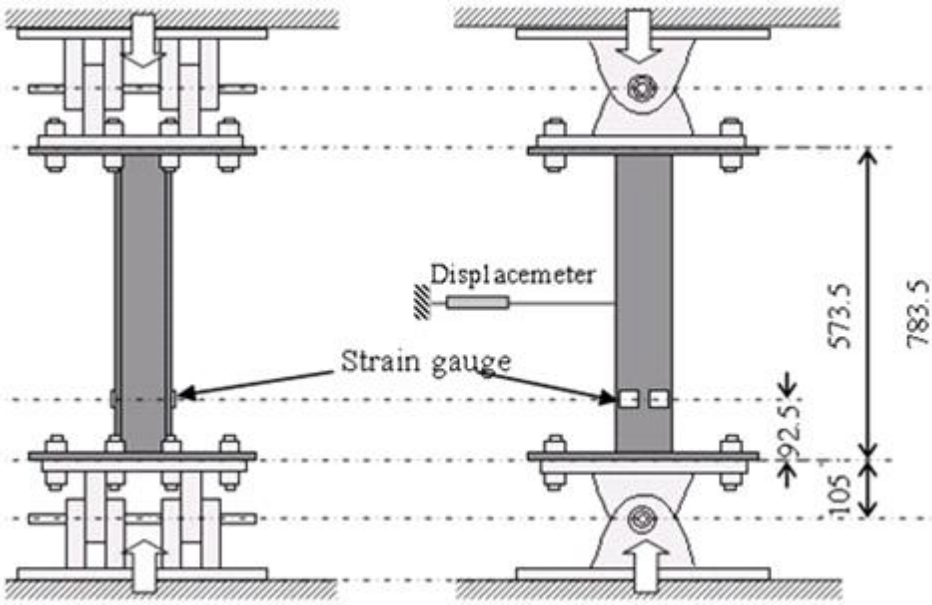

(b)

Fig. 2.13. (a) Test setup and (b) detail of specimen

2.6 Test Result

The compression test deformation result and the load-deformation relationship are shown in the figure below.

2.6.1. Failure Mode

The failure mode of test result is presented in the figure 7. The figure shows that the test specimen buckles around the central part and in addition before the specimen buckles globally, the flanges of the specimen buckles locally in both cases.

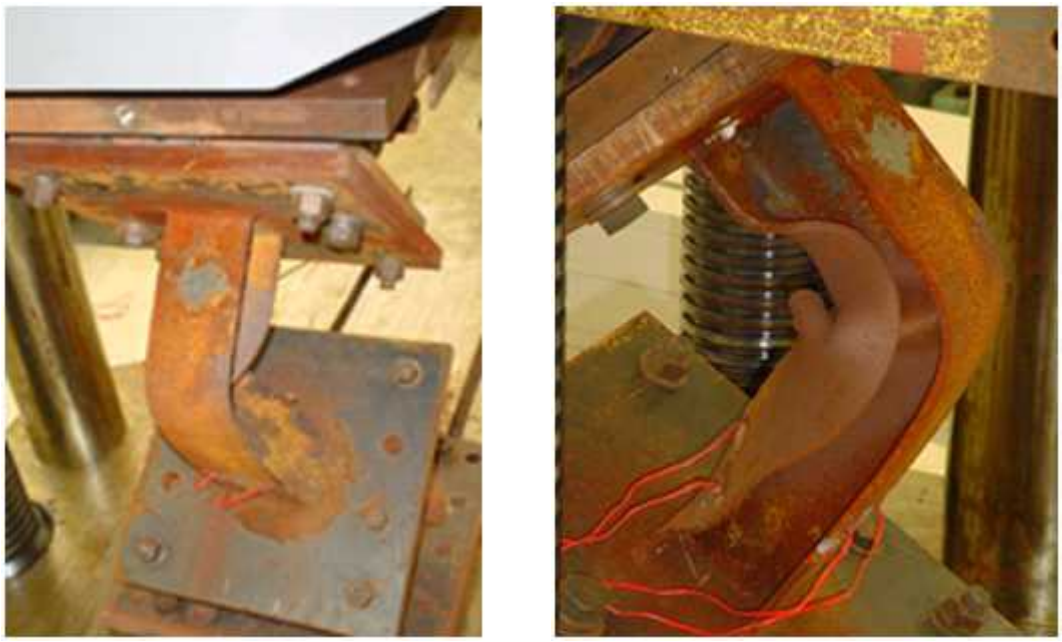

Fig. 2.14 Strong axis deformation shape of test specimen

Fig. 2.15. Weak axis deformation shape of test specimen

2.6.2. Load-deformation relationship

The load-deformation relationship of compression test result is presented on figure 8 below. In this case, the strength of the column member after attaining maximum load it declines rapidly for both strong and weak axis. But for weak axis the strength degradation is more rapidly compared with strong axis.

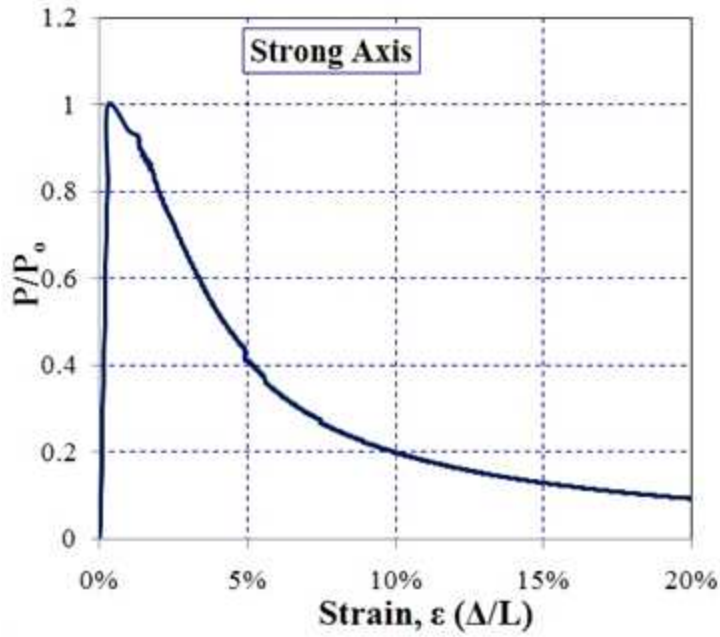

Fig. 2.16. Load-deformation curve of test result (Strong Axis)

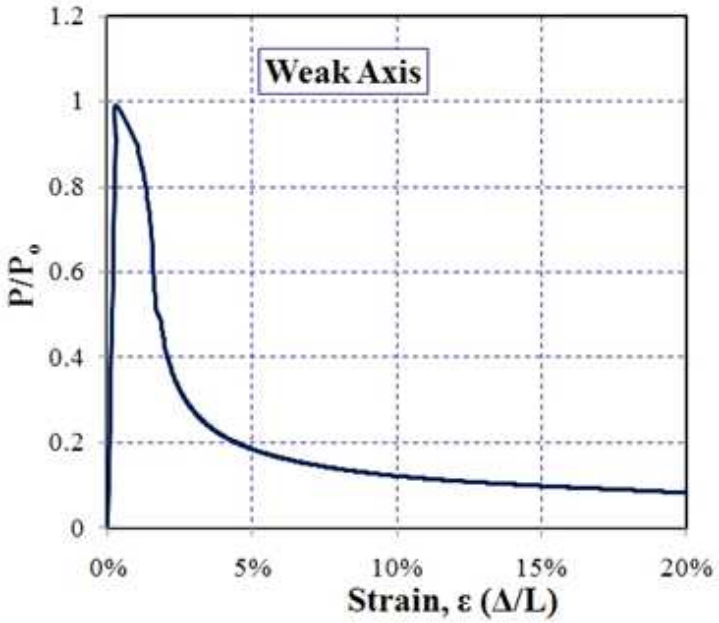

Fig. 2.17. Load-deformation curve of test result (Weak Axis)

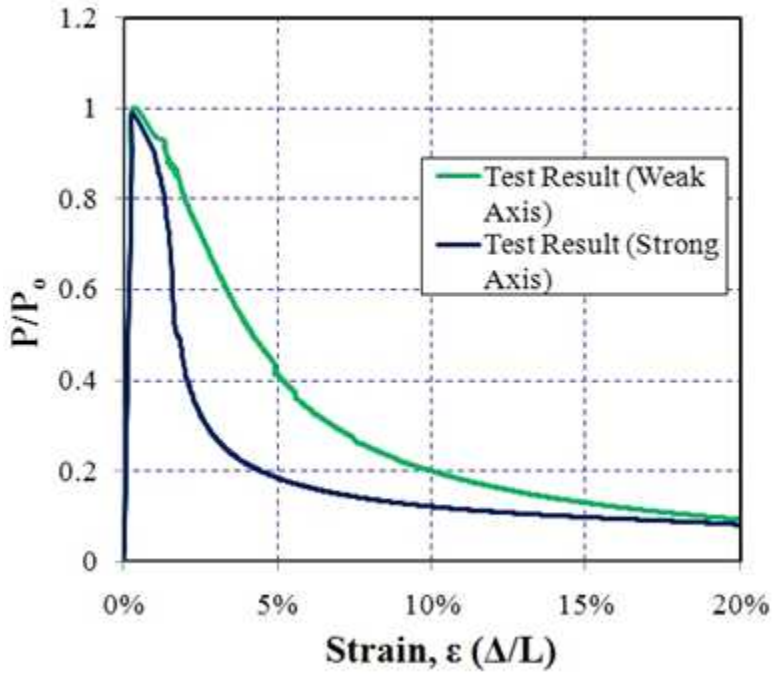

Fig.2.18. Comparison of Test results

2.7 Comparison of Analysis and Test Results

To demonstrate the applicability of the methods described above for predicting the postbuckling and failure behavior or deformation shape of H-shape column, analysis results of an exemplary models are presented and compared to experiment results. In addition, the comparison of numerical, analysis and experiment graphical results are discussed.

2.7.1 Deformation Mode

The inelastic buckling mode of analysis and test result was compared for both strong and weak axis constraint condition. In both case, local buckling of flange at

the central part is observed.

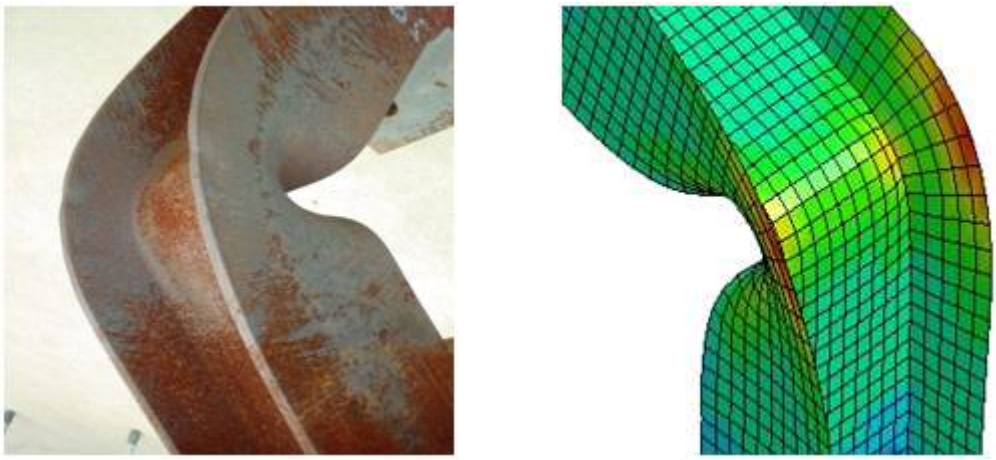

Fig.2.19. Comparison of deformed shape of test and analysis result on weak axis

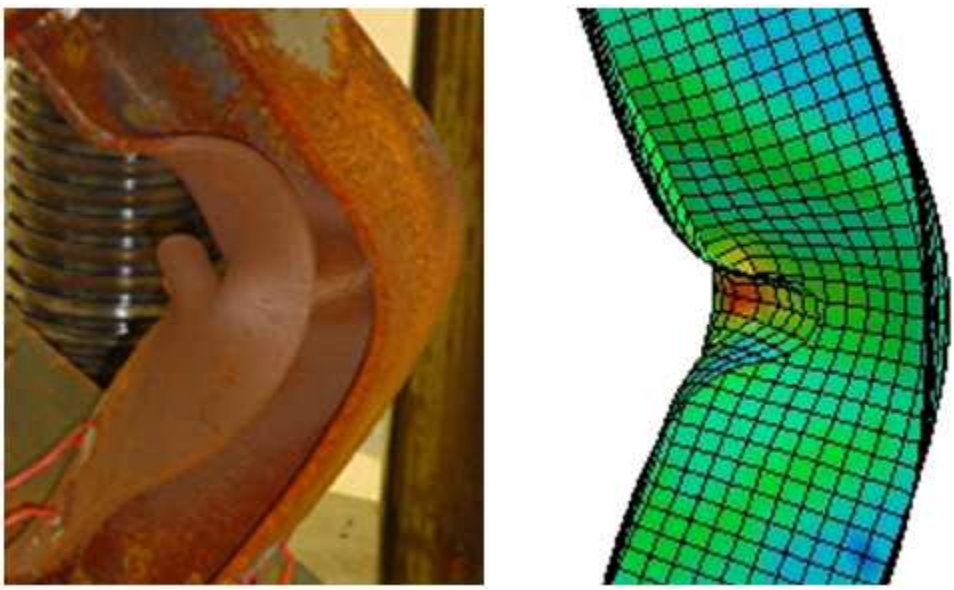

Fig. 2.20. Comparison of deformed shape of test and analysis result on strong axis

2.7.2 Load-deformation

Figure 2.20 and 2.21 presents the load-deformation relationship of analysis and test result. In both cases, for weak and strong axis constraint condition, the deformation in the elastic range is quite match and of course after attaining the maximum resisting capacity, inelastic range or post buckling part, also the matching is good. However, at the pick point there is some difference that the analysis result kept constant for short period whereas in the test result the strength degrades rapidly after attaining the maximum load.

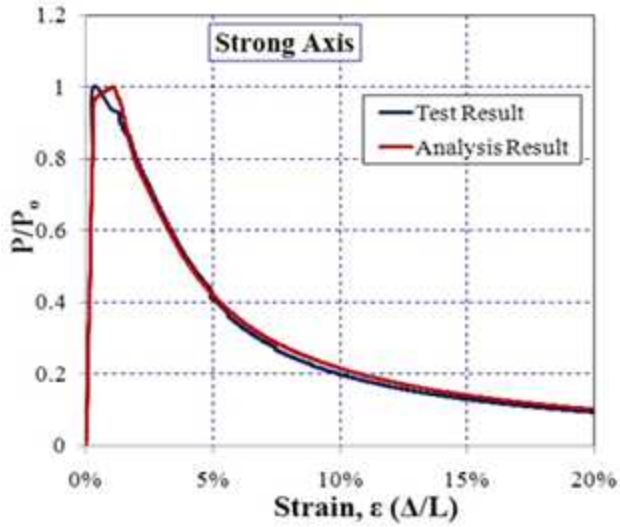

Fig. 2.21. Comparison of load-deformation curve for strong axis

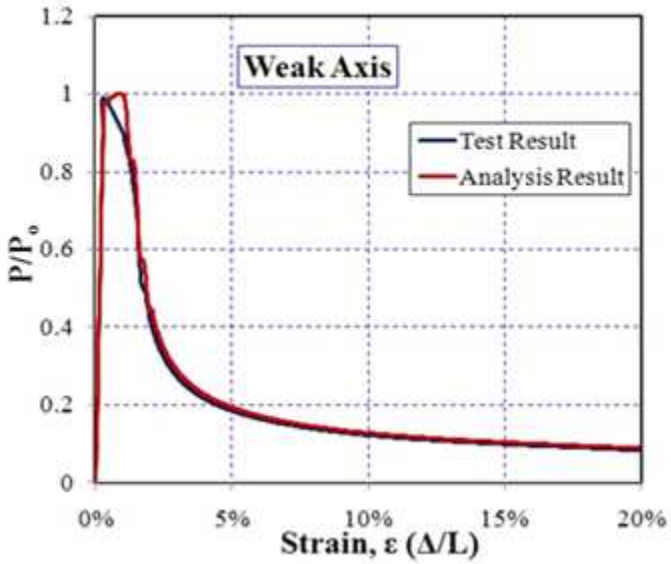

Fig. 2.22. Comparison of load-deformation result for weak axis

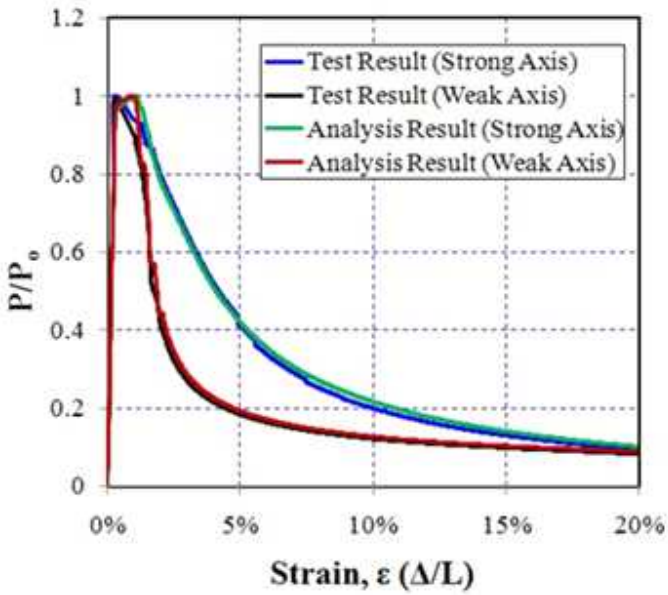

Fig. 2.23. Comparison of test and analysis results

2.7.3 Energy Absorption

The energy absorption capacity of the column member computed from the area under fig. 12 and presented in fig. 13. The analysis and test results of cumulative energy absorption capacity compared. The energy absorption capacity of column member on strong axis for both test and analysis result higher than on the weak axis. In comparison to same axis for the two approaches, analysis result shows little bit higher value but the difference is not significant. In the weak axis the slight difference starts early and continues parallel up to the end. Unlike weak axis, strong axis the difference starts lately compared with weak axis. Generally, the analysis carried out in this study can clearly and precisely determine the inelastic buckling behavior of steel column with an H-shape.

Effect of flange and web total energy called part total energy is also evaluated from FE analysis result. Fig. 14 presents the part total energy curve. From the graph, the total part energy of flanges is higher than the total part energy of web. The effect will be more significant in the case of weak axis constraint condition. The most important point to be noted here is that, the sum of the total part energy of flange and web is almost equal to the cumulative energy absorption capacity presented under fig. 13.

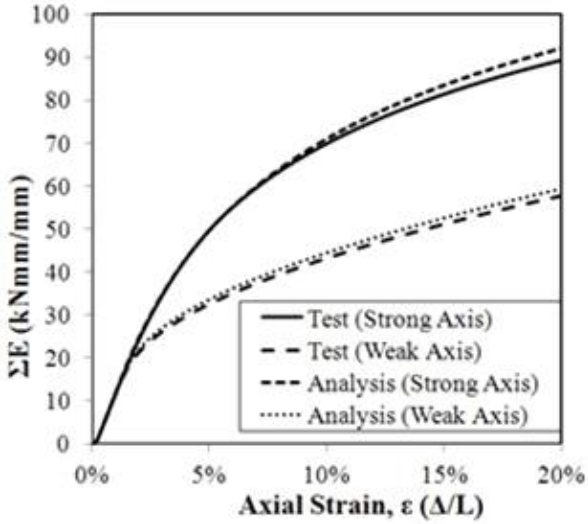

Fig. 24. Comparison of cumulative Energy absorption Capacity

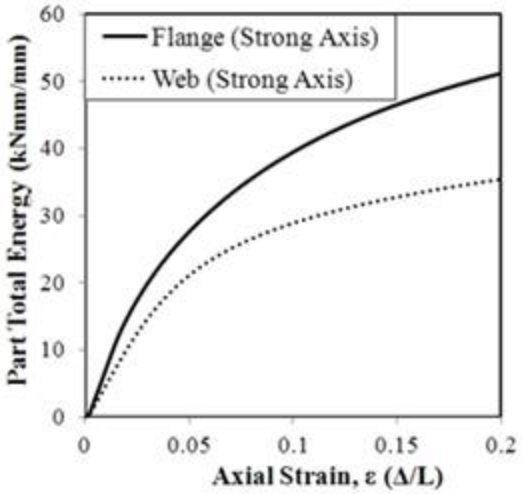

Fig. 2.25 Part total energy for strong axis

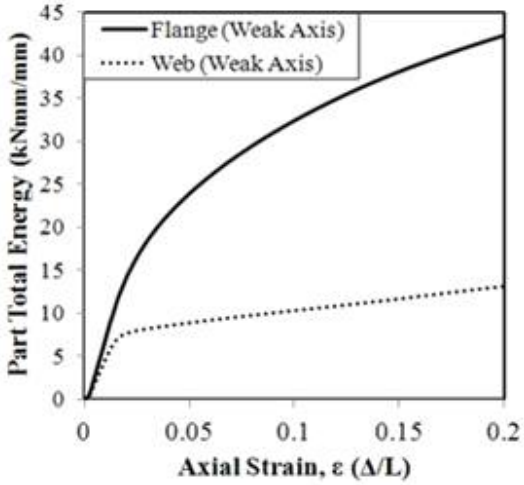

Fig. 2.26. Part total energy for weak axis

2.8 Summary

The inelastic buckling behavior and residual strength of H-shaped steel column member when axial compression loading have been studied comprehensively by FE analysis followed by experiment and the following conclusion have been drawn.

A nonlinear FE model conducted to investigate the inelastic buckling behavior of steel column validated using measured data and observed damage state from the experiment. The deformation mode observed from the test for both strong and weak axis constraint condition is the same as the result obtained from analysis. In addition, from the result of load-displacement relationship, it is noted that the analysis model was capable of accurately simulate the inelastic buckling behaviorof steel column member.

Furthermore, the energy absorption capacity of the test specimen and analysis model has also been compared and a great match is found with an overall error less than 5%. The part total energy of the analysis specimen (flange and web) was evaluated. The sum of the total part energy (of flange and web) is almost equal to the cumulative energy calculated from the load-deformation curve.

CHAPTER 3 INELASTIC BUCKLING EVALUATION OF H-SHAPE FIXED-FIXED STEEL COLUMN MEMBER

3.1. Theoretical Investigation of Buckling Behavior

In this case there are no more researchers that investigate this issue in detail as it is difficult to differentiate on which axis does the member buckles. Fig. 3.1 shows the conceptual model of the theoretical buckling of column members under compression load. The model describes both end fixed column, constraint rotation in all direction at both ends and only allows translation in the vertical direction by constraining in other direction as shown in the fig. As the compression force increases, three plastic hinges for both end fixed column member as shown in figure 3.1(b) is formed. The maximum force at which the column member starts to buckle is the critical force (P_{cr}) for elastic buckling. From the condition of moment equilibrium of the half-column as a free body Fig.1c, the axial load and from the buckling geometry, the displacement due to axial load is given by:

$$P = \frac{4M_p}{Lsin\theta} \tag{3.1}$$

$$\Delta = \frac{L}{2}(1-\cos\theta) \tag{3.2}$$

From buckling geometry (using trigonometric theory):

$$\sin\theta = \frac{2\sqrt{L\Delta - \Delta^2}}{L} \tag{3.3}$$

and substituting for axial force to eliminate Θ, the post-buckling behavior can be approximated by:

$$P = \frac{2M_p}{L\sqrt{\frac{1}{4} - \left[\frac{1}{2} - (\Delta/L)^2\right]}} \tag{3.4}$$

where is the plastic moment of the column section (which depends on section shapes and material properties), Δ is displacement due to axial compression force and Θ is the plastic rotation. From equation 1 the displacement Δ is:

$$\Delta = \frac{L - \sqrt{L^2 - (4M_p/P)^2}}{2} \tag{3.5}$$

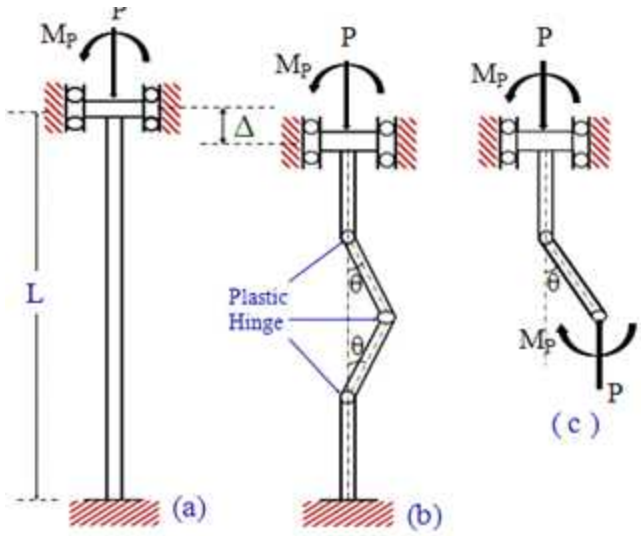

Fig. 3.1 (a), General layout (b), Bazant's plastic buckling mechanism model, (c) Free body diagram

By considering the material property and sectional property of the specimen; the plastic moment of the section is given by and , and finally the plastic moment becomes:

$$M_p = \frac{Z_p \bullet P_y}{A} \tag{3.6}$$

So equation 3.5 becomes:

$$\frac{\Delta}{L} = \frac{1}{2} - \sqrt{\frac{1}{4} - (2Z_p/LA)^2 * \left(\frac{1}{P/P_y}\right)^2} \tag{3.7}$$

where Z_p is the section modulus at plastic state, A-cross sectional area and P_y is the force at yield state. The general load-deformation curve of equation 2is shown in fig.3.

3.2 Finite Element Analysis Model

3.2.1 Material Modeling

The analysis model under consideration has components consisting of H-shaped a common mild SS400 steel specimen with cross sectional dimension of H-100x100x6x8 and upper and lower rigid bodies. Explicit non-linear analysis using LS-Dyna of version 12.0 was carried out with reasonable accuracy. The analysis material is modeled as a shell element and the following two conditions are considered. First, we consider large deformation kinematics to simulate the residual displacement. Of course, without large deformation kinematics, the deformation behavior cannot be predicted in the analysis model. Second, the nonlinear, inelastic plastic kinematic material behavior is considered.

Generally there are different hardening rules; isotropic, kinematic or the combination of isotropic and kinematic hardening rules as explained in chapter 2.

Isotropic and kinematic contribution may be varies by adjusting the hardening parameter β between 0 (kinematic hardening) and 1 (isotropic Hardening). In this case the kinematic hardening model was used. The detail of the kinematic hardening model is shown in figure 3.2 below.

The buckling and postbuckling behaviors depend on the material and section property of the member. The mechanical property used in the analysis and the sectional property is indicated in Table 3.1 and 3.2 respectively. For comparison purpose the effect of slenderness ratio is considered for different ratios as shown in table 3.2.

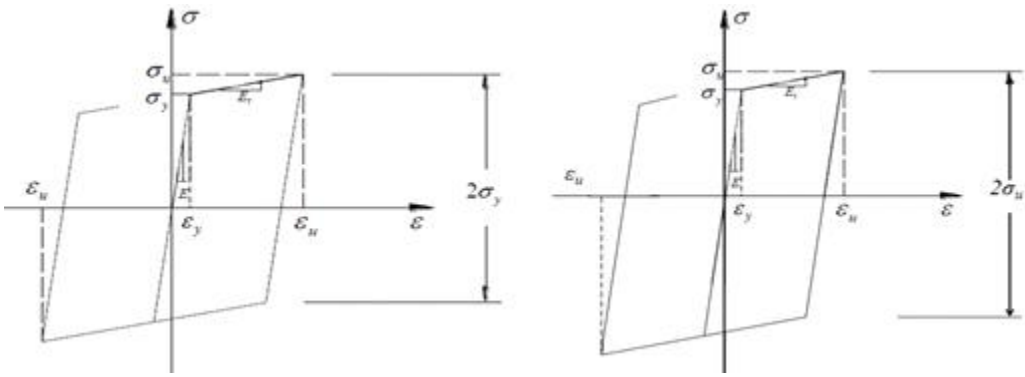

Fig. 3.2 Kinematic and Isotropic Hardening Model

Table 3.1 The property of material used in the analysis

Property	Specimen	Upper and Lower Rigid body
Young's Modulus (GPa)	205	205
Poison's ratio	0.3	0.3
Density (kg/m^3)	7860	7700
Yield Strength (MPa)	345	
Tangent Modulus (MPa)	756	
Hardening Parameter	0.0	
Strain rate [C] (s^{-1})	40	
Strain rate [P]	5.0	
Failure Strain	0.75	

Table 3.2 Sectional property of specimen, different cases considered

Section Property		Type	Slenderness ratio	
Area	2190mm^2	Type I	λ_x	6
Radius of Gyration (r_x)	41.8mm		λ_y	10
Radius of Gyration (r_y)	24.7mm	Type II	λ_x	12
			λ_y	20
Moment of area I_x(mm^4)	3.83x10^6	Type III	λ_x	24
			λ_y	40
Moment of area I_y(mm^4)	1.34x10^6	Type IV	λ_x	48
			λ_y	80

Given the cross-sectional properties of the specimen the length of each specimen is calculated from the relationship of:

$$L = \kappa * \lambda \tag{3.8}$$

where k: radius of gyration and given by:

$$K = \sqrt{\frac{I}{A}} \tag{3.9}$$

So that the length of each Type of specimen will be 250mm, 500mm, 750mm and 1000mm respectively.

3.2.2 Constraint and Loading Condition

The constrained condition modeled to have an axial compression, the lower rigid body is fixed in all direction, and both translation and rotation is constrained. As shown in figure 4, the upper rigid body is modeled to have translation only in Y axis and constrained in the X and Z-axis and constrained rotation in all directions. A linear incremental load is applied in the vertical direction (in the Y-axis) on the upper rigid body. There are basically two ways of applying load: the constant

stress loading and the constant strain loading. In the constant stress loading, a uniform load is prescribed while not constraining the displacements i.e. to the maximum displacement. On the other hand, the constant strain loading requires the member to be constrained to have the same prescribed displacement. Here it is used constant strain loading by setting maximum allowable strain. Vertical load is applied with respect to time to have the maximum strain set.

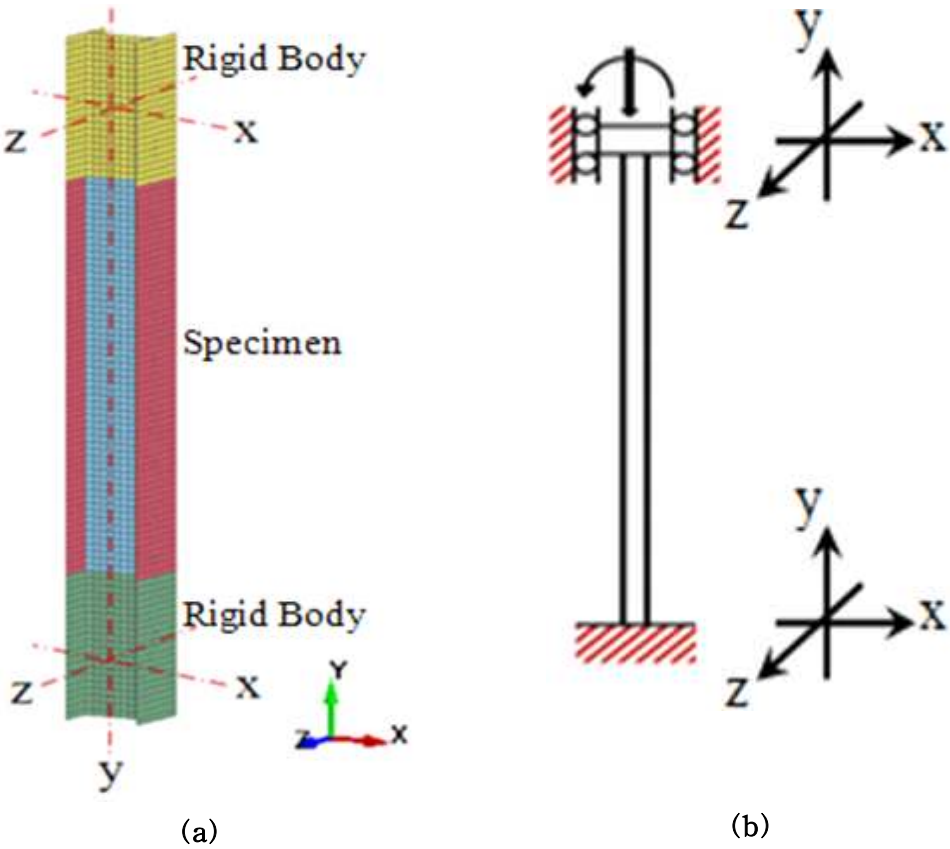

Fig. 3.3 (a) Analysis model, (b) Loading and constraint condition

3.3. Result and Discussion

The failure mode and load-displacement is shown in figure 3.4 and 3.5 respectively. Plastic deformation of in the column member is causes when the stress is sufficient to permanently change its shape in a way that is not reversible. It is indicated in the fig. 3.4 for deformation at strain level of less than the yielding point; the stress will cause elastic deformation, so that its original shape will be back if the stress is removed in another word the strain will be recoverable.

3.3.1 Failure Mode

In a vast majority of situations, failure occurs by buckling after a portion of the cross-section has yielded. The deformation or failure mode of the specimen is shown in fig. 3.4 below. As shown in the figure, the column member buckles at the center and at both ends. In addition, local buckling of flanges also observed around the places. The deformation shape of analysis result is the same as the Bazant's theoretical plastic deformation shown in figure 3.1 above. Before the column member buckles totally, the flange of the member buckles locally around the center after reaching the critical force. But In common applications local buckling cannot be significantly restricted because it occurs for short periods. It is followed by the global buckling of the member. And it is noticed that for all considered cases the failure mode is the same. Generally buckling in the both end fixed column member was occurred around these indicated portions (as shown in figure 3.4(a)).

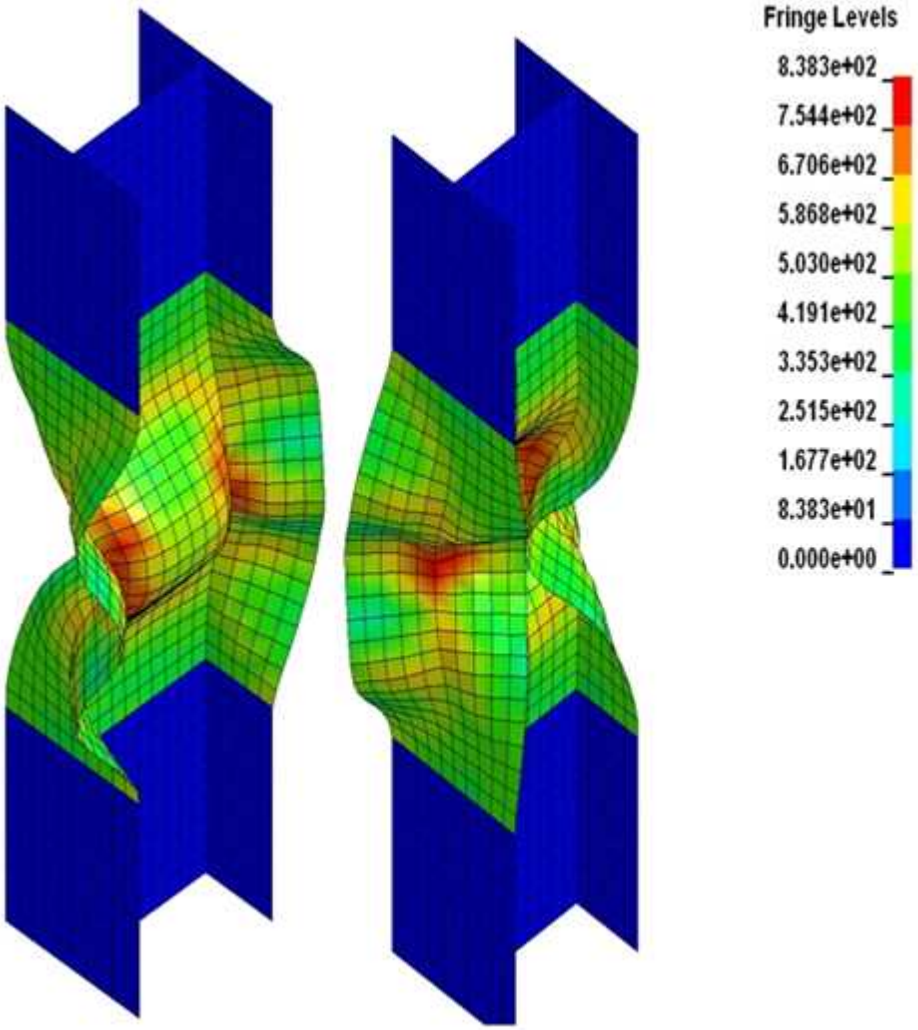

(a) The buckling mode of analysis result for Type I Specimen

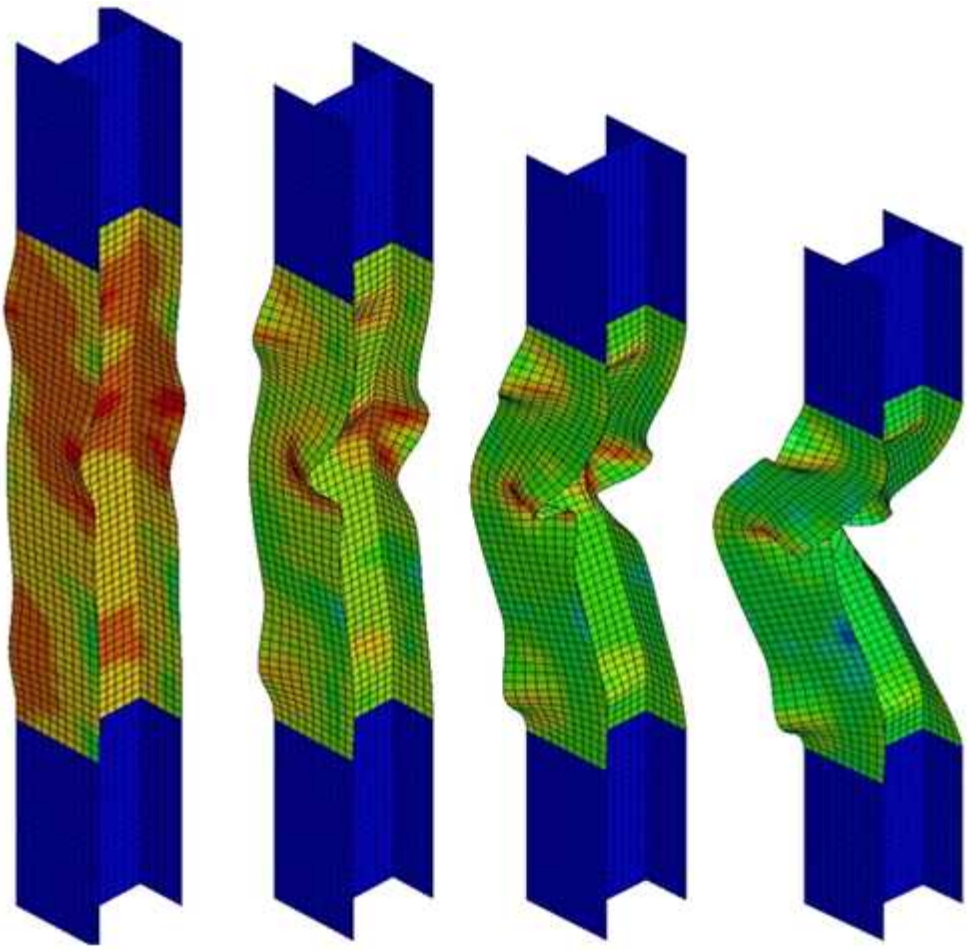

5% strain 10% strain 15% strain 20% strain

(b) The buckling mode of analysis result for Type II Specimen

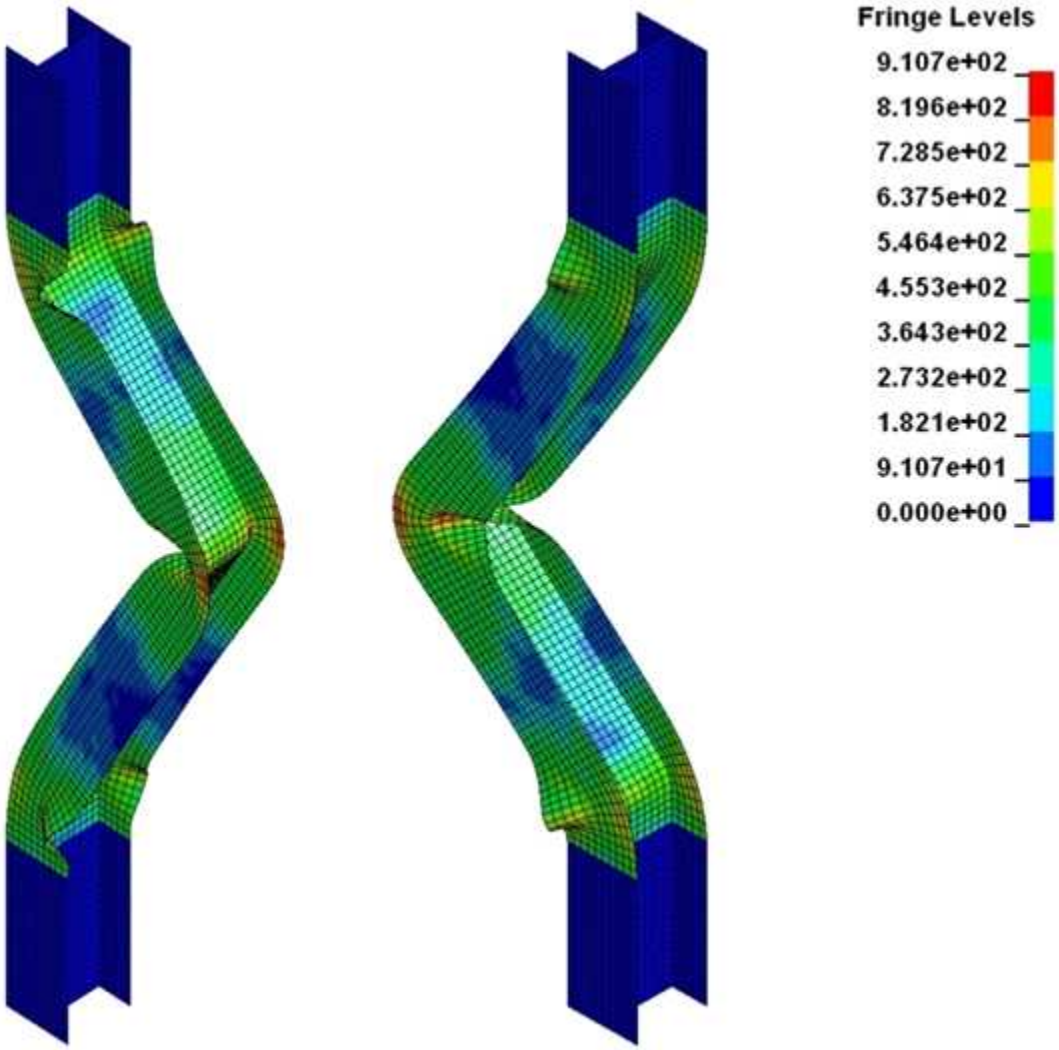

(c) The buckling mode of analysis result for Type III Specimen

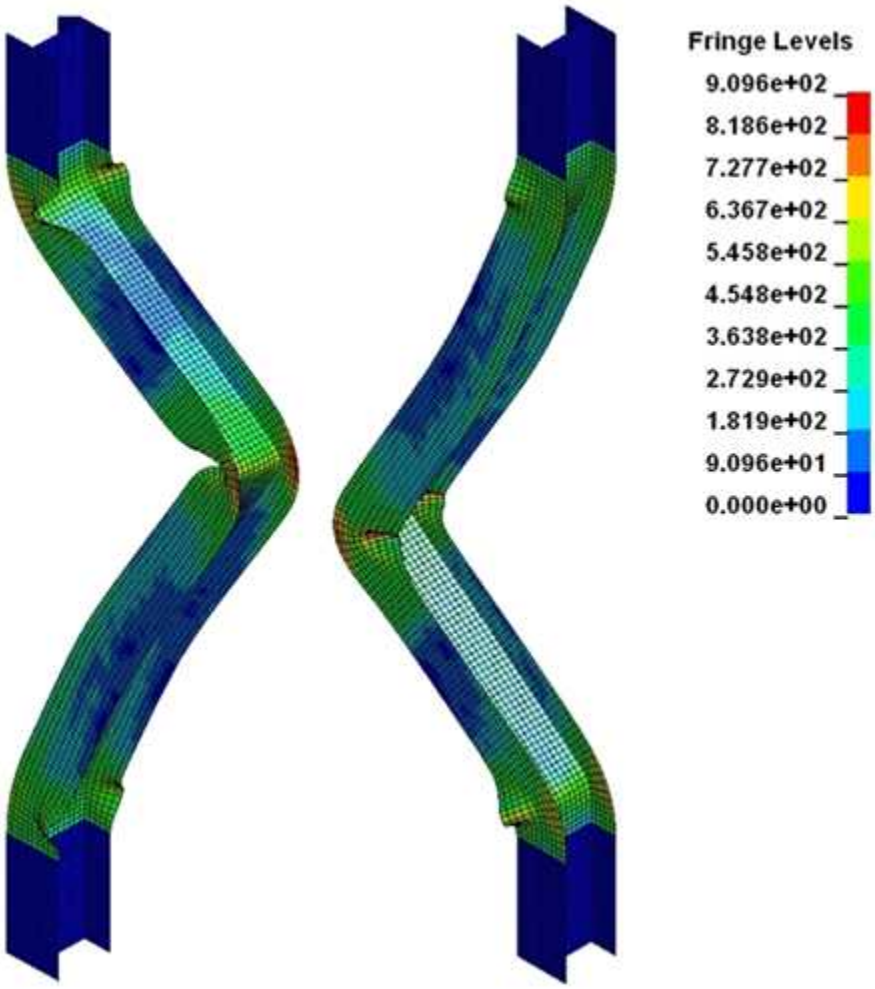

(d) The buckling mode of analysis result for Type IV Specimen

Fig. 3.4. The buckling mode of analysis result

3.3.2 Equivalent Plastic Strain

The load-displacement analyses result in the figure 3.5. For all cases the strength kept constant after reaches the critical load and then degrades after some period though the period is different. Short column (Type I) the strength kept

maximum for longer period compared to other cases as the strength kept constant up to strain about 4%. If we consider for the strain of 4%, the resisting values are: 0.2353, 0.3883, 0.7204 and 0.9460 for Type I to IV respectively. On the other hand, for the force ratio (P/P_o=0.4),the strain values are:16.68%, 8.42%, 3.89% and 2.83% for Type I-IV specimen respectively.

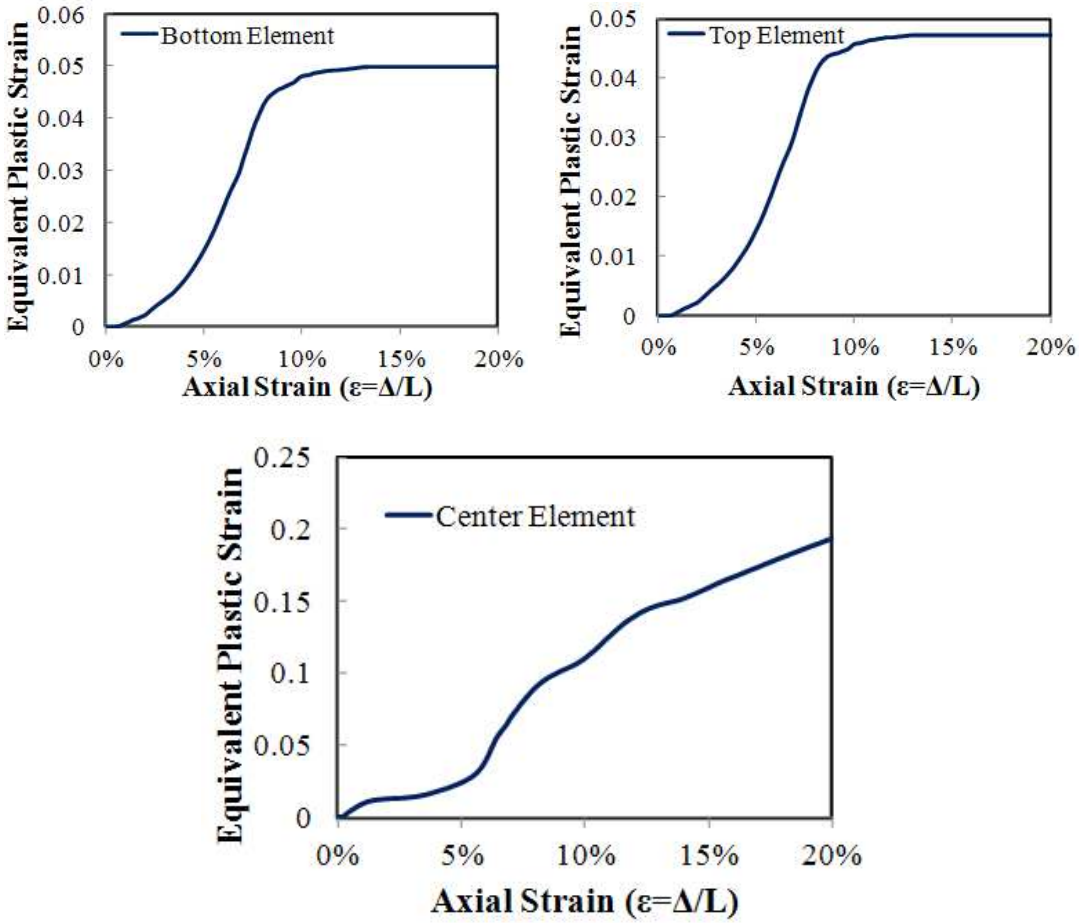

Fig. 3.5 Effective plastic strain of element for Type I

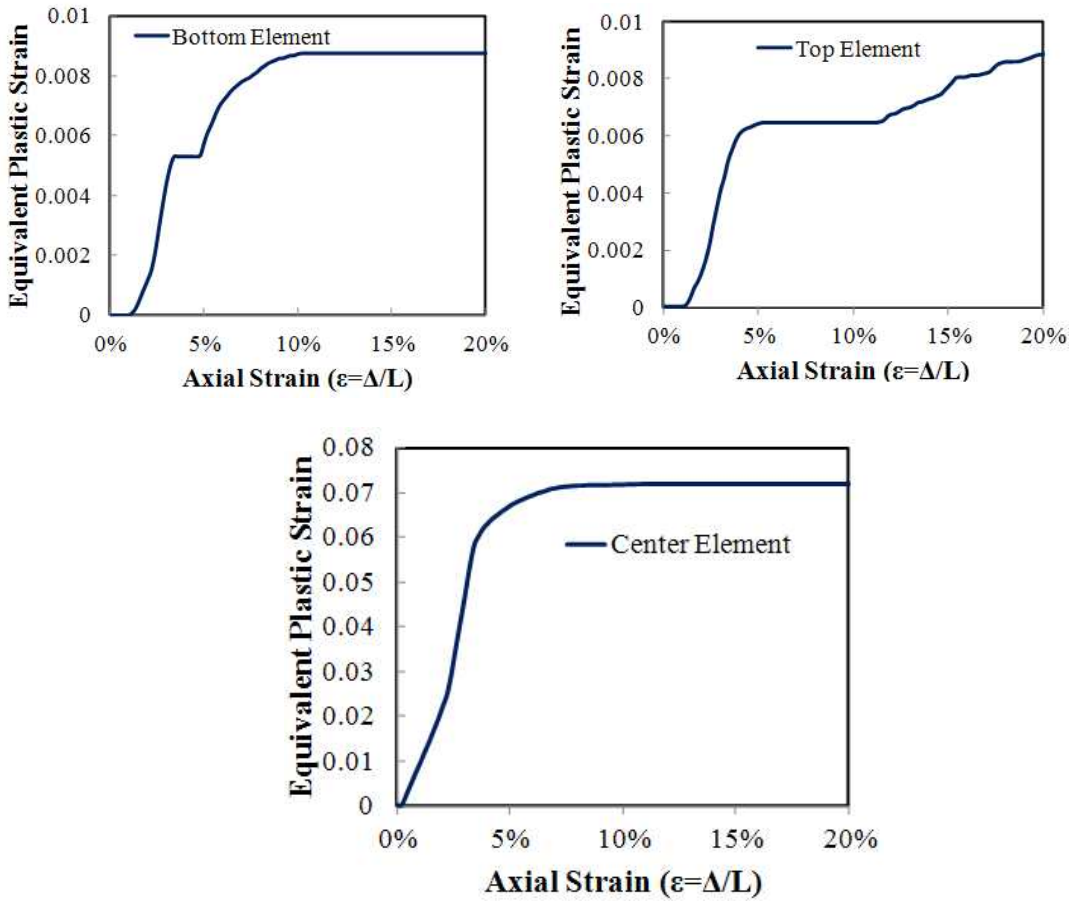

Fig. 3.6 Effective plastic strain of element for Type II

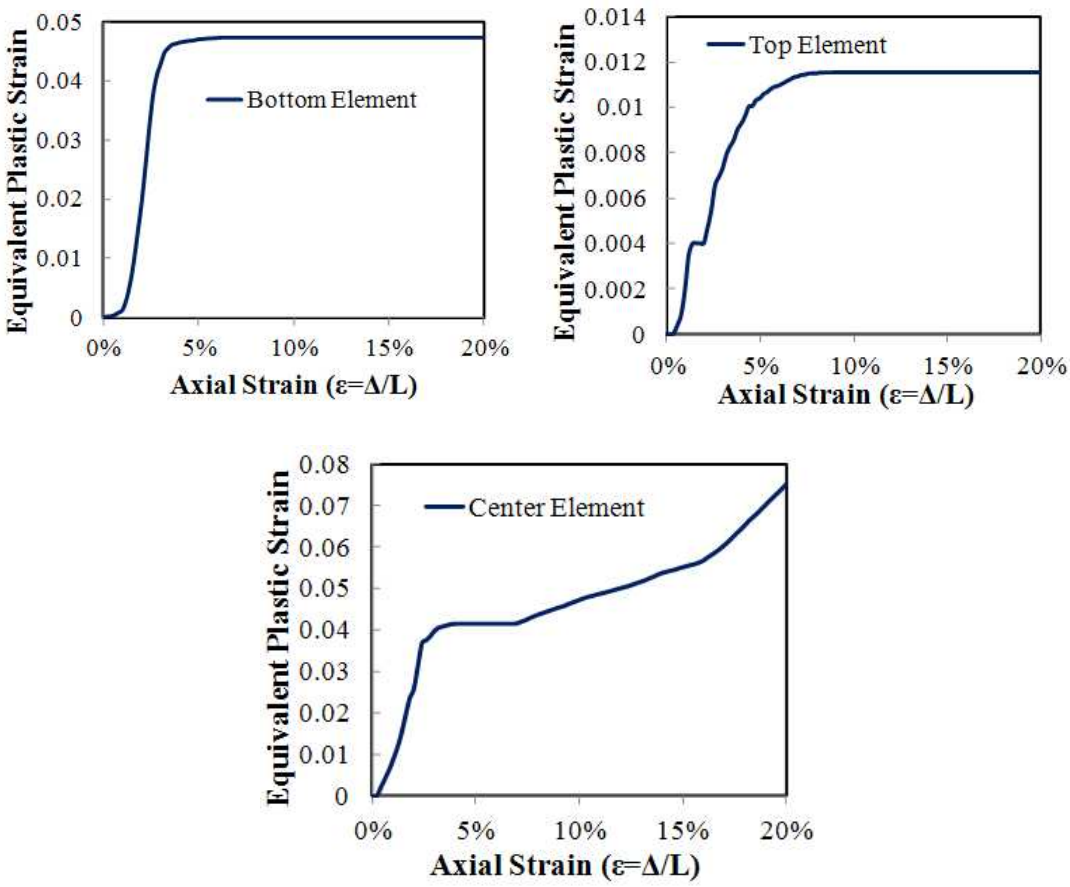

Fig. 3.7 Effective plastic strain of element for Type III

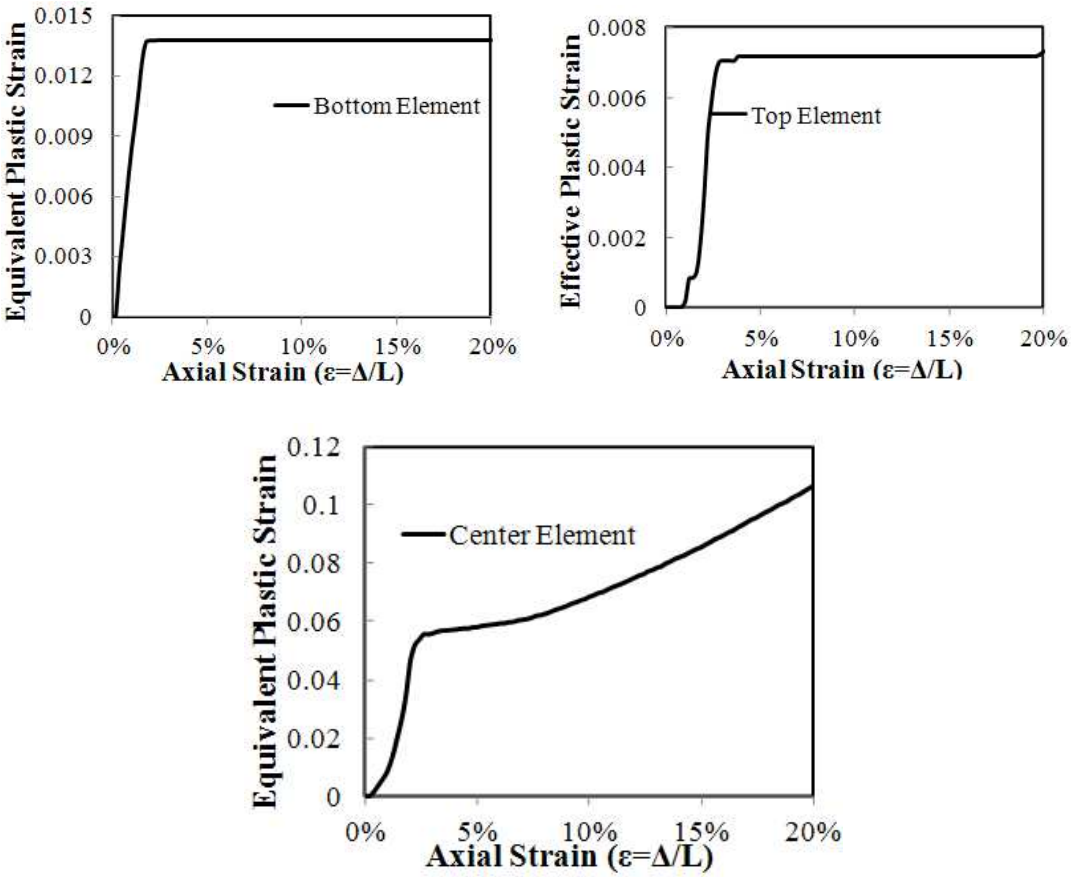

Fig. 3.8 Effective plastic strain of element for Type IV

3.3.3 Load-displacement and Energy absorption Curve result

The load-displacement analyses result in the figure 3.5. For all cases the strength kept constant after reaches the critical load and then degrades after some period though the period is different. Short column (Type I) the strength kept maximum for longer period compared to other cases as the strength kept constant up to strain about 4%. If we consider for the strain of 4%, the resisting values

are: 0.2353, 0.3883, 0.7204 and 0.9460 for Type I to IV respectively. On the other hand, for the force ratio (P/P_o=0.4),the strain values are:16.68%, 8.42%, 3.89% and .83% for TypeI to IV respectively. The energy absorption capacity (the area under load-deformation curve) of slender column is less than short column. As the slenderness ratio increase, the energy absorption capacity of the member is decreases. The strength degradation for Type III and VI is rapidly compared to other cases. But short column exhibits slight strength degradation. Energy absorption capacity (the area under load-deformation curve) of column member is highly dependent on slenderness ratio, fig. 3.6. The initial or at the elastic state the energy absorption capacity of the member is the same for all slenderness rations. However in the inelastic state the absorption capacity is quite different. As shown in the figure, short column has more energy absorption capacity. When the slenderness ratio doubled, the overall energy absorption capacity or the resisting capacity of column member will decrease about twice.

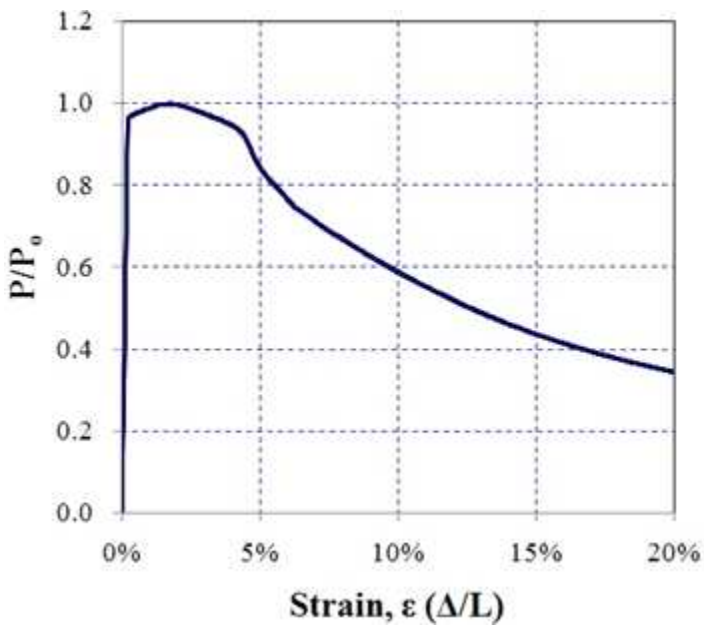

Fig. 3.9 Load-displacement relationship analysis result for Type I

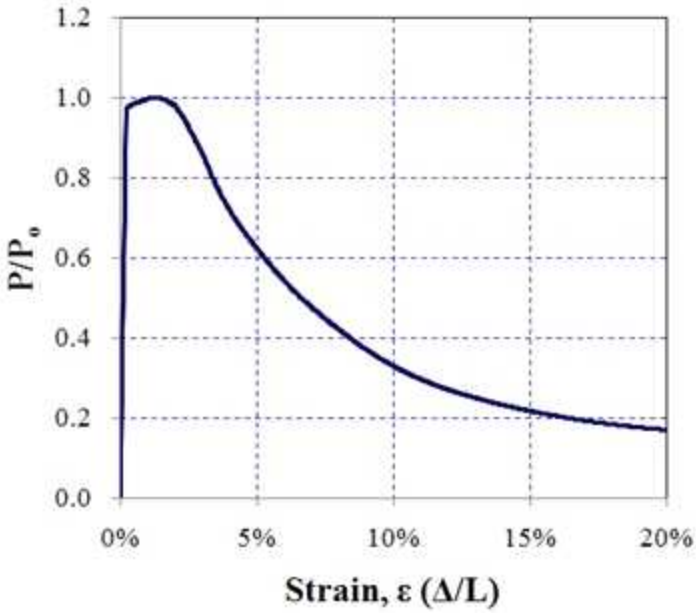

Fig. 3.10 Load-displacement relationship analysis result for Type II

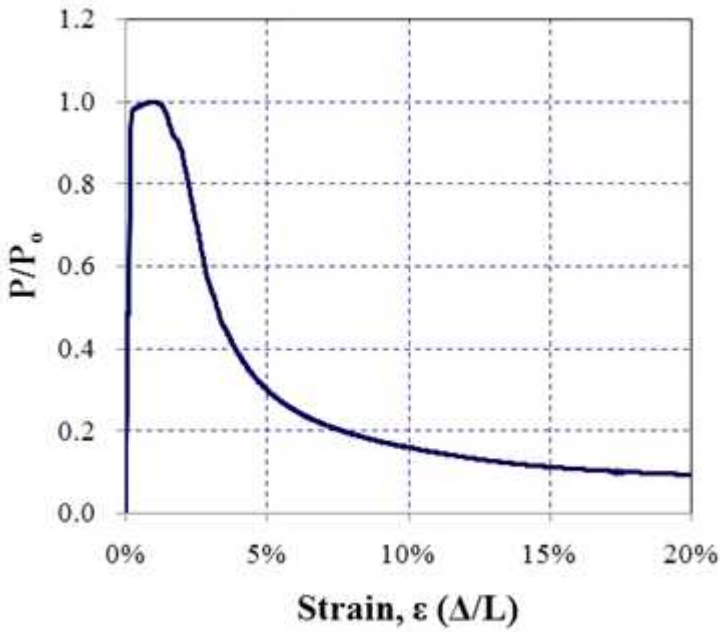

Fig. 3.11 Load-displacement relationship analysis result for Type III

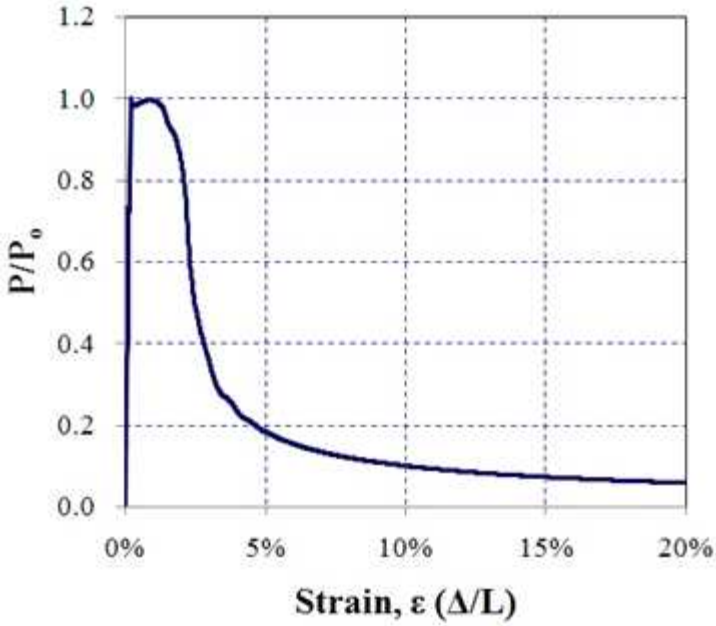

Fig. 3.12 Load-displacement relationship analysis result for Type IV

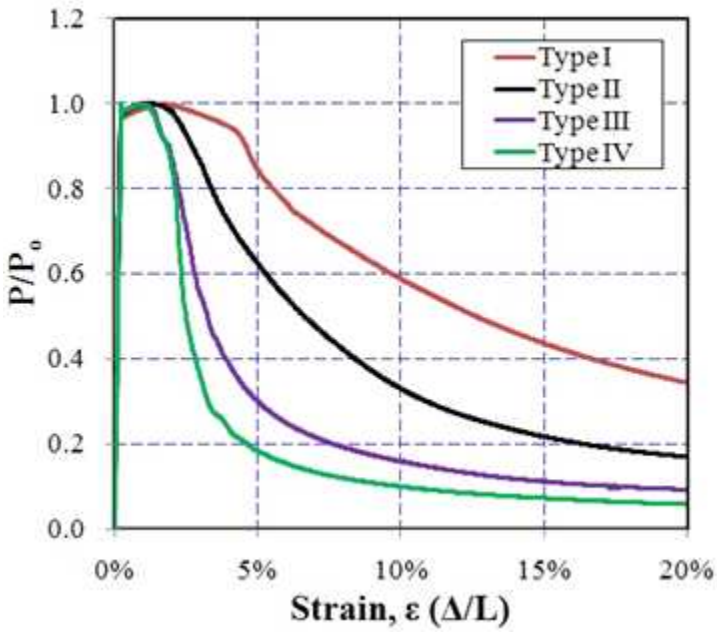

Fig. 3.13 comparison of load-deformation curve

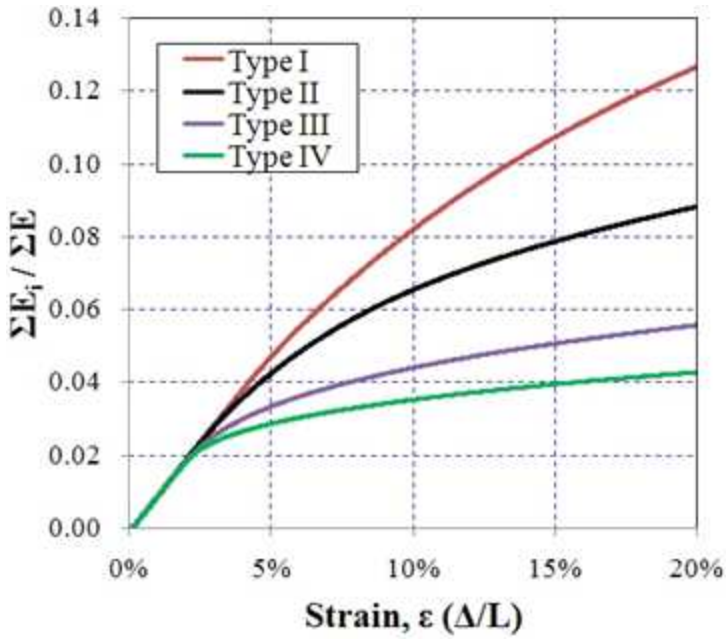

Fig. 3.14 Comparison of cumulative energy absorption of analysis result

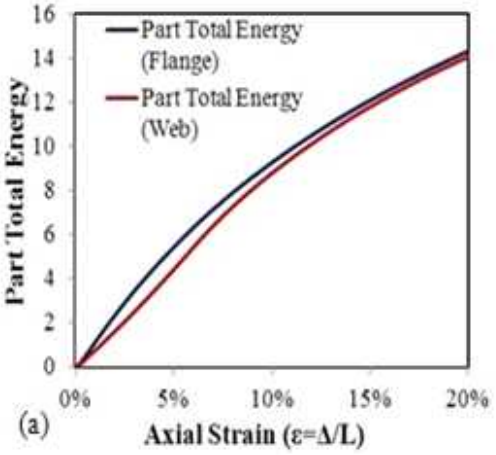

Type I

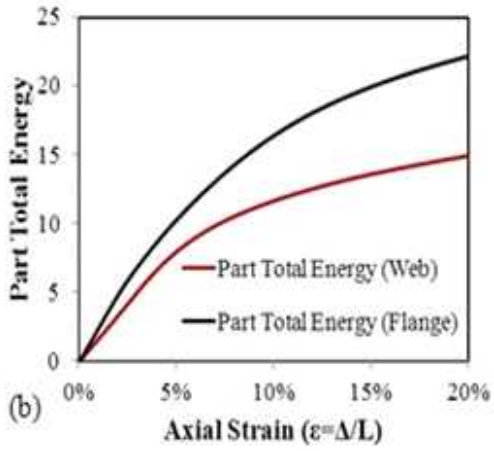

Type II

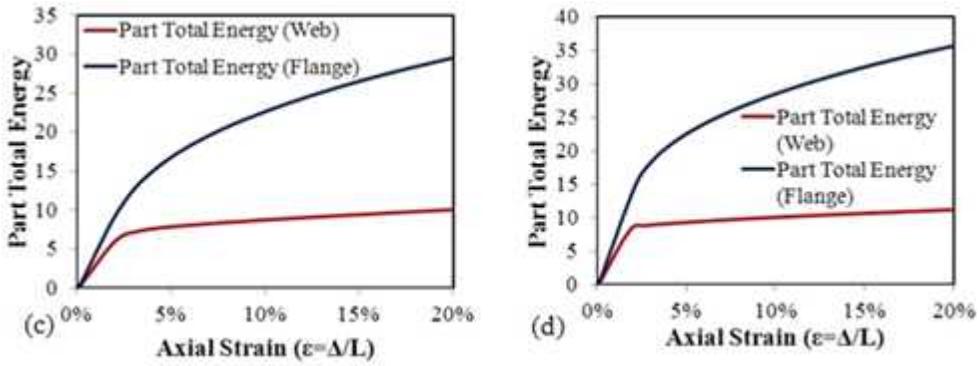

Type III Type IV

Fig. 3.15 Comparison of Part total energy of analysis result

3.4 Summary

The plastic deformation behavior and residual strength when vertical loads were applied to H-shaped SS400 steel columns of both end fixed condition has been studied and have the following main conclusion.

The failure mode of column member under axial compression load in analysis result shows that buckling at the central part and at both ends. In addition local buckling of flange is also observed. However, it is difficult to assume the buckling axis in both end fixed column model.

The strength kept constant after reaching the critical load and the strength decreases slightly for short column but for slender column the strength degrades rapidly as shown in the result load-deformation curves.

The energy absorption capacity decreases with an increase in slenderness ratio. An increase in slenderness ratio in twice will decrease the energy absorption capacity about in half.

The theoretical plastic buckling, considers only in plane buckling where as the analysis result shows both in plane and out of plane buckling, is applicable only for slender column in load-deformation curve though it is not fit able for both elastic curve and inelastic buckling curve. Whereas, for short column the theoretical load-deformation curve relation can't be exactly determined.

CHAPTER 4 INELASTIC RESPONSE OF H-Section AND CHS STEEL BRACING MEMBER UNDER CYCLIC LOADING

4.1 Introduction

Since the load-bearing capacity of the structures depends on the buckling characteristic of the bracing members, in this chapter the bracing member under cyclic loading for different constraint condition was studied. During a severe earthquake and high lateral load (wind), the structures are subjected to reversed cyclic loading, and subsequent inelastic buckling of the bracing members is encountered. One of the best options to withstand the earthquake effect on the building structure is using bracing member. This means that the earthquake resistance of building structures can be effectively provided through the utilization of braced-frame configurations. Rectangular (RHS) and square (SHS) hollow sections are often employed as bracing members for structural as well as aesthetic reasons [1]. Here, steel members having cross section of an H-shape and circular hollow is used as a bracing member. For a severe seismic event, the main design objective is to maintain overall structural integrity without collapse. As part of the capacity design philosophy, energy is dissipated through critical members and components, which are expected to undergo inelastic cyclic deformations without suffering significant loss of strength. Clearly, in the case of braced frames, these critical members are the diagonal braces, for which a detailed assessment of cyclic response is fundamental to the seismic design process. Many researchers have been studied experimentally the inelastic cyclic deformation of bracing members having cross section of RHS and SHS. [1][2][3] In this study steel member of H-section and circular hollow section with different constraint condition is studied analytically.

4.2. Literature Review On Bracing System

So many scholars had been studied steel braces that resist only tensile forces or to resist both tensile and compressive axial forces. For this study I revised a number of publications and different papers. The studies had been conducted more of experimentally and simulation. The experiments have shown that, in general, tension-compression braces (braces under cyclic loading) provide better performance during an earthquake, but their behavior under severe cyclic loading is complicated and not yet well understood. The cyclic inelastic behavior of brace members is complex due to the influence of the following physical phenomena: yielding in tension, buckling in compression, post-buckling deterioration of compressive load capacity, deterioration of axial stiffness with cycling, low-cycle fatigue fractures at plastic hinge regions, and the Bauschinger effect. These factors complicate the formulation of efficient analytical models that are capable of accurately simulating the inelastic behavior of steel braces. Nevertheless, practical and reliable analytical tools are essential for the transition from current prescriptive seismic codes to performance-based design specifications, which require accurate predictions of inelastic limit states up to structural collapse.

Study of Zayas, Popov and Mahin (1980): in this research program six tubular steel braces were tested. The objectives of their study were to resent the experimental data in a form which can later be utilized in analytical studies, and to interpret the experimental observations. The findings of this study are used as a benchmark in this thesis because local buckling was observed in the experiments and its occurrence is well documented.

The specimens tested by Zayas et al. were one-sixth scale models of bracing members used in offshore structures. All specimens had a diameter of 102 mm.

The specimens had either 2.1 mm or 3.1 mm wall thickness which resulted in a diameter-to-thickness ratio of 48 and 33, respectively. Of the six specimens, four had pinned ends while the other two had fixed ends. For the pin ended specimens the length of structural tubing was 1407 mm. All specimens were made of AISI 1020 mild steel tubing which is similar in carbon content and properties to ASTM A36 steel. Because of the drawing process used in its manufacture, the material properties of this tubing in the as-received condition are considerably different from the A36 steel. Four of the specimens were annealed by heating and oven cooling to obtain material properties that are similar to the one of A36 steel. All specimens were subjected to quasi-static cycles of reversing axial displacement. These cycles included compressive inelastic buckling followed by tensile stretching. In a typical experiment applied load, axial and lateral displacements and strains at certain critical points were recorded. The test layout used for this study is illustrated in Figure 4. and the test result is also presented.

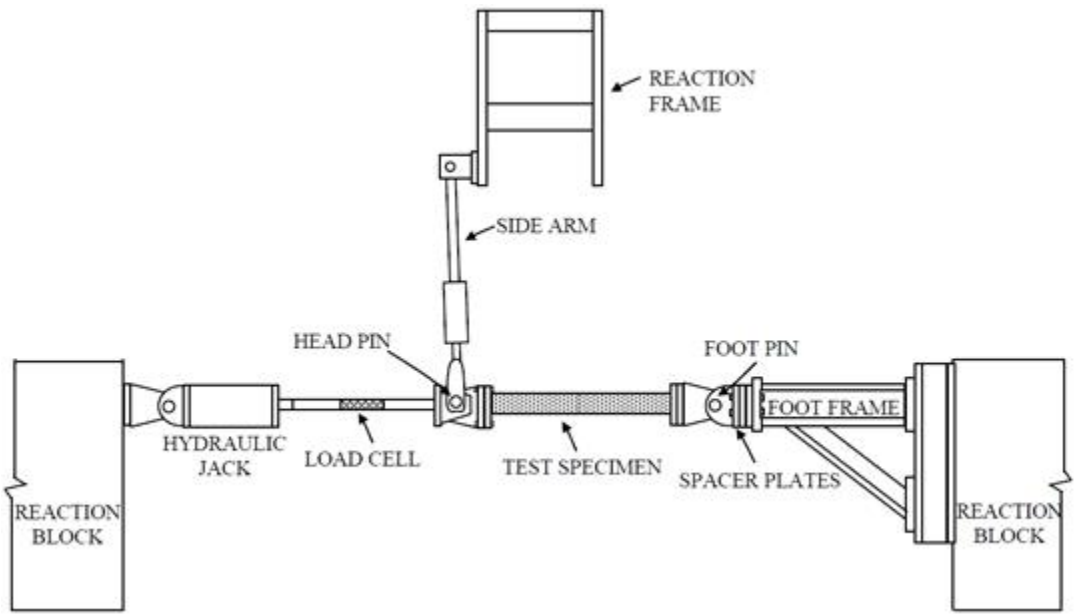

Fig. 4.1. Test Layout for Zayas et al. (1980)

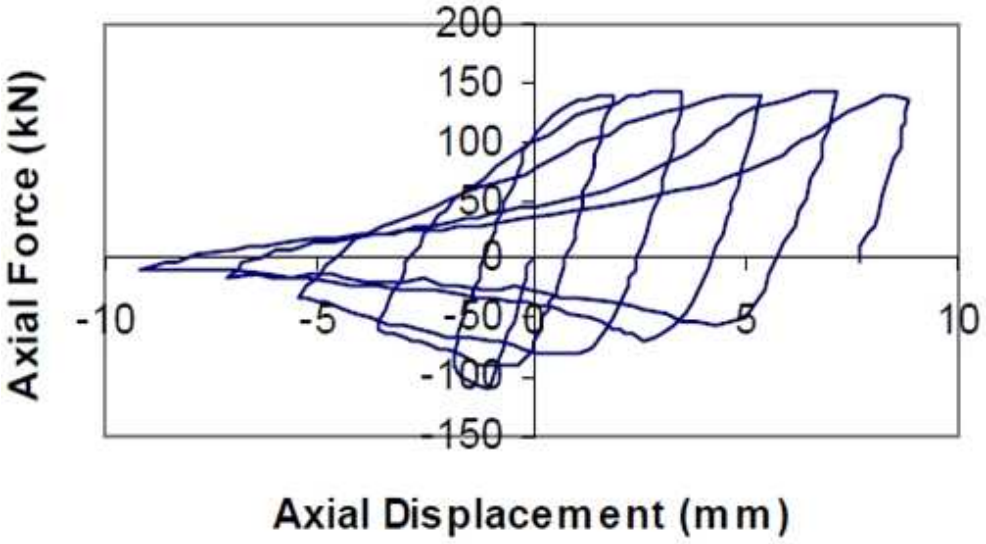

Strut 1 Experimental (Zayas et al.)

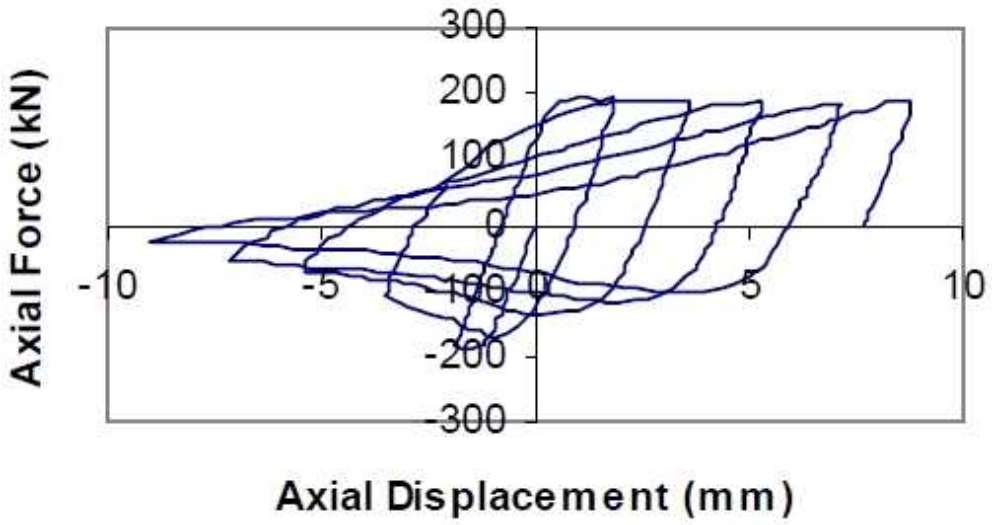

Strut 2 Experimental (Zayas et al.)

Fig. 4.2. Axial force-axial displacement relationship of Zayas et al. Experiment

Study of Jun Jin et al. (2003): Studied the inelastic cyclic model for steel braces. In his study, he presents a formulation for a beam - column element that can be used to simulate the inelastic cyclic behavior of tubular steel braces.

Black et al. (1980) conducted cyclic axial loading experiments on 24 structural steel struts with a wide range of cross-section geometries.

The axial load-axial displacement relationship for one full cycle is predicted by Alexander and Warren et al.(1996) are presented. Fig. 4.7. shows the typical hysteretic behaviour of a steel member when subject to axial cyclic loading. In their study they also presented the division of the cycle to a set of zones corresponding to different behavioral characteristics following the approach of Ikeda and Mahin (1984). A cycle is divided into four general categories for a better representation of cyclic behaviour: the elastic zone, plastic zone, elastic buckling zone and yield zone. The terms "elastic" and "plastic" correspond to the state of the plastic hinge, while the term "yield" is associated with the state of the beam segments. After that, the elastic zone is subdivided into the elastic shortening (both member length and axial load decrease) and the elastic lengthening zone (both member length and axial load increase). Finally, the elastic shortening, elastic lengthening and plastic zones are further subdivided into the zones in compression and those in tension. As a result, the eight zones are incorporated to properly define the axial force-deformation curve.

Zone P1 and P2 are the plastic zone in compression and tension respectively. The brace model presented takes into account the strain-hardening material behaviour in two plastic zones P1 and P2.

Elastic state shortening(ES1) is under elastic region under compression loading and ES2 is elastic shortening under unloading. In the same way elastic state lengthening(EL1) the first lengthening under tension load increase up to original member length and EL2 is the lengthening in tension zone up to the second plastic zone.

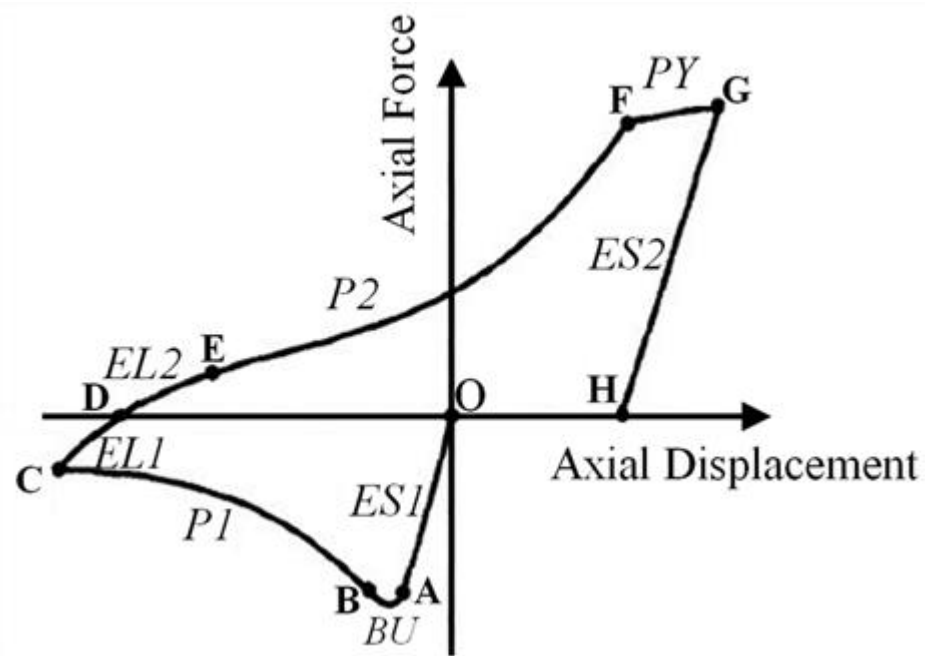

Fig. 4.3. Definition of different zones

Robert Tremblay et al. (2002) studied about the inelastic seismic response of bracing members. He revised the past experimental studies on the inelastic response of diagonal steel bracing members subjected to cyclic inelastic loading was carried out to collect data for the seismic design of concentrically braced steel frames for which a ductile response is required under earthquakes.

He identified resistance of concentrically braced steel frames to earthquake ground motions relies on the capacity of the bracing members to undergo several cycles of inelastic deformations including stretching in tension and buckling in compression. Fig. 4.4 shows the typical hysteretic response (P vs δ plot) of an RHS brace as measured in a quasi-static test in which the amplitude of the applied deformation was increased stepwise at every other cycle up to fracture of the brace presented by Robert Tremblay. Py and δy in the figure correspond

respectively to the yield capacity and deformation at yield of the brace. In this test, the brace was loaded first in tension but also buckled in the first cycle when the load was reversed. After buckling has occurred, the compressive strength decreased as a plastic hinge formed near the brace mid-length. Upon load reversal, elastic recovery took place and the brace was straightened up through inelastic rotation in the plastic hinge. During the second and subsequent cycles, the compressive resistance degraded significantly due to the Baushinger effect and to residual out of- plane deformations from previous cycles. In tension, the brace reached its tensile yield resistance and developed some strain hardening. At every cycle, the brace also accumulated permanent elongation and, hence, could only developed its yield resistance after larger axial deformation was imposed in tension. The amount of inelastic rotation imposed to the hinge at every cycle increased as the brace elongated and the imposed deformation increased. Eventually, local buckling of the cross section developed at the hinge location, which induced high localized strains in the steel material and contributed to reduce further the brace compressive strength. Fracture took place at the hinge when the brace was stretched in tension after local buckling has occurred.

4.3. Non-linear Inelastic buckling

The non-linear finite element analysis and theoretical buckling mode is presented here. In bracing system the influence of the end constraint condition is needs to be investigated. All the detail is presented below.

4.3.1 Non-linear FE Analysis

4.3.1.1 Material Model

The material modeling of analysis specimen was the same as used in chapter 2, 3 above the only difference is the loading and constraint condition. Nonlinear, inelastic, plastic kinematic properties of material is used with combined isotropic and kinematic hardening model of strain hardening characteristics. Three different constraint condition was considered: 1. Pinned – Pinned, 2. Pinned – fixed and 3. Fixed – fixed. The effect of slenderness ratio on the inelastic buckling behavior as well as on the load resisting capacity of bracing member is another parameter to be identified. But for this study this cannot be considered.

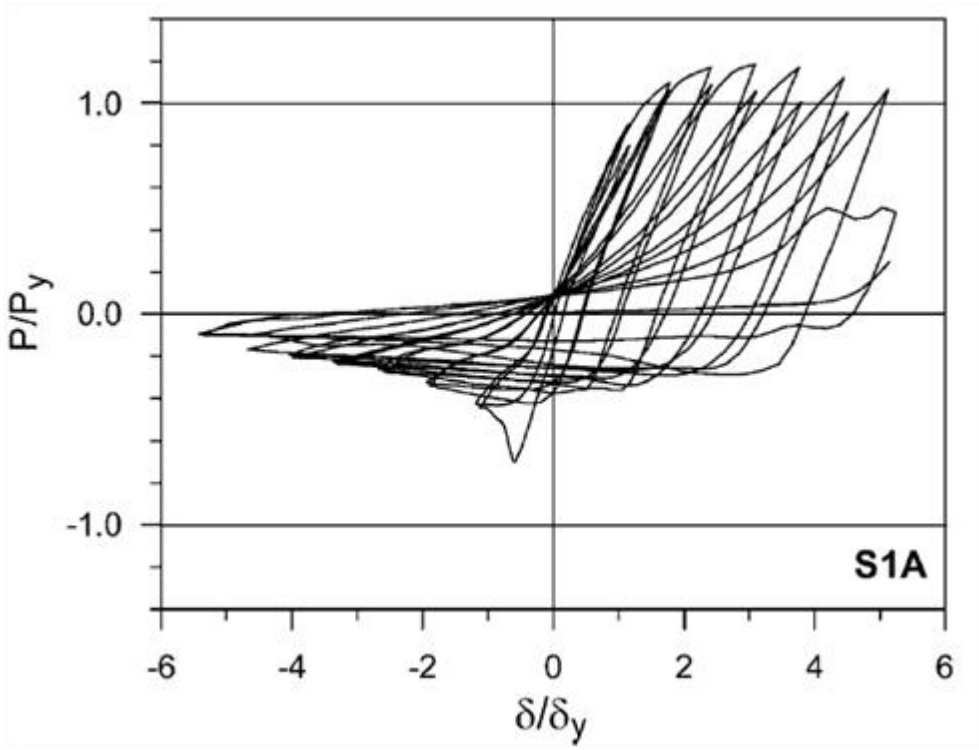

Fig. 4.4. Typical brace hysteretic response under symmetrical cyclic loading (Robert Tremblay 2002).

4.3.1.2 The Constraint and Loading Conditions

4.3.1.2.1 Constraint Condition

As mentioned above three different constraint conditions are considered. Fig. 4.1 (a) to (c) refers to the ideal constraint conditions modeling. The pinned-pinned bracing member is modeled to have free translation and rotation in all direction.

(a). Pinned-Pinned Support Condition

(b). Fixed-Pinned Support Condition

(c). Fixed-Fixed Support Condition

Fig.4.5. Different Constraint Condition Model Considered

4.3.1.2.2 Loading Condition

The loading condition is the same as that used in Chapter 2 and 3 above with constant strain loading. The displacement protocol used shown in figure below. For

all the considered slenderness ratios by setting the maximum strain up to fracture. the cyclic displacement protocol is shown in Fig. 4.2.

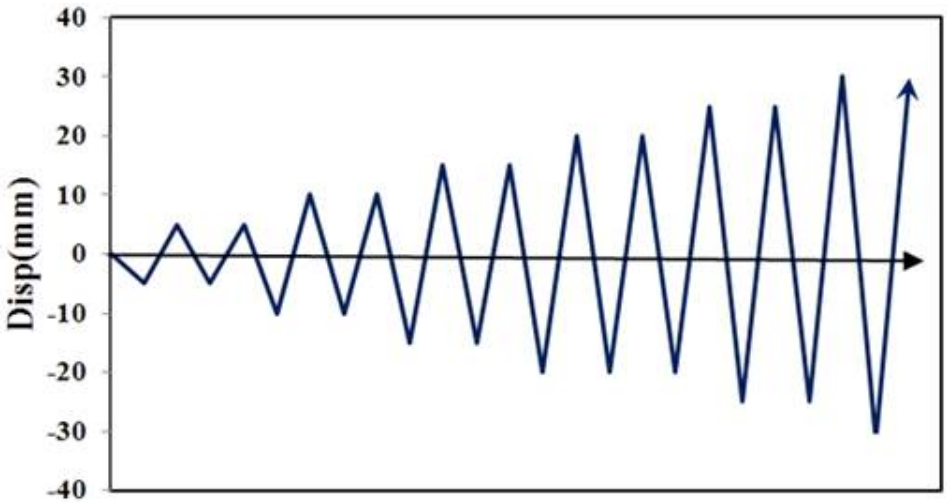

Fig.4.6. Displacement Protocol

4.3.2. Theoretical Investigations

Theoretically braces under compression loading, of course for pinned-pinned and fixed-fixed constraint condition is already presented on Chapter 2 and 3 above, the buckling mode with length of effective length is presented below.

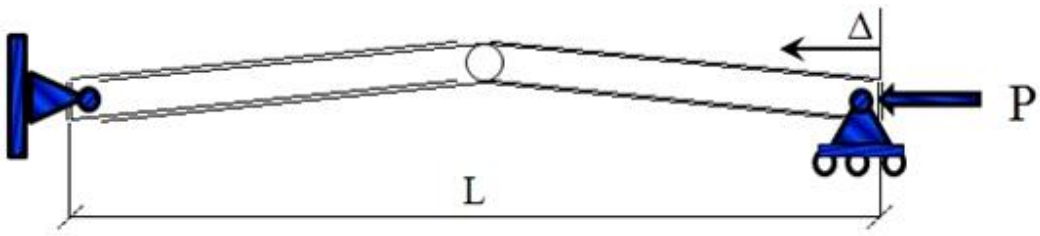

(a). Pinned-pinned Model

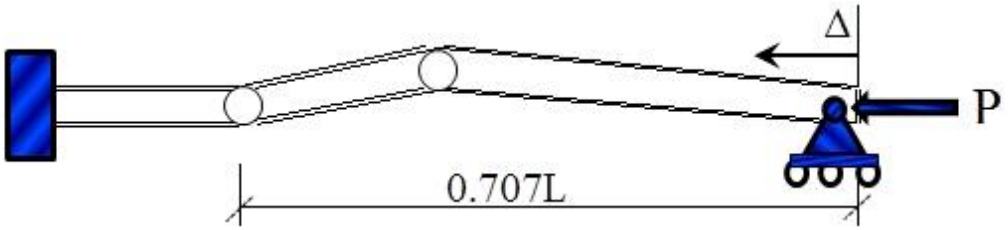

(b). Fixed-pinned model

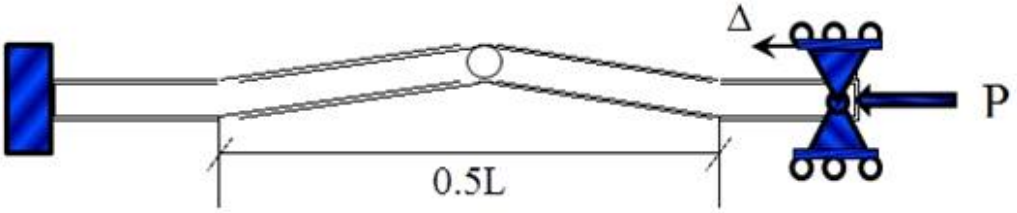

(c). Fixed-fixed model

Fig. 4.7. Theoretical Buckling mode of bracing member under compression loading

The axial shortening for pinned-pinned constraint condition is derived and given by:

$$\frac{\triangle}{L}=1-\sqrt{1-(\frac{2Z_p}{LA})^2*(\frac{1}{P/P_y})^2} \qquad (4.1)$$

Where: $\triangle$ is axial shortening, L; length from pin to pin, Z_p: is the plastic section modulus, A: cross sectional area, P: applied load and P_y: axial force at yield state.

In the same way for fixed-fixed constraint condition the relationship axial shortening and axial force from the theoretical buckling is given by:

$$\frac{\Delta}{L}=\frac{1}{2}-\sqrt{\frac{1}{4}-(2Z_p/LA)^2*\left(\frac{1}{P/P_y}\right)^2} \qquad (4.2)$$

For fixed-pinned constraint condition, the derivation is complex, the derivation of load-deformation relationship is under process.

4.4. Analysis Result

4.4.1 Buckling Mode of CHS Bracing Member

For pinned-pinned and fixed-fixed support condition a plastic hinge forms at the brace midpoint when the member buckles. For Fixed-pinned constraint condition the plastic hinge is formed at around $(\frac{2-\sqrt{2}}{2})L$ length from the fixed end and the other is some distance to pin end form the first hinge as indicated in fig. 4.11. The plastic hinge region is prone to local buckling. Local buckling can cause high localized strains which eventually trigger low cycle fatigue and may result in fracture of the member during repeated inelastic cycles. Therefore, local buckling leading to fracture may represent a limitation on performance. Fracture developing after local buckling is particularly important for hollow structural section (HSS) brace members (Hassan and Goel 1991; Tang and Goel, 1989; Tremblay 2002). The analysis result of buckling mode followed by fracturing type of simply supported bracing members is presented in Fig. 4.9.

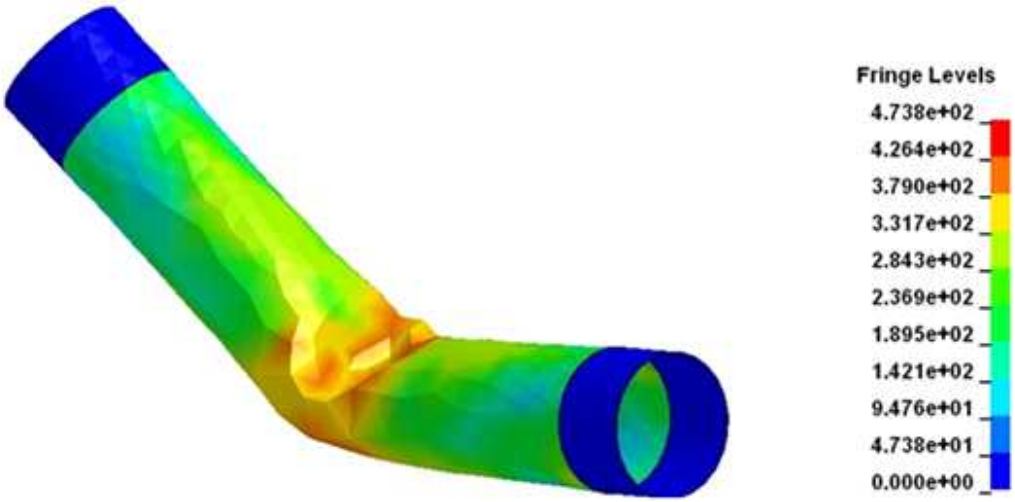

Fig. 4.8. Buckling mode and von Mises's stress distribution for pinned-pined support condition of CHS

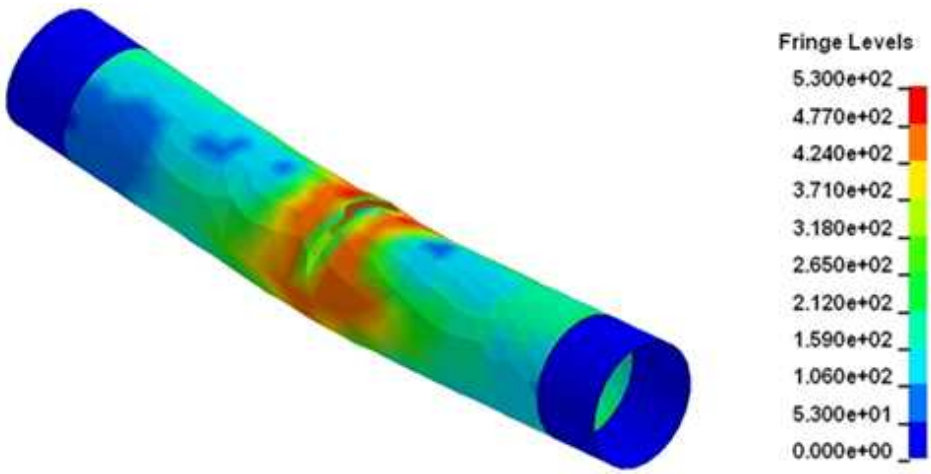

Fig. 4.9. Fracturing and von Mises's stress distribution for pinned-pined support condition

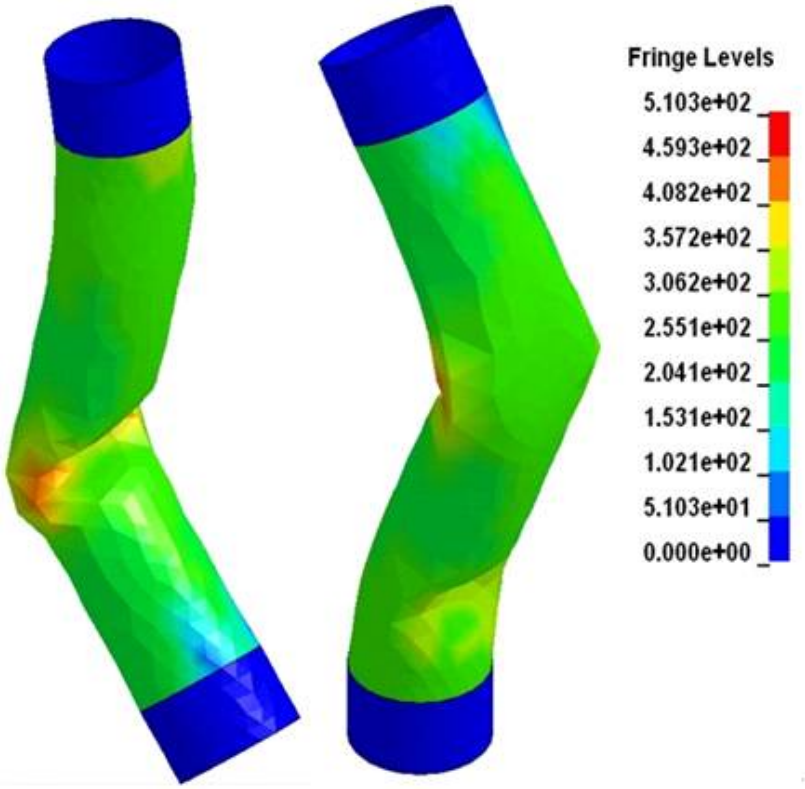

Fig. 4.10. Buckling mode and von Mises's stress distribution for fixed-pined support condition

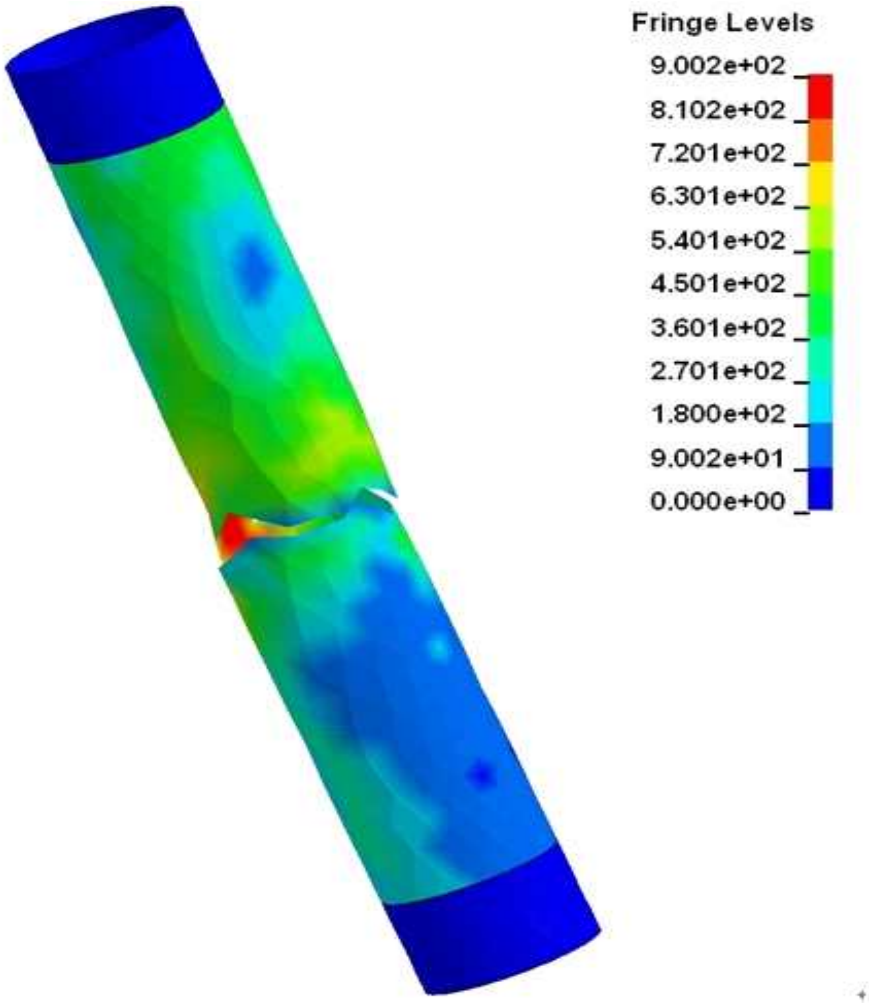

Fig. 4.11. Fracturing and von Mises's stress distribution for fixed-pined support condition

4.4.2AxialLoad-AxialDisplacementRelationshipForCHS

The axial force - axial displacement relationship is presented in fig. 4.8 below.

From the fig. we can notice that the load resisting capacity of fixed ended higher

compared to fixed-pinned and pin ended constraint condition. It is obvious that both end fixed member has high resisting capacity. This situation is also seen on the axial load-axial deformation relationship.

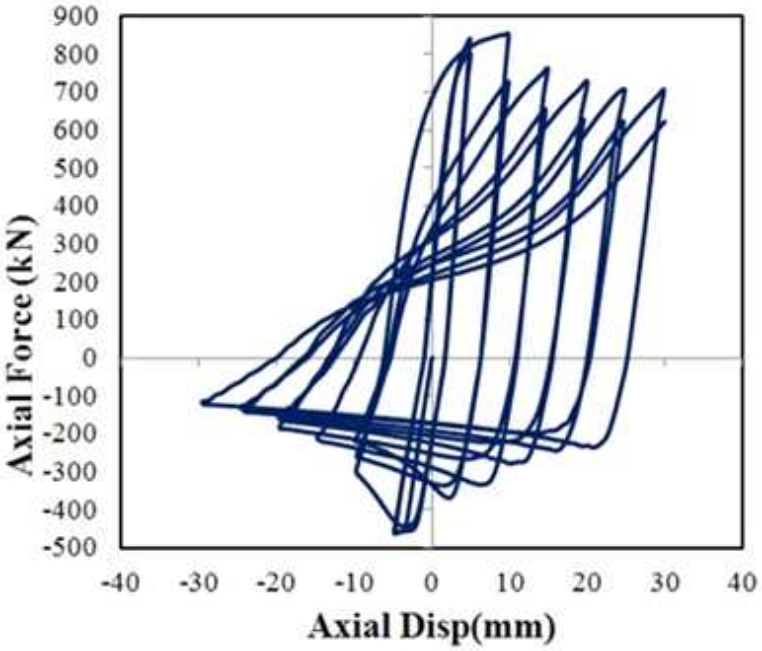

(a). Analysis Result for Fixed-Fixed model

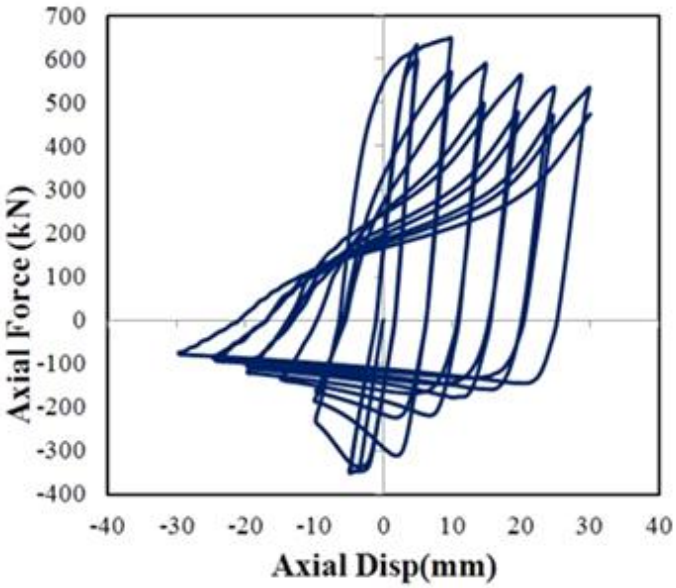

(b). Analysis Result for Fixed-Pinned model

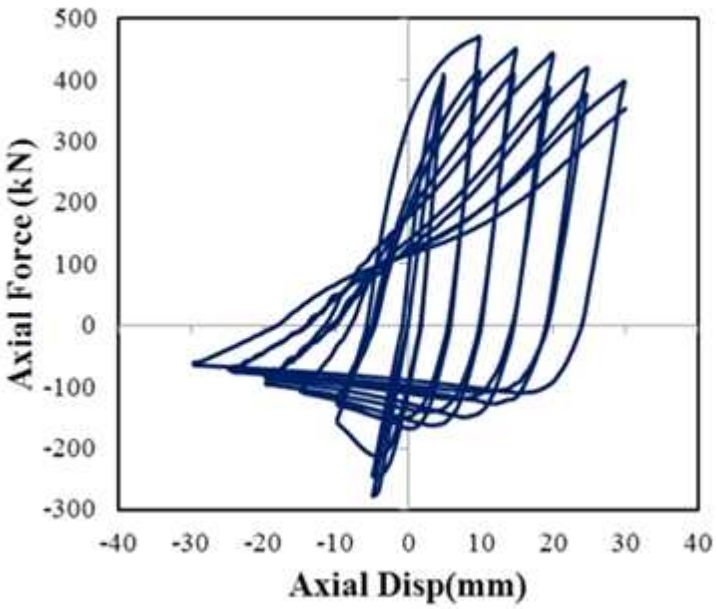

(c). Analysis Result for Pinned-Pinned model

Fig. 4.12. Hysteresis loops of analysis Result for CHS model

4.4.3 Buckling Mode of H-Section Bracing Member

The same situation is repeated for H-section bracing members. Here for the simply support condition and Fixed-pinned support condition two different cases are considered constraining on the strong axis and weak axis. It is necessary to identify the effect of these conditions for bracing members unde cyclic loading in both buckling mode and load-displacement relationships. It is not worthy to present all the results. Here it is better to present the buckling mode and the fractured member for fixed-fixed support condition as shown in Fig. 4.9 and 4.10 respectively.

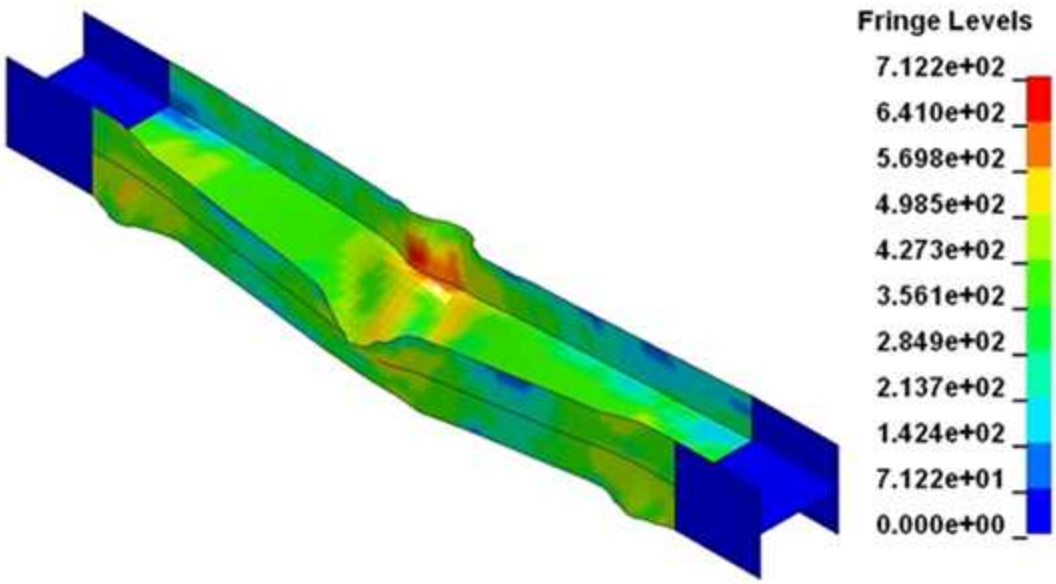

Fig. 4.13. Buckling mode and von Mises's stress distribution for fixed-fixed support condition (H-Section)

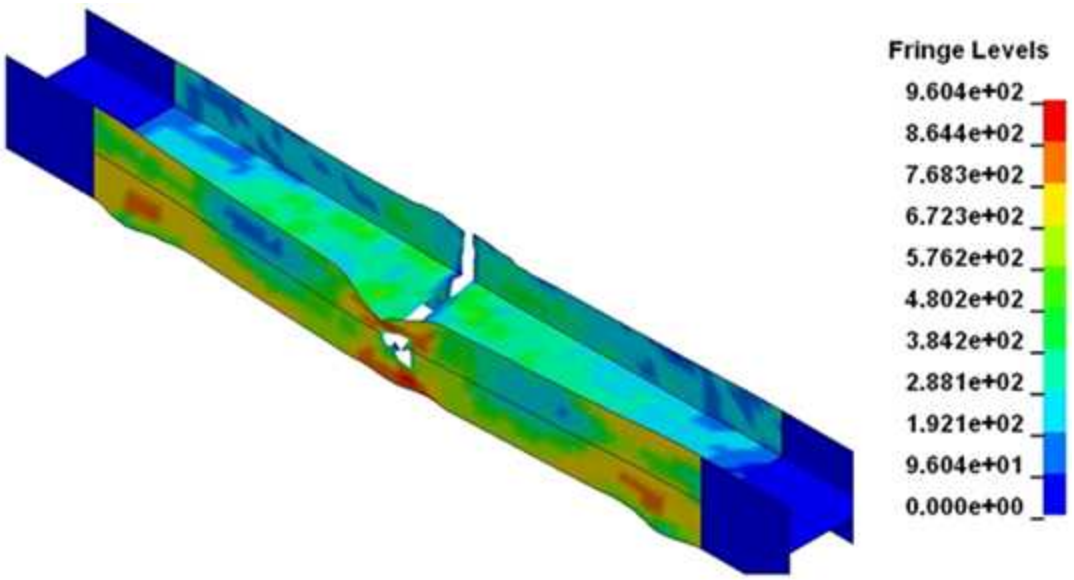

Fig. 4.14. Fracturing and von Mises's stress distribution for fixed-fixed support condition (H-Section)

4.4.4AxialLoad-AxialDisplacementRelationshipForH-Section

The same process is repeated here. The load resisting capacity of H-section bracing member is higher than the equivalent circular hollow section bracing member. The compression load resisting capacity in the elastic range increases. Once the member yields the compression laod resisting capacity decreases in each cycle. However, on the tension part in the elastic range the resisting force is lower than after yielding. As described in sub-title 4.4.2 above, the cyclic loops predicted works for the H-section bracing members as well.

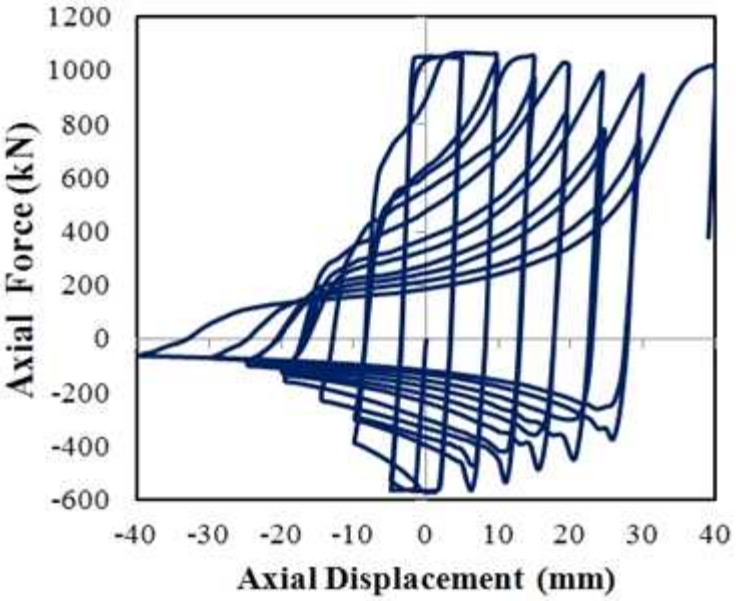

(a). Analysis Result for Fixed-Fixed model

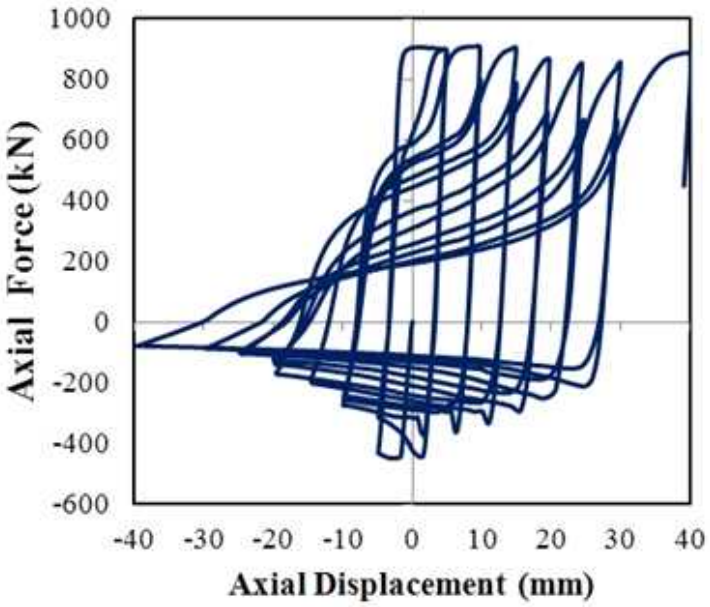

(b). Analysis Result for Fixed-Pinned model

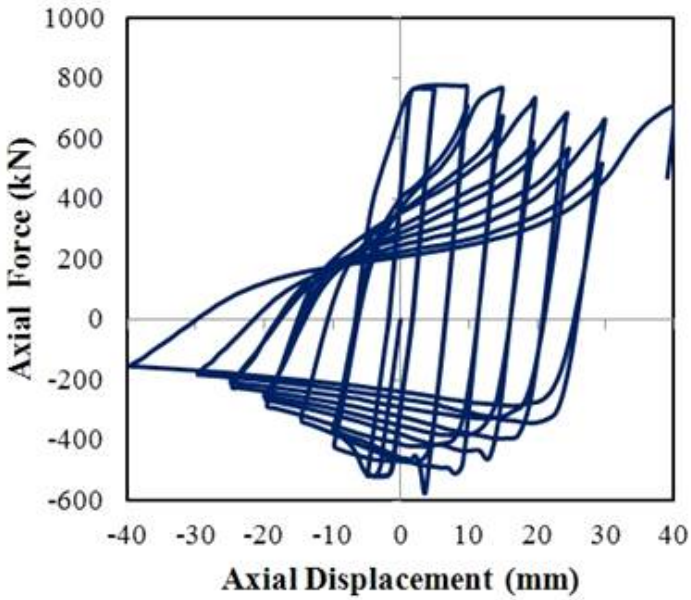

(c). Analysis Result for Pinned-Pinned model

Fig. 4.15. Hysteresis loops of analysis Result for H-Section model

4.5 Lateral brace Deformation

Significant in-plane or out-of-plane lateral deformation of braces were observed in tests and in past earthquakes and such movements must be accounted for in design if it can produce damage to and collapse of non-structural elements such as walls and cladding elements. Such lateral deformations develop upon application of a compression load to a previously buckled brace. Observations of brace behaviour during tests suggest that simple models as those shown in Fig. 4.14 can be used to relate the lateral deformation, $\triangle$, to the applied compression displacement, δ_c. For a pin-ended brace subjected to small axial deformation (Fig.4.14a), a sinusoidal function closely represents the deformed shape and it can be shown that the amplitude of the lateral displacement is equal to:

$$\triangle = \frac{2}{\pi}\sqrt{\delta_c * L_H} = 0.64 * \sqrt{\delta_c * L_H} \qquad (4.3)$$

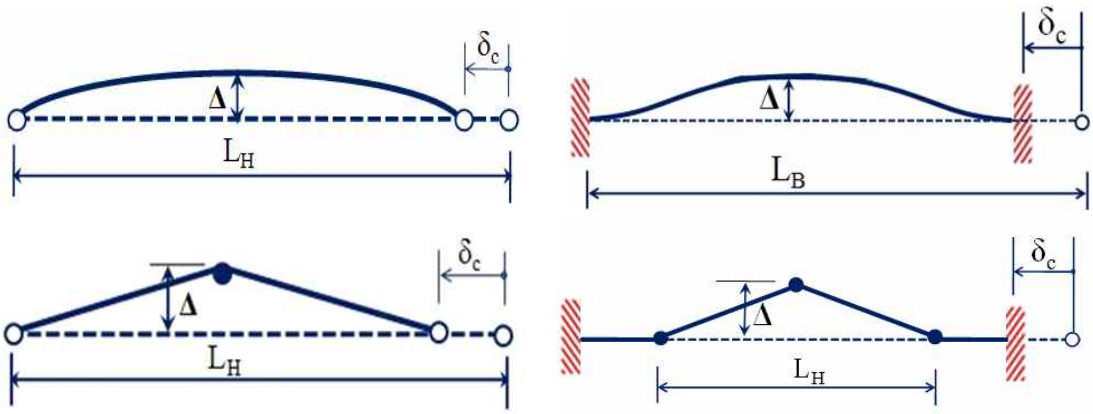

Fig. 4.16. Out-of-plane deformation of braces: (a) elastic with pinned ends; (b) inelastic with pinned ends; (c) elastic with fixed ends; (d) inelastic with fixed ends.

Under higher ductility levels, a plastic hinge forms at mid-span and a rigid-plastic stick model represents more closely the brace response, as shown in Fig. 4.14(b). With that model, the lateral deformation is given by:

$$\triangle = \frac{1}{\sqrt{2}}\sqrt{\delta_c * L_H} = 0.71 * \sqrt{\delta_c * L_H} \qquad (4.4)$$

For braces with rotational end restraints, the deformation will typically be smaller. For instance, the maximum lateral deformation for a fixed - fixed end connected brace at low ductility (Fig. 4.14c) is given by:

$$\triangle = \frac{1}{2\pi}\sqrt{\delta_c * L_B} = 0.16 * \sqrt{\delta_c * L_B} \qquad (4.5)$$

At higher ductility plastic hinges develop in the braces (Fig. 4.14d), can be obtained using Eq. (4.4) with the distance L_H being equal to the distance between the hinges that form near the ends. Based on observations during tests, these hinges can be assumed to be located at a distance from the brace ends equal to the depth of the member measured in the plane of buckling. Considering that lateral deformations are generally critical at high ductility levels, Eq. (4.4) with a factor 0.7 can then be used for all end conditions.

4.6 Summary

In this chapter bracing member with circular cross section and H-section has been presented. The hysteresis response under cyclic loading as well as the deformation mode of the bracing members under different constraint condition was presented. though the analysis result is verified directly by experiment, form literatures reviewed, and presented in this chapter, the both the buckling mode and hysteresis loops shape is matches with the experimental studies.

Since the behavior of bracing member is not yet identified clearly, further study will be needed on this chapter. Not only this but also the system and form of bracing member has a wide range to be studied.

CHAPTER 5 CONCLUSION

This study have two parts:

1. Inelastic buckling behavior of steel members
2. Inelastic seismic response of steel structures.

Under the first part, column member considering effect of: (a) constraint condition (b) slenderness ratio has been identified analytically. The analysis result, the buckling mode and load-displacement relationship, were of course verified in some cases. From the comparison a great match was obtained. From this it is possible to say the finite element analysis carried out in this study can evaluate inelastic buckling behavior of steel column member under axial compression loading. Depending on the constraint condition, the strength degradation varies. Fixed ended model kept constant after attaining the maximum load and the strength degradation is slightly compared to pin ended model. The pin ended model constraint in strong and weak axis is also same up to the maximum resisting force; however the after attaining the critical load the strength degrades rapidly for weak axis constraint condition relative to other constraint condition.

The second part deals with inelastic response of bracing members under cyclic axial loading was also evaluated. Though the hysteresis curve is compared directly with the test results, the cyclic shape is similar with already done experiments from literatures. This chapter needs to be studied further because the cyclic characteristics of bracing member is complex. But generally the result obtained reveals that the FE analysis carried out can evaluate the cyclic response of bracing members.

In addition, the inelastic seismic response of steel dampers, shear panel and circular pipe dampers has also been presented in Appendix A and B.

1) Shear Panel Damper: the parameters considered are: material strength and depth to thickness ratio. generally three different failure mode has been observed in both test and analysis. These are: panel fractured with an X-shape, welding part of the panel to the end plate is fractured and the last one is where the welding part of flange to the end plated were fractured. In the first case where the panel fractured with an X-shape, because of an early yielding of the panel the strength degrades at initial displacement. Comparison of the two material (low yield point steel and conventional steel) with equivalent size shows that low yield point steel have high cyclic resisting capacity though the maximum resisting load of conventional steel is higher compared to the corresponding low yield point steel.

2) Circular Pipe Damper: here also two different strength steel material has been used. The parameters considered is aspect ration which is the depth to diameter ratio. Aspect ratio of $\sqrt{3}$ is found to be the effective size of circular pipe damper. Of course the size less and greater than the effective size has also been studied. In the same way, the cyclic deformation capacity and cumulative energy absorbing capacity of the equivalent CPD has been compared. It has been noticed that LYP100 (low yield point steel) has high seismic energy absorbing capacity than the common conventional steel (SS400).

In the analysis carried out in this study the strain hardening characteristics of steel material is given more attention especially in the LS-Dyna where there is a choice in strain hardening behavior.

Generally the combined strain hardening model is the governing strain hardening characteristics for steel structures. Combined strain hardening means the combination of kinematic and isotropic hardening model it shows both translation and expansion of initial yield surface. Low yield point steel behaves more of isotropic characteristics compared to conventional steel which shows kinematic hardening characteristics.

REFERENCES

CHAPTER 1

[1] Wikipedia, the free encyclopedia

[2] Park, Hwon-Mo, D. Yeshewawork, Kim, Hyun Soo, Choi, Jae-hyouk 'Analytical Evaluation of Residual Strength for Steel Frame in Case of Column Member Loss' Journal Of Computational Structural Engineering Institute of Korea 2011, pp.675-683

[3] Hwonmo P. Evaluation on the Post-buckling Energy Absorption of H-Shaped Steel Column for Prevention Progressive Collapse, Master, Chosun University, Gwangju, Korea, 2011

CHAPTER 2and3

[1] D. Yeshewawork, JH. Choi 'Nonlinear Inelastic Buckling Behavior and Residual Strength of H-Section Steel Column' international journal Advanced Materials Research [approved and waiting publication]

[2] D. Yeshewawork, JH. Choi, JY. Kim, 'An Evaluation on Post-buckling Residual Strength of H-Section Steel Column for Fixed Constraint Condition' Journal of Korean Society of Mechanical Engineers, Vol. 37, No. 1.[approved and waiting publication]

[3] D. Yeshewawork, J.H Choi and S.K Lee, 'Evaluation on Postbuckling Residual Strength and Stain Recovery of H-section Steel Column' Proceeding of the 9th International Symposium on Architectural Interchange in Asia, 2012, pp. 20.

[4] Zdenek BZ, Yong. Z, Why Did the World Trade Center Collapse? - Simple Analysis, Journal of Engineering Mechanics, ASCE; 2002; p.2-6

[5] Phill-Seung Lee, Hyuk-Chun Noh, Inelastic buckling behavior of steel members under reversed cyclic loading, Engineering Structures 32 (2010) 2579_2595

[6] R.K. Livesley, Introduction to matrix structural analysis; 1968; Baifukan

[7] Shanley. F.R, Inelastic Column Theory, Journal of Aeronautical Science; 1947; 14, p.261-264

[8] Daisuke ST, Ahmer WD, Post-buckling Behavior of Pre-stressed Steel Stayed Columns, Engineering Structures; 2008; 30, 1224-1239

[9] ANSYS LS-Dyna user's manual version 12.0

[10] Zenglin L, Ken'ichi OI, Takumi IT. Sensitivity Analysis on Vertical Load Carrying Capacity of Framed Structures to Member Disappearance, Journal of Constructional Steel;2003;11,p.325-332

[11] Ben KT, Hiroshi AK, Keihiko IN. Post-buckling Behavior of Short Steel Columns, Transactions of the Architectural Institute of Japan 1975; 299, p.67-76

[12]Yeong CY. Post-buckling Behavior of Tapered Columns under a Combined Load using Differential Transformation, Architectural Research 2006; 8, p.47-56

[13] Architectural Institute of Japan: Limit State Design Guide lines of steel structures, 1998

[14] P.C. Paris. Limit Design of Columns, Journal of the Aeronautical Sciences; 1954. 21, p.43~49

[15] Choelho L, Seonwoong K, Kyungkoo L, Kyuhong H, Simplified Nonlinear Dynamic Progressive Collapse Analysis of Welded Steel Moment Frames Using Collapse Spectrum, Journal of Korean Society of Steel Construction ;2009;100,267-275

[16] Kyung koo L, Evaluation of Residual Capacity of Steel Compressive Members under Blast Load, Journal of Architectural Institute of Korea; 2010; 264, 37-44

CHAPTER 4

[1] B.M. Brodericka,*, J.M. Gogginsa, A.Y. Elghazoulib 'Cyclic performance of steel and composite bracing members' Journal of Constructional Steel Research 61 (2005) 493 - 514

[2] Popov EP, Zayas VA, Mahin SA ' Cyclic inelastic buckling of thin tubular columns.' Journal of the Structural Division, ASCE 1979; 105 (ST11):2261 - 77.
[3] Jain AK, Goel SC, Hanson RD. Hysteretic cycles of axially loaded steel members.'Journal of the Structural Division, ASCE 1980; 106 (ST8):1777 - 95.
[4] Zayas VA, Popov EP, Mahin SA. 1980. Cyclic inelastic buckling of tubular steel braces. Earthquake Engineering Research Center, Report No. UCB/EERC-80/16, University of California, Berkeley
[5] Tremblay R. 2002. Inelastic seismic response of steel bracing members. Journal of Constructional Steel Research, 58: 665-701.
[6] Alexander M. Remennikov and Warren R. Walpole, ' Modeling the Inelastic Cyclic Behavior of a Bracing members for work-hardening Material.' Int. J. Solids Structures Vol. 34, No. 27, pp. 3491-3515, 1997
[7] Jun Jin and Sherif El-Tawil, P.E., M.ASCE, 'Inelastic Cyclic Model for Steel Braces.' Journal of Engineering Mechanics, 2003, pp 548-557
[8] ANSYS LS-Dyna user's manual version 12.0

APPENDIX A

[1] D. Y. ABEBE, J.Y. IN and J.H. CHOI 'Study on Structural Performance Evaluation of Shear Panel Hysteresis Damper' Proceeding of 2nd International Conference on Computational Design in Engineering, 2012, pp 311.
[2] ANSYS LS-Dyna user's manual version 12.0
[3] D. Yeshewawork and J.H. Choi "A Study on Structural Performance Evaluation on Advanced Shear Panel Steel Damper' Proceeding of Korea Institute for Structural maintenance and Inspection, 2012. pp. 153-156
[4] J.H, Park, T.W. Park, W.J. Kim, D.B. Lee, 'Study on characteristic of steel hysteresis damper and evaluation methodology of damper application effects', Korean Architecture Association Theses Collection, pp. 33-36, No.1, Vol. 26,
[5] Park, Ji-Hyung, Park, Tae-Won, Kim, Wook-Jong, Lee, Do-Beom (2006) Study

on characteristic of steel hysteresis damper and evaluation methodology of damper application effects, pp. 33-36, No.1, Vol. 26, Korean Architecture Association Theses Collection.

[6] Geum, Dong-Seong, Yoon, Myung-Hoon (2002) Introduction to performance design cases of ultrahigh building over 200m using hysteresis type steel damper, Korea Steel Structure Academy Book, pp. 134-141, No.3, Vol. 14.

APPENDIX B

[1] D. Yeshewawork, and J.H. Choi, 'Structural Performance Evaluation on Hysteresis Characteristics of Circular Pipe Steel Damper'. Proceeding of IUMRS-ICA2012 (2012) pp. 132.

[2] D. Yeshewawork, and J.H. Choi, 'Hysteresis characterstics of circular pipe steel damper Using LYP100' [approved and waiting publication] the proceeding of international conference on Steel Innovation 2013.

[3] ANSYS LS-Dyna and ANSYS Workbench user's manual version 12.0

[4] YASUI Nobuyuki., 2010, "Cyclic Loading test using plastic deformation for evaluation of performance of cold-formed circular steel pipe columns," Journal of Japanese society of steel construction, Vol.17, No.68, pp1~12.

[5] Kazuhiko Kasai、Yanghui Xu., 2002, "Experimental Parameter Study on Cyclic Inelastic Behavior of Bolted Angle Connections," Journal of Structural and Construction Engineering, No.560、pp169~179.

[6] Neto, Eduardo de Souza. Computational methods for plasticity: theory and applications / Eduardo de Souza Neto, Djordje Peric, David Owens.

APPENDIX C

[1] X. Q. Yang and X. X. Huang 'A nonlinear Lagrangian approaches to Constrained Optimization Problems' SIAM J. OPTIM. Society for Industrial

and Applied Mathematics, Vol. 11, No. 4, pp. 1119 - 1144, 2001

[2] Liang Xue, Zhongqin Lin and Zhengxu Jiang 'Effect of Initial Geometrical Imperfection on square Tube Collapse'

[3] Philippe Le Grognec, Pascal Casari and Dominique Choqueuse 'Influence of residual stresses and geometric imperfections on the elastoplastic collapse of cylindrical tubes under external pressure' Marine Structures, Volume 22, Issue 4, Pages 836-854, 2009.

[4] Raul H. Andruet 'Special 2-D and 3-D Geometrically Nonlinear Finite Elements for Analysis of Adhesively Bonded Joints' thesis for Doctor of philosophy in Engineering Science and Mechanics.

APPENDIX A

INELASTIC RESPONSE OF SHEAR PANEL HYSTERESIS STEEL DAMPER

A.1 Introduction

Low yield point steel (SLY120) has low strength and high plasticity, this property makes it more pliable and thus more it is able to absorb energy through plastic deformation during earthquake. The shear panel damper (SPD) using low yield point steel is a new and now applicable type of energy dissipating device based on the concepts structural seismic control. During the vibration of building due to earthquake or wind, its rational design enables it to first enter a plastic state so that it can absorb a large part of the seismic energy by way of shear hysteresis on a metal plate. SPD devices dissipate energy passively based on plastic yielding and nonlinear shear deformation in metal materials. Its energy dissipation capacity depends crucially on plastic deformation and fatigue resistance. Subjected to earthquake load, SPD devices must have sufficient ductility to withstand the maximum possible shear deformation and thereby reduce earthquake damage. Therefore, the large deformation capacity of an SPD must be determined and its cumulative dissipated energy evaluated. A series of experiments were carried out for different thickness 120SYP panel and the results were compared with the analysis result. For comparison purpose it is conducted by using common mild steel SS400 with thickness of 3.5mm.

A.1.1 Material Properties of Specimen

To find out mechanical characteristic of low yield point steel (SLY120) and general structural steel (SS400), tensile coupon test of the specimen was performed and the results are shown in Fig. 2 and Table 1.

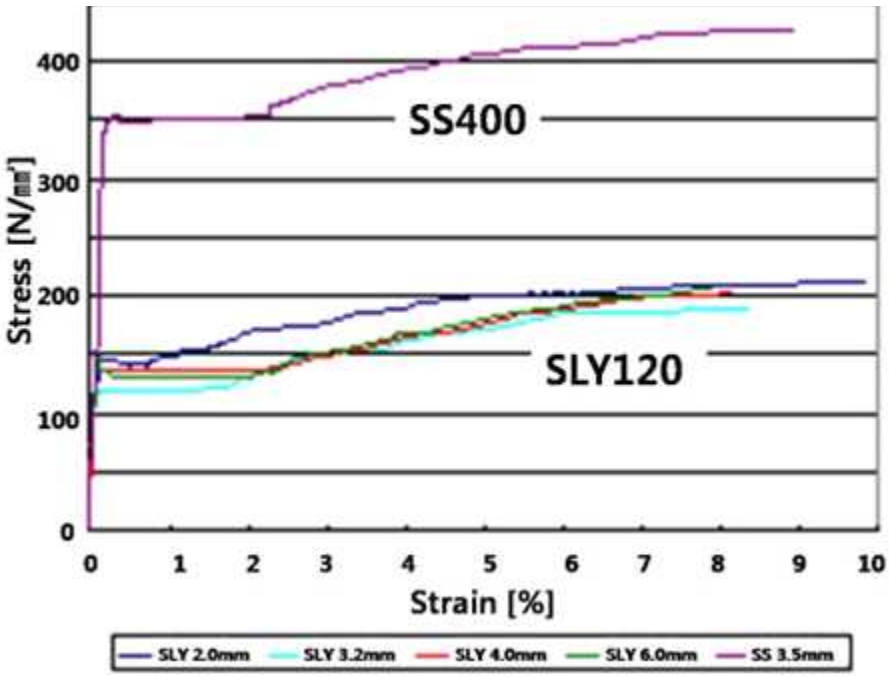

Fig. A.1. Experiment result of tension strength.

Table A.1 Mechanical Properties of specimen (Test result)

Material	Yield Strength (σ_u)	Ultimate Strength (σ_u)	Max. Strain ϵ_u	Strength $\tau_y = \sigma_y / \sqrt{3}$
SS400	347.4MPa	425.8MPa	28.1%	200.6MPa
SLY120	126.7MPa	202.8MPa	41.7%	73.1MPa

In the specimen tensile coupon test results, it was confirmed that yielding strength of low yielding point steel used in this experiment was less than 1/2 of general structural steel but it was very sufficient in plasticity deformation ability as 41.7% for low yield point steel.

A.2 Finite Element Analysis Model

A.2.1 Material Modeling

The panel of specimen was modeled with two different strength steel, SLY120 and SS400 steel. Whereas the in both cases the flange and the two end plates (rigid bodies) are modeled by the conventional steel SS400. The detail dimension is shown in figure 4.1 below. Non-linear analysis was carried out with reasonable accuracy with low yield point steel and for comparison purpose we also analyze SPD with the common mild steel SS400. The analysis material is modeled as a shell element in the case of explicit nonlinear finite element analysis and as a solid element for the case implicit finite element analysis. In both cases the following two conditions are considered. First, we consider large deformation kinematics to simulate the residual displacement. Of course, without large deformation kinematics, the deformation behavior cannot be predicted in the analysis model. Second, the inelastic material behavior, including the cyclic characteristics, is considered.

Plastic kinematic model carried out here is the same as that done on Chapter 2. Considering combined kinematic and isotropic strain hardening models. The detail of the plastic kinematic modeling is presented in table A.2.

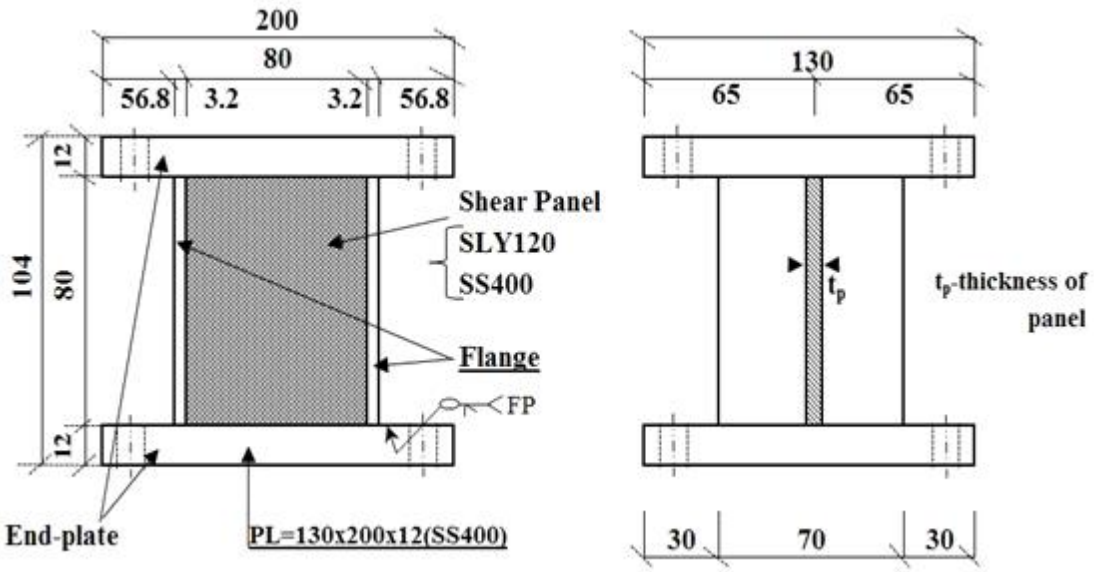

Fig. A.2 Detail of specimen

Table A.2 The property of material used in the analysis

Properties	Web (Panel)		Flanges	Upper and Lower End Plate
	SLY120	SS400		
Young's Modulus	205	205	205	205
Poison's ratio	0.26	0.3	0.3	0.3
Density(kg/m3)	7800	7860	7860	7700
Yield Strength	126.7	347.4	347.4	
Tangent Modulus	550	756	756	
Hardening Parameter	0.25	0.5	0.5	
Strain rate [C]	50	40	40	
Strain rate [P]	5.0	5.0	5.0	
Failure Strain	0.8	0.75	0.75	

The analysis is carried out for five specimens having different panel thickness in both experimental and analysis simulation. The detail is presented in table below.

Table A.3 Specimen detail

Specimen Code	Material Type	Measurements [mm]		d/t_p
		depth (d)	thickness of panel (t_p)	
L2.0	SLY120	80	2.0	40
L3.2	SLY120	80	3.2	25
L4.0	SLY120	80	4.0	20
L6.0	SLY120	80	6.0	13.33
L3.5	SS400	80	3.5	22.86

A.2.2 Constraint and Loading Condition

The constraint condition was modeled to have a shear effect on the panel, the lower rigid body is fixed in all direction, i. e. both translation and rotation is constrained. As shown in the figure 3 below, the upper rigid body is modeled to have translation only in X and constrained all other directions in the Y & Z-axis and constrained rotation in all directions. A linear incremental load is applied in the horizontal direction (in the X-axis) on the upper rigid body. The displacement control loading system is shown in the figure 4 for both analysis and experimental simulation. With this displacement protocol, the load is applied to the upper rigid body to allowable strain.

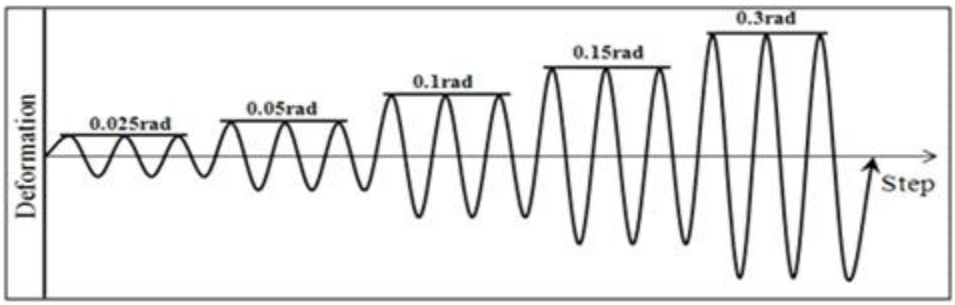

Fig. A.3 Displacement Protocol

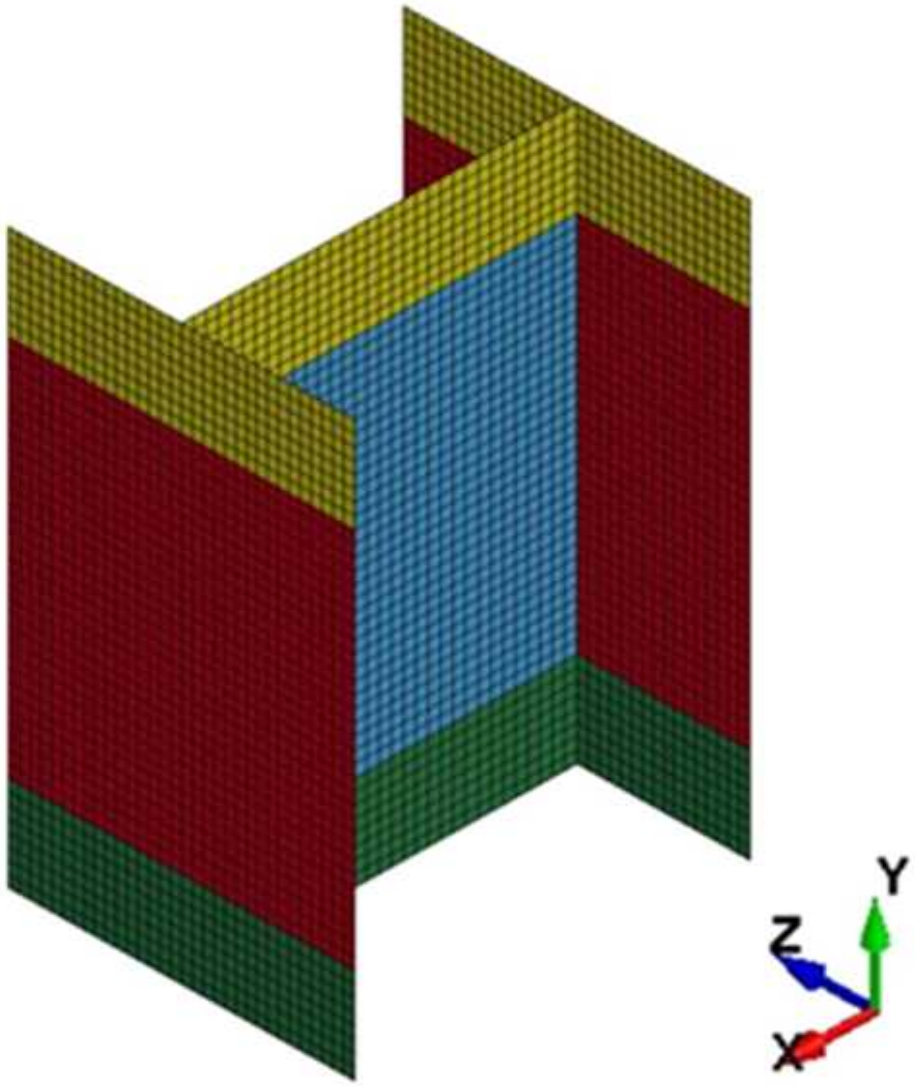

Fig. A.4 Meshed 3-D Analysis Model

A.3 Verification and Validation of Analysis Model

To verify the feasibility and reliability of the proposed nonlinear finite element analysis, experiment was undertaken on the low yield steel panel. The failure mode

and stress-strain relationship was obtained and compared to analytical results.

A.3.1 The Test Program and Process

The detail of experimental specimen is shown in fig. 5.1. was used for the test with equal and the same material with that of analysis specimen. Fig. 5.10 shows a loading experiment equipment system. As loading experiment equipment system, Pantograph was installed so that rotation angle does not occur at the top part of experiment specimen while load was applied horizontally at experiment specimen of low yield point shear panel damper. By installing Counter Weight using the principle of a pair of scale, it was arranged that axial force is not applied to experiment specimen.

Displacement meters for measuring displacement of low yield point shear panel dampers was installed at the top end plate and the bottom end plate of the experiment specimen. Average value of the right and left side displacement devices was evaluated as displacement value of the experiment specimen. In addition, horizontal force on the experiment specimen was measured by installing load cell adding actuator.

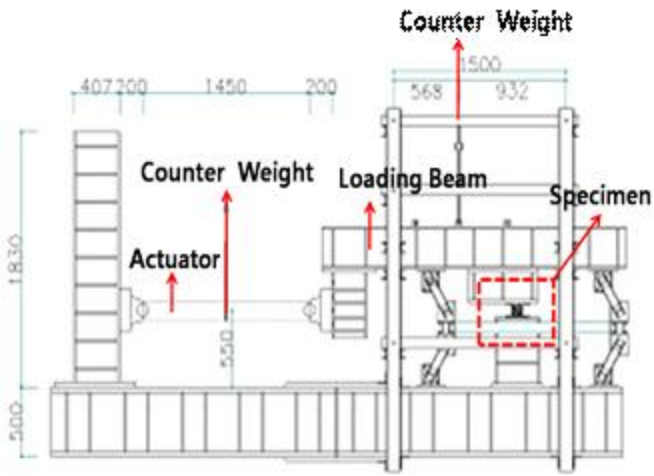

Fig. A.5. Load experiment equipment

A.4 Comparison of the Results

The result of finite element analysis and loading test have been compared in both failure mode and hysteresis curve.

A.4.1 Failure Mode

The failure mode or deformation type of all specimens is presented in figure below for both analysis and loading test. The specimen model is presented both with the von Mises's stress distribution. Generally three types of fracturing are seen in both cases.

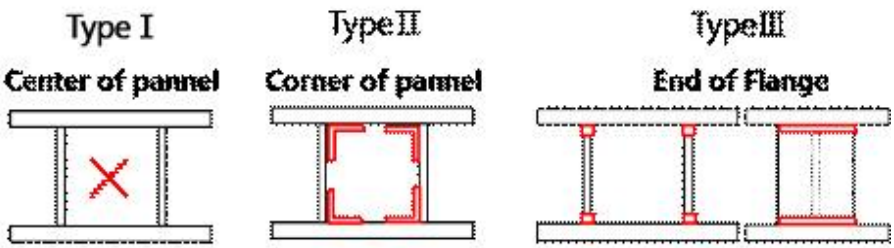

Fig. A.6 Failure Type

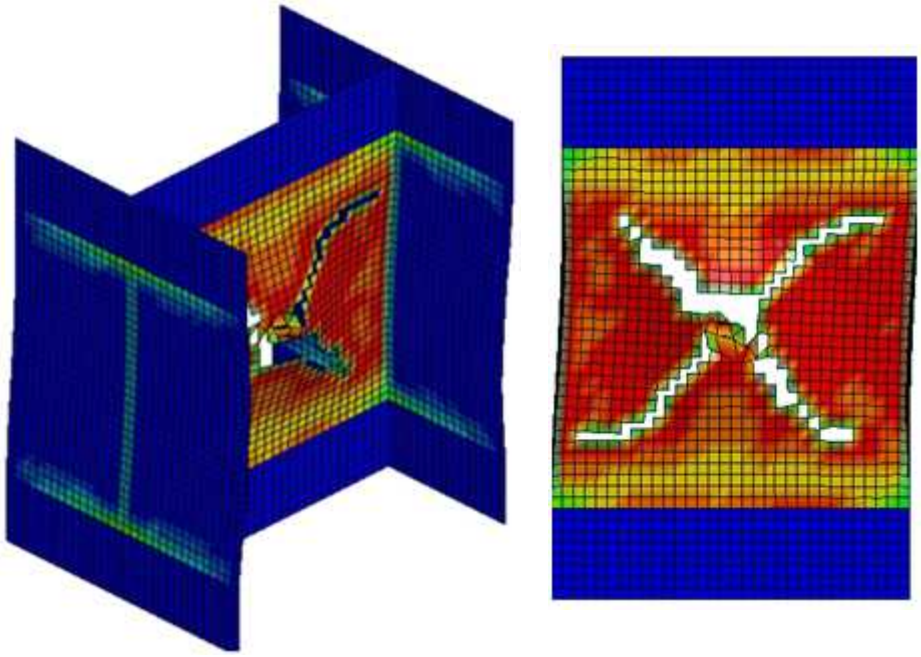

Failure mode and von Mises's stress distribution (L2.0, SLY120)

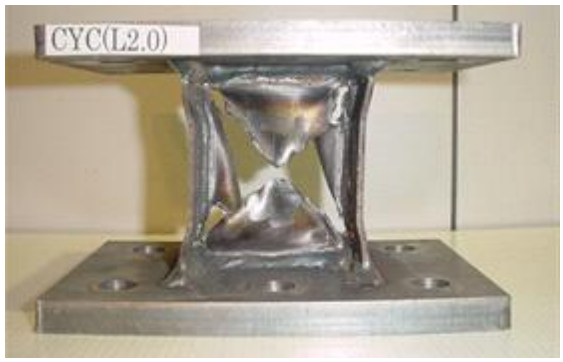

Failure mode of loading test result (L2.0, SLY120)

(a) Type I failure type

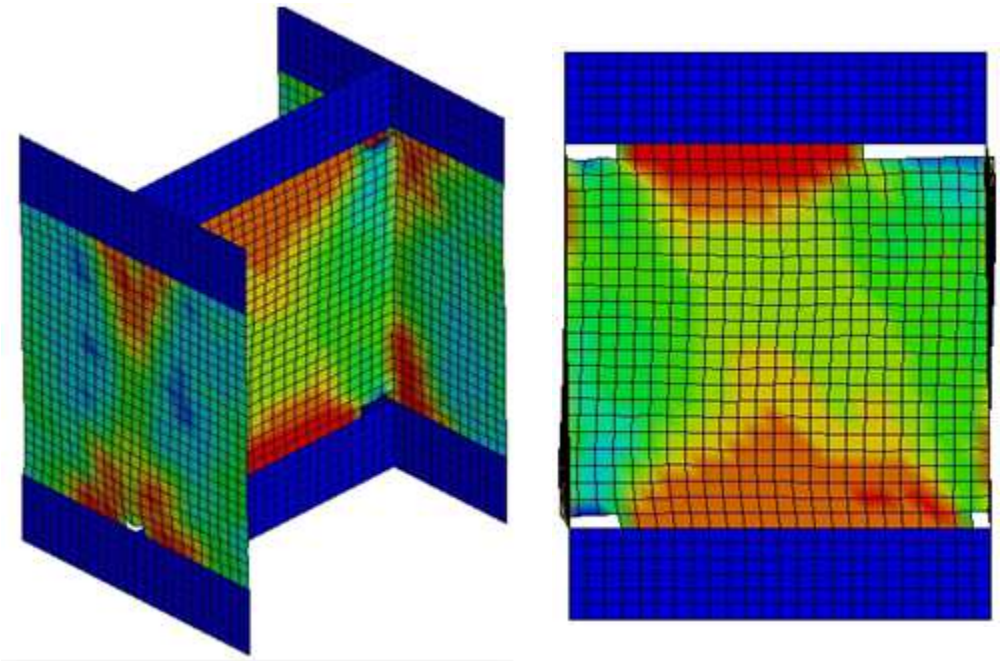

Failure mode and von Mises's stress distribution (L3.2, SLY120)

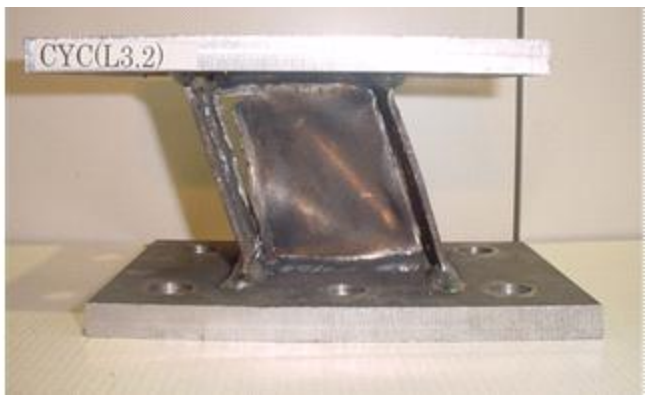

Failure mode of loading test result (L3.2, SLY120)

(b) Type II failure type

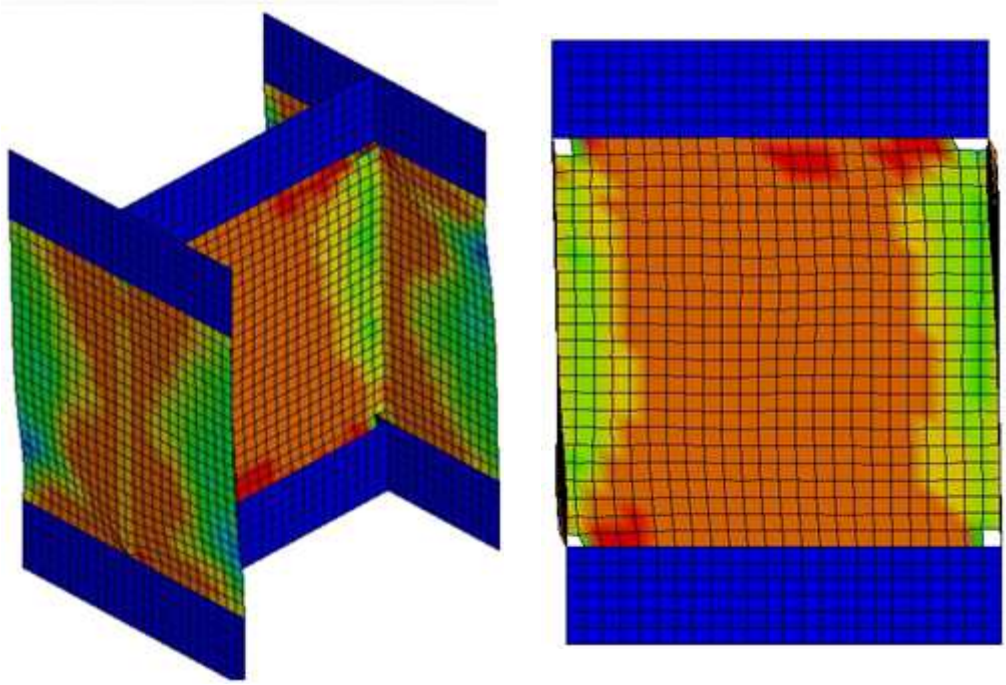

Failure mode and von Mises's stress distribution of analysis result (L4.0, SLY120)

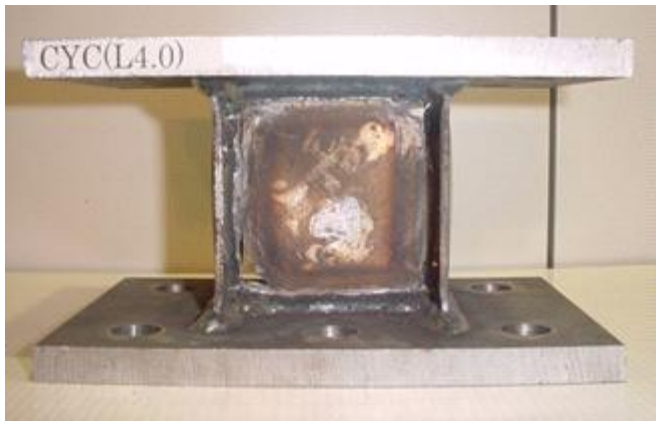

Failure mode of loading test result (L4.0, SLY120)

(c) Type II failure type (L4.0, SLY120)

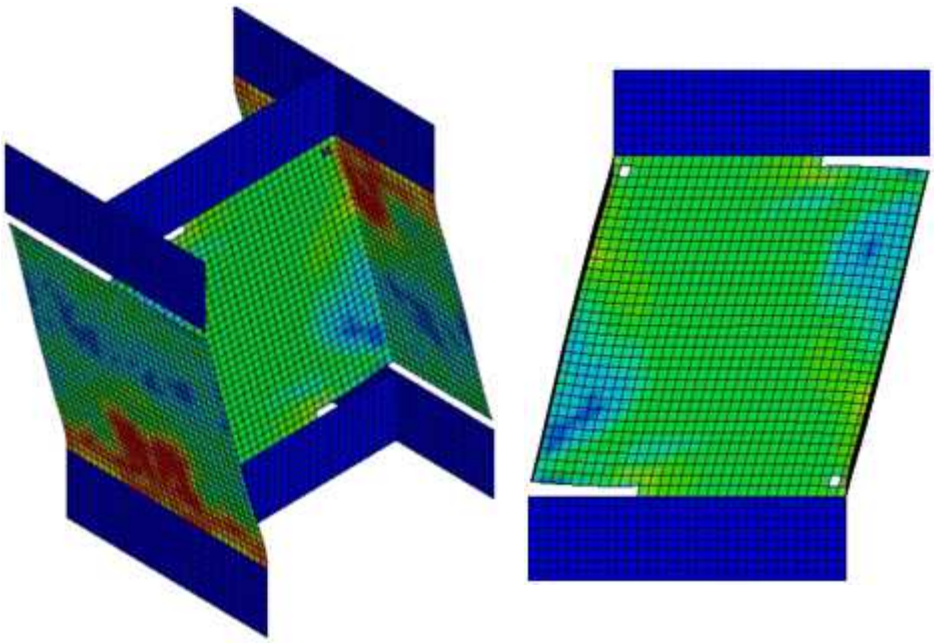

Failure mode and von Mises's stress distribution (L6.0, SLY120)

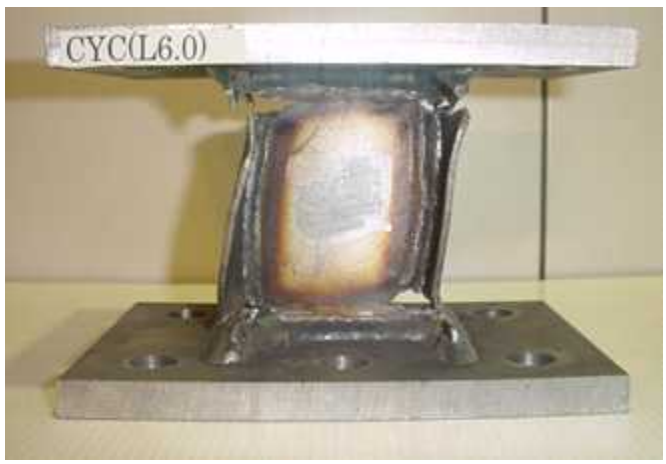

Failure mode of loading test result (L6.0, SLY120)

(d) Type III failure type (L6.0, SLY120)

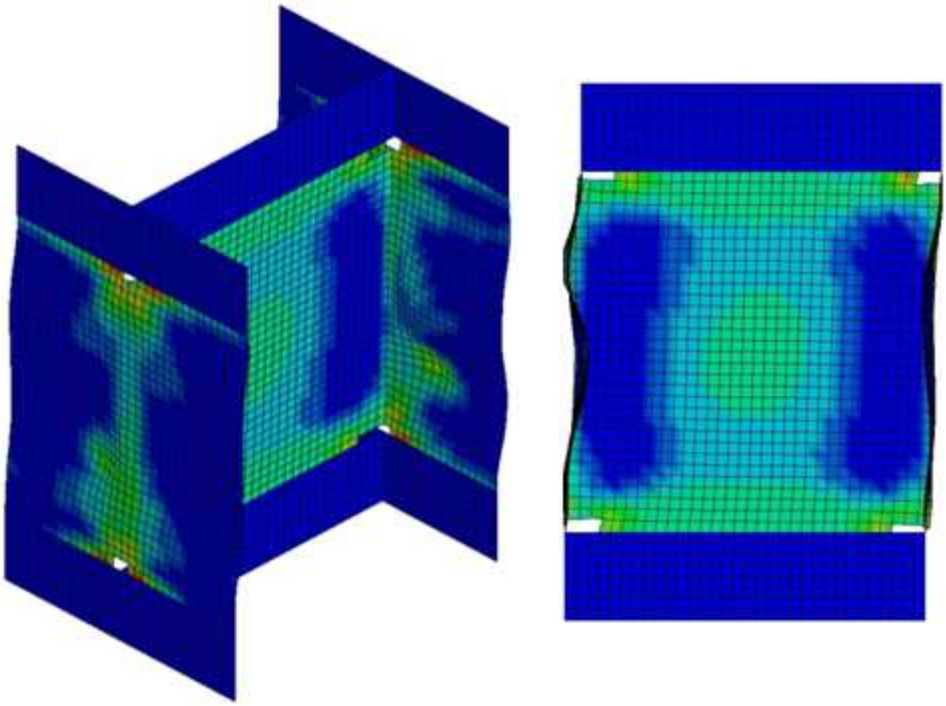

Failure mode and von Mises's stress distribution (L3.5, SS400)

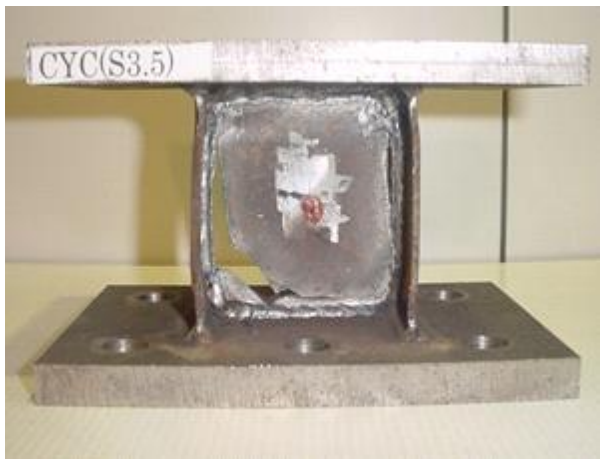

Failure mode of loading test result (L3.5, SS400)

(e) Type II failure type (L3.5, SS400)

Fig. A.7 Failure Modes of Analysis and Test Result

A.4.2 Comparison of Analysis and Test Result Hysteresis Curves

For all the considered specimen the hysteresis loops have been compared for analysis and test results. Generally, form the hysteresis loops we can notice that the shape and the maximum load resisting capacity is same. However, the initial yielding and in each cyclic behavior a slight difference is observed. Low yield steel having thin panel, Fig A.12 (a), the strength value degrades at the initial displacement. This is because of an early yielding of the panel. As the thickness of the panel increases the decrease in the strength at zero displacement becomes slightly. This situation doesn't observed in the conventional steel panel. (Fig A.12 (e). The resisting capacity of conventional steel is high but the deformation capacity is lower than the low yield point steel.

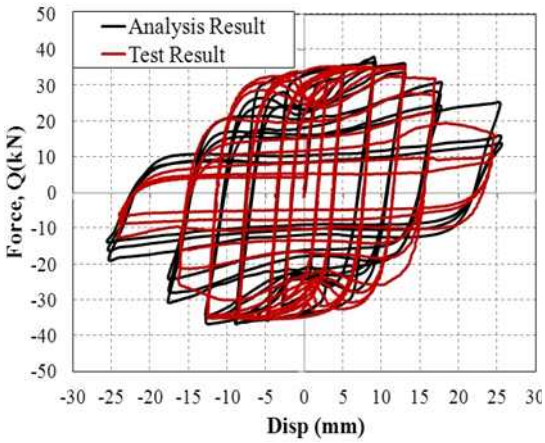

(a). Comparison of the hysteresis loops for specimen L2.0, SLY120

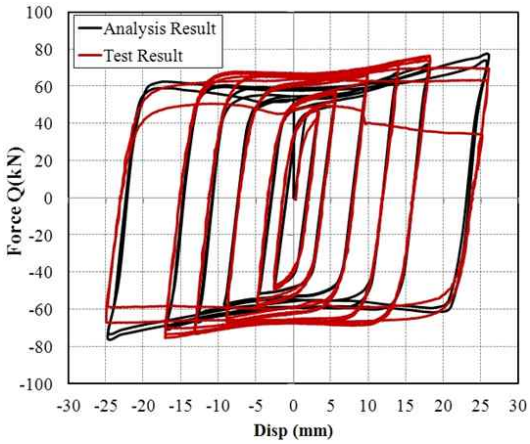

(b) Comparison of the hysteresis loops for specimen L3.2, SLY120

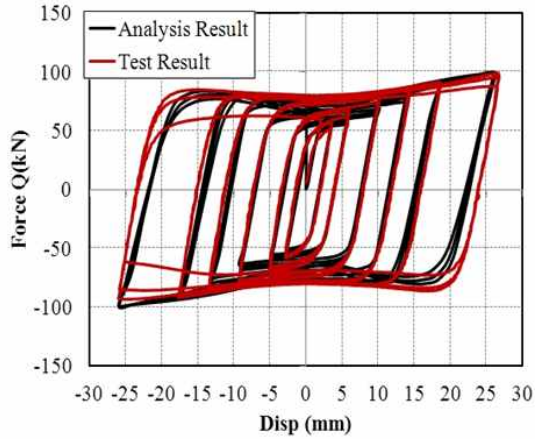

(c) Comparison of the hysteresis loops for specimen L4.0, SLY120

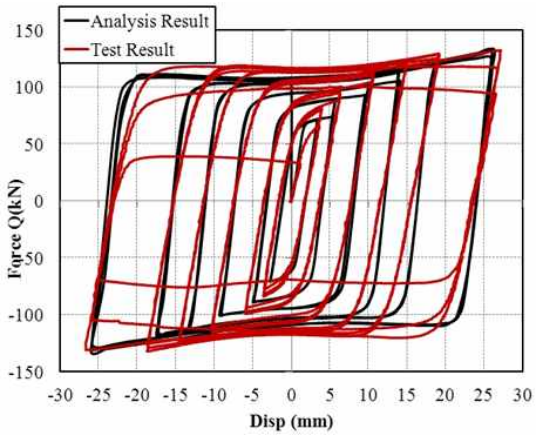

(d) Comparison of the hysteresis loops for specimen L6.0, SLY120

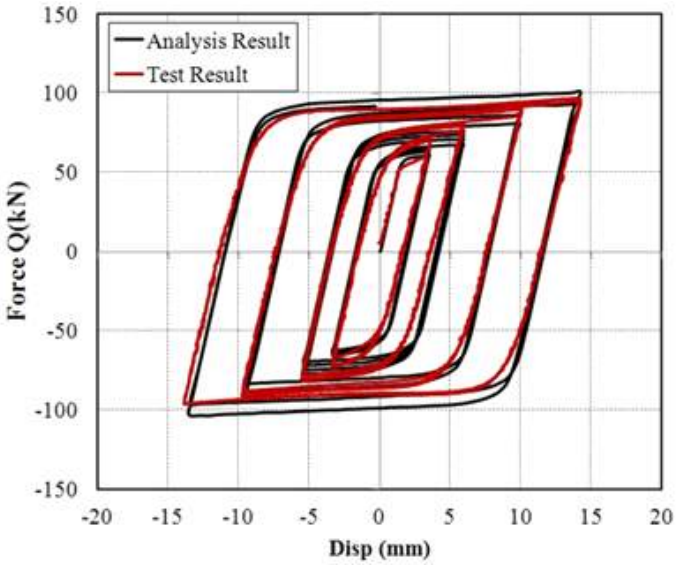

(e) Comparison of the hysteresis loops for specimen L3.5, SS400

Fig. A.8 Comparison of the hysteresis loops for specimen L3.5, SS400

The maximum load monotonic loading test and cyclic loading of test and analysis result as well the failure mode is summarized in table below.

Table A.4 Comparison of Analysis and Test results for yield and maximum forces.

Experiment specimen	Measurement (mm)			Comparison of the Results				Failure Mode
				Monotonic Loading		Cyclic Loading $Q_u(kN)$		
	d	t_p	d/t_p	$Q_y(kN)$	$Q_u(kN)$	Test	Analysis	
L2.0	80	2	40	21.2	35.6	37.46	39.11	Type I
L3.2	80	3.2	25	27.3	62.5	76.58	78.24	Type II
L4.0	80	4	20	34.9	92.3	99.16	98.26	Type II
L6.0	80	6	13.33	49.5	175	132.42	134.14	Type III
S3.5	80	3.5	22.86	51.9	95	96.42	100.38	Type II

A.5 Inelastic Response of Shear Panel Damper

When the shear panel damper is loaded with cyclic load with displacement protocol shown in Fig 5.4, the inelastic response of the damper for one full cycle is represented as in the fig. below.

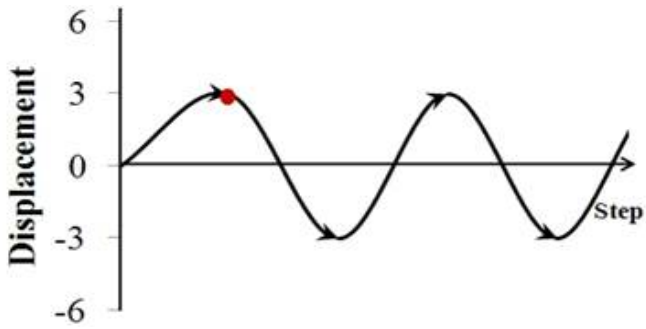

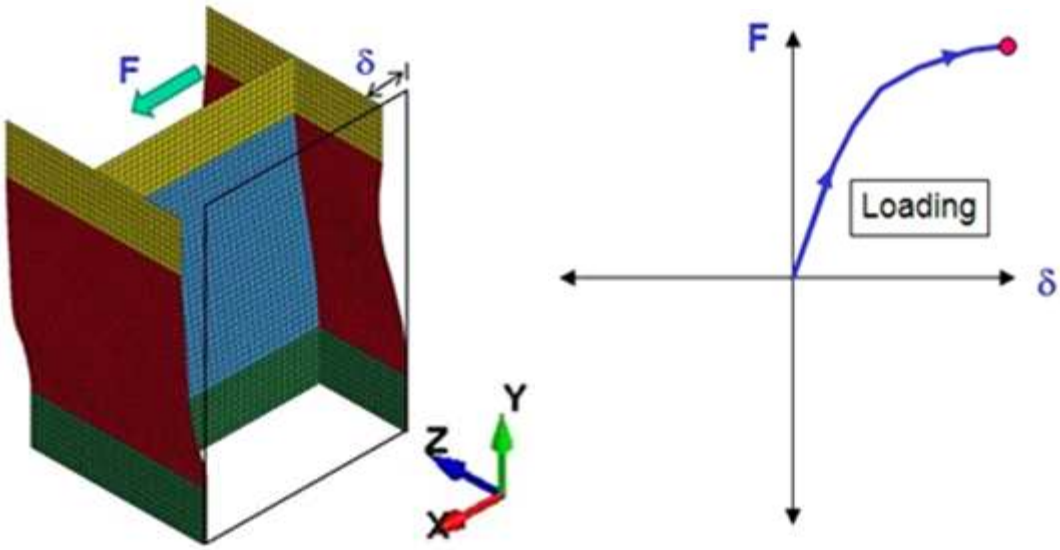

Fig.A.9 Inelastic response under loading

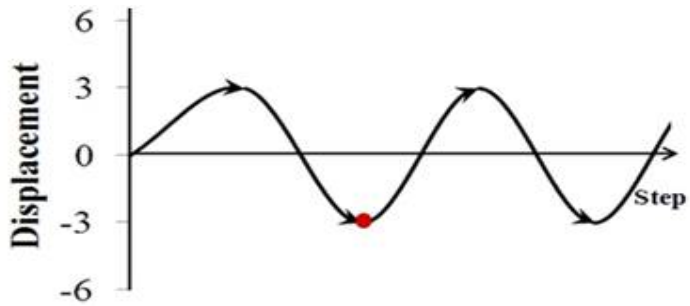

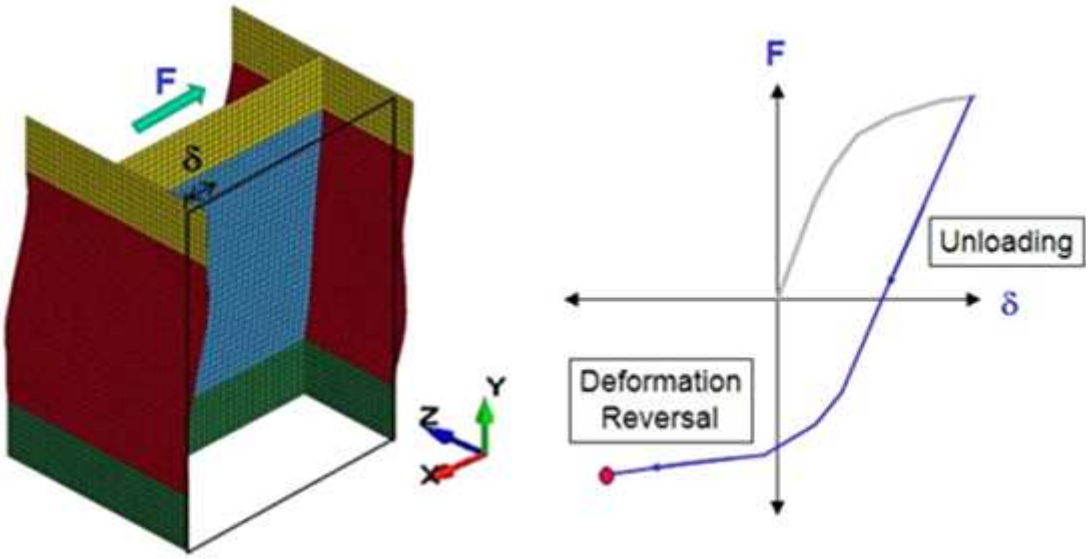

Fig.A.10 Inelastic response under unloading

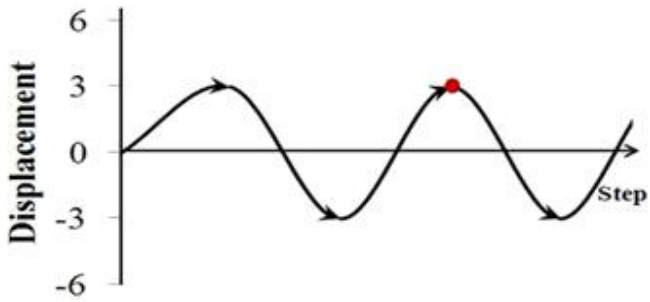

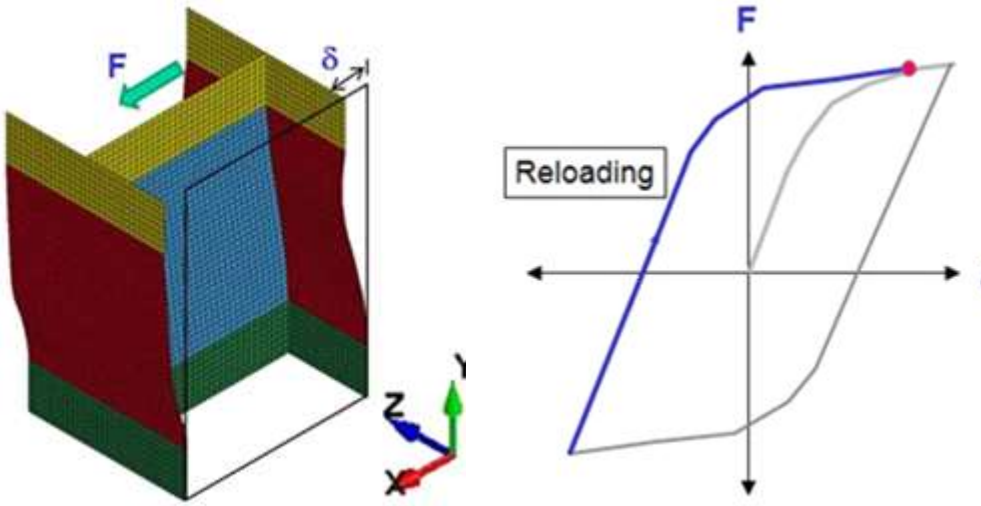

Fig. A.11 Inelastic response under reloading

A.6 Cumulative Energy Dissipation

The area within the hysteresis loop is the energy dissipated BY ONE FULL CYCLE of deformation. The dissipated energy is irrecoverable. The total hysteretic energy dissipation will be the sum of the areas for all loops. The accumulated hysteretic energy dissipation is the total energy dissipated up to some point in time.

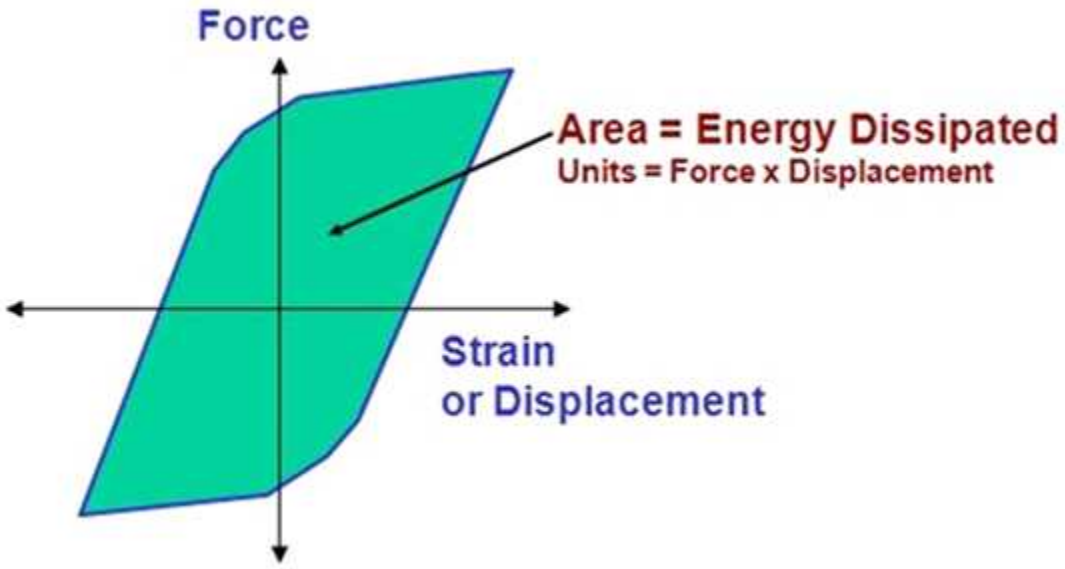

Fig. A.12 One full CYCLE energy dissipation

A.7 Summary

Shear panel dampers with different depth to thickness ratios has been studied in this chapter. It is proved that the low yield point steel has high energy absorption capacity compared to the corresponding equivalent conventional steel.

This is mainly because of low yield point steel has high elongation capacity than the common steel which have high load resisting capacity.

The failure mode as well as the hysteresis loops was identified. Three different types of failure mode was observed. In both test and analysis result of hysteresis loops low yield point steel has high cyclic deformation capacity.

APPENDIX B
INELASTIC RESPONSE OF CIRCULAR PIPE STEEL DAMPER

B.1 Introduction

Many studies have been conducted on seismic controlled structures, and many seismic response control techniques have been proposed. Among these techniques improving damping performance of a building means fitting mechanism that artificially absorbs vibration energy. Various energy absorbing devices have been designed and used for seismic response control. Steel dampers are among these energy absorbing devices designed by different types of structural steels. These steels are of different types depending on the chemical composition and mechanical properties. The advance of steel production has made the new structural steel available; Low Yield-Point Steel (LYP steel) possesses extremely low yield strength and high elongation properties. It is obvious that steels used as hysteresis dampers must become plastic in an earthquake prior to other structural members, such as columns and beams, at designed stress level. Since steel dampers, in earthquake, are exposed to repeated high plastic strain; consequently, low fatigue properties are important. Circular pipe steel damper (CPD) is one of energy dissipating device used in a base of building structures (under column member). CPD devices dissipate energy passively based on plastic yielding and nonlinear shear deformation in metal materials. Of course the energy dissipation capacity is not much but can resist load in all direction. Its energy dissipation capacity depends crucially on plastic deformation and fatigue resistance especially at around the welded part. As the action force during earthquake is so multi-dimensional, the CPD can resist load in all directions, as its advantage of using CPD among other

types of steel dampers. The stresses developed in the cross section during loading are: bending, shear stress as well as combined bending and shear stresses depend on the size and shape (diameter to the depth ratio) of the CPD. In this paper, it studied circular pipe steel damper for both conventional steel and low yield point steel using Experimental and nonlinear FE analysis.

B.2 Properties of Specimen

B.2.1 Chemical Composition

The chemical composition of steel used, SS400 equivalent to ASTM A36 and LYP100, are shown in table 1. The composition affects the yield strength only through the variation in alloying elements such as carbon (C), silicon (Si), manganese (Mn), phosphorus (P), sulfur (S) and nitrogen (N).

Table B.1. Chemical compositions of steel used in this study.

Material	C	Si	Mn	P	S	N
SS400	0.13	0.01	0.47	0.011	0.009	-
LYP100	≤ 0.01	≤ 0.03	≤ 0.2	≤ 0.025	≤ 0.015	≤ 0.006

B.2.2 Mechanical Properties

To measure the mechanical property of steel used in this paper, tensile strength (coupon test) was carried out. The mechanical properties, yield strength, ultimate strength and elongation, of the tensile test result are shown in table2. The stress-strain relationship from the tensile strength test is also obtained as shown in fig. 1 for both conventional (SS400 steel) and LYP100 steel.

Table B.2 Mechanical Properties of Specimens (coupon test result)

Material	Yield Strength σ_y (MPa)	Ultimate Strength σ_u (MPa)	Elongation (%)
SS400	369	411	13.1
LYP100	202.6	265.4	-

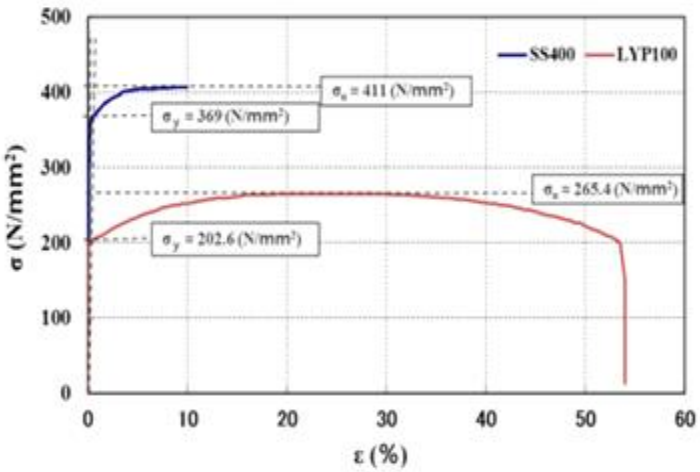

Fig. B.1 Stress-strain curve of test result.

B.3 Theoretical Equations

Theoretically the whole system of CPD is considered as a fixed ended beam as presented in fig. 2. The bending stress distribution and shear stress distribution on the cross-section is shown in fig. 3(a), (b) respectively. The optimum and economical use of material size is determined. The bending stress and shear stress as well as the stiffness are derived as follows.

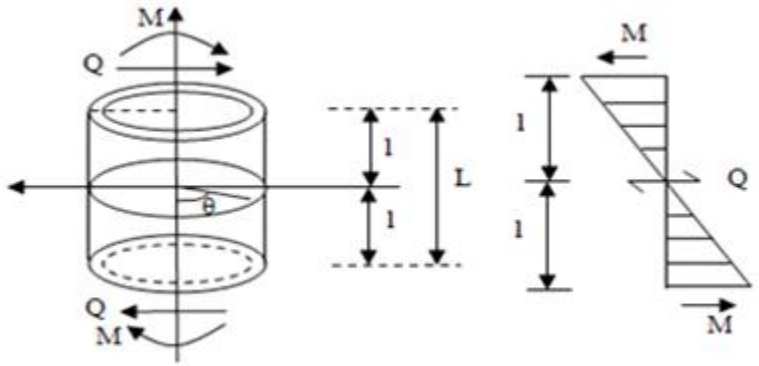

Fig. B.2 (a) Loading condition under shear

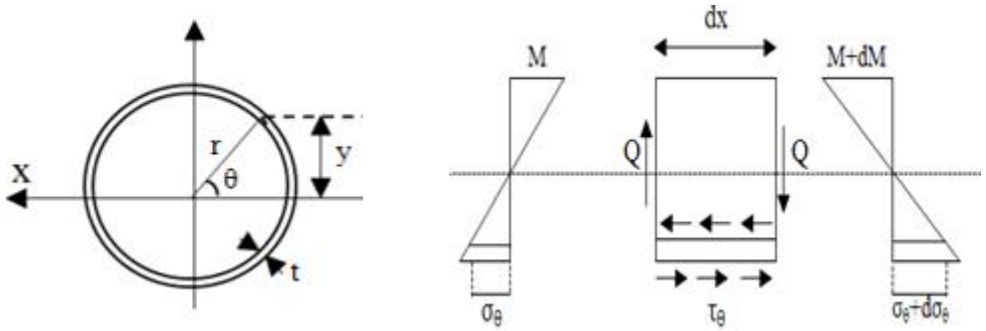

(a) cross-section of the stress distribution

(b) cross-section of shear stress distribution

Fig. B.3 Stress distribution

The bending stress on the cross-section is given by:

$$\sigma_\theta = \frac{M}{I} y \tag{B.1}$$

$Where,\ y = r sin\theta, \text{and}\, I = \pi r^3 t$ So that the bending stress will be:

$$\sigma_\theta = \frac{M}{\pi r^2 t} sin\theta \tag{B.2}$$

The maximum bending stress is found at $\theta = \frac{\pi}{2}$, substituting θ in equation (6.2):

$$\sigma_{max} = \frac{M}{\pi r^2 t} \tag{B.3}$$

Whereas the shear stress (τ) is defined as:

$$\tau_\theta = \frac{Q r^2}{I_x} cos\theta \tag{B.4}$$

substituting for $I = \pi r^3 t$ and $Q = \frac{M}{l}$ in the above equation, the shear stress will be:

$$\tau_\theta = \frac{M}{\pi r t l} cos\theta \tag{B.5}$$

The shear stress is maximum for Θ = 0^o, at which the cosΘ = 1, then

$$\tau_{max} = \frac{M}{\pi r t l} \tag{B.6}$$

The uni-axial and shear yield stresses for the von Mises criterion [7]are related by:

$$\sigma_y = \sqrt{3}\,\tau_y \tag{B.7}$$

Substituting equation (2) and (4) to equation (5) we can have $\sqrt{3}=\frac{l}{r}$, this section is considered as the optimum and economical use of material at which both bending and shear stresses are occurred simultaneously. It can be summarized as:

$$\frac{l}{r}=\frac{L}{D}=K \qquad \text{(B.8)}$$

Depending on the aspect ratio CPD can be classified as: bending stress, shear stress and combined bending and shear stress resisting damper for $K>\sqrt{3}$, $K<\sqrt{3}$ and $K=\sqrt{3}$ respectively. The analysis and test was conducted taking as a reference, i.e. for values less than $\sqrt{3}$ for K = 1 and greater than $K=\sqrt{3}$ for K = 2 as listed in table 4.

To derive the deformation and stiffness consider the fig. 4. In this fig. it is obvious that L: the total length ($L = 2l$) and D: is the diameter ($D = 2r$)

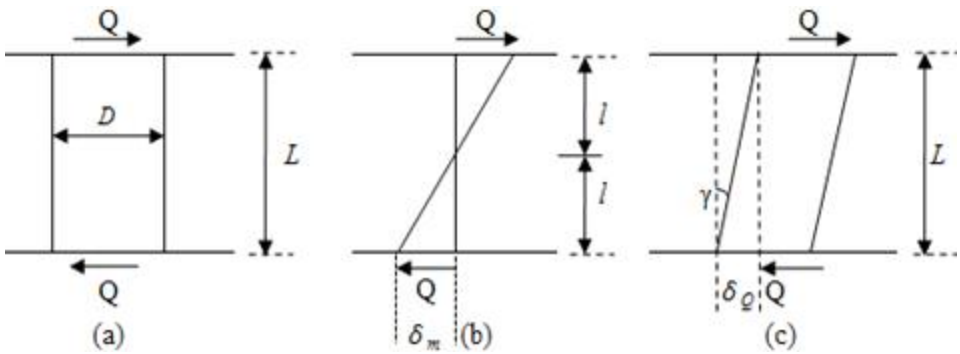

(a) Loading condition of CPD (b) bending deformation (c) shear deformation

Fig.B.4 Loading Condition and Deformation mode

The bending deformation is given by:

$$\delta_m = \frac{Q.(2l)^3}{12EI} = \frac{2Ql^3}{3EI},\ Q = \frac{M}{l} \tag{B.9}$$

At yield state,

$$\sigma_{\max} = \sigma_y = \frac{My}{\pi r^2 t} \Rightarrow M_y = \sigma_y \pi r^2 t. \tag{B.10}$$

Form this the shear force at yield state is derived as:

$$Q = \frac{M_y}{l} \Rightarrow Q_y = \sigma_y \frac{\pi r^2 t}{l} = \frac{1}{K}\pi r t \sigma_y. \tag{B.11}$$

where $K = \frac{l}{r}$

The shear deformation from fig. 4 is calculated as:

$$\delta_Q = 2\gamma l. \tag{B.12}$$

The shear stress at $\theta = 0$ is:

$$\tau = \frac{M}{\pi r l t} = \frac{Q}{\pi r t}. \tag{B.13}$$

The shift angle (γ) is given by:

$$\gamma = \frac{\tau}{G}. \tag{B.14}$$

Thus, the shear deformation will be:

$$\delta_Q = \frac{2K}{G\pi t} Q. \tag{B.15}$$

The maximum shear stress from equation 6.7:

$$\tau_{\max} = \frac{\sigma_y}{\sqrt{3}} = \frac{M_y}{\pi r l t} = \frac{Q_y}{\pi r t} \tag{B.16}$$

Then the shear force will be:

$$Q_y = \frac{1}{\sqrt{3}} \pi r t \sigma_y \tag{B.17}$$

Total deformation, which is the sum flexural and shear deformation, is given as:

$$\delta = \delta_m + \delta_Q = \frac{2K}{E\pi t} \frac{1}{3} K^2 + 2(1+\nu) Q \tag{B.18}$$

The initial stiffness is given by:

$$k = \frac{Q}{\delta} = \frac{3E\pi t}{2KK^2 + 6(1+\nu)} \tag{B.19}$$

B.4 Non-linear FEM analysis

B.4.1 Material Model

Non-linear analysis was carried out with reasonable accuracy with low yield point steel and conventional steel. During analysis of steel deformation elastoplastic modeling are widely used and here it is considered large deformation kinematics to simulate the residual displacement. Of course, without large deformation kinematics, the deformation behavior cannot be predicted in the analysis model. The strain hardening behavior of steel was considered and a simplified bilinear hardening model is used to describe the stress-strain relationship in steel for analysis. Fig. 5 shows a schematic of the bilinear model of a kinematic hardening. The analysis models have components consisting of a circular pipe (the specimen) and end plates. The specimen was modeled by low yield point steel (LYP100) and conventional steel (SS400) with different aspect ratios (and end plates are modeled by SS400 steel; the detail dimensions for is shown the figure 5.

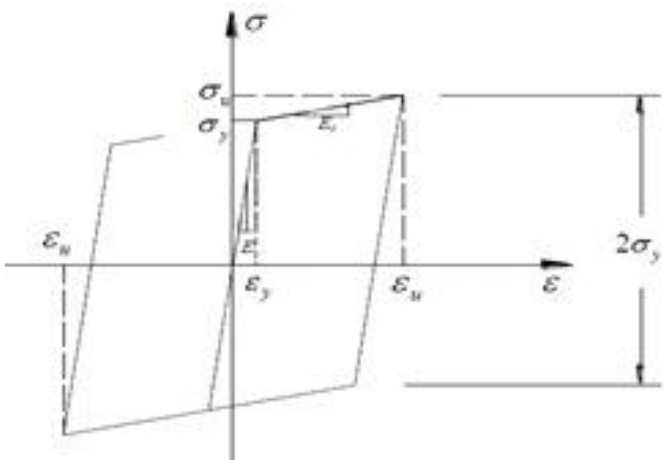

Fig. B.5 Bilinear model with a kinematic hardening

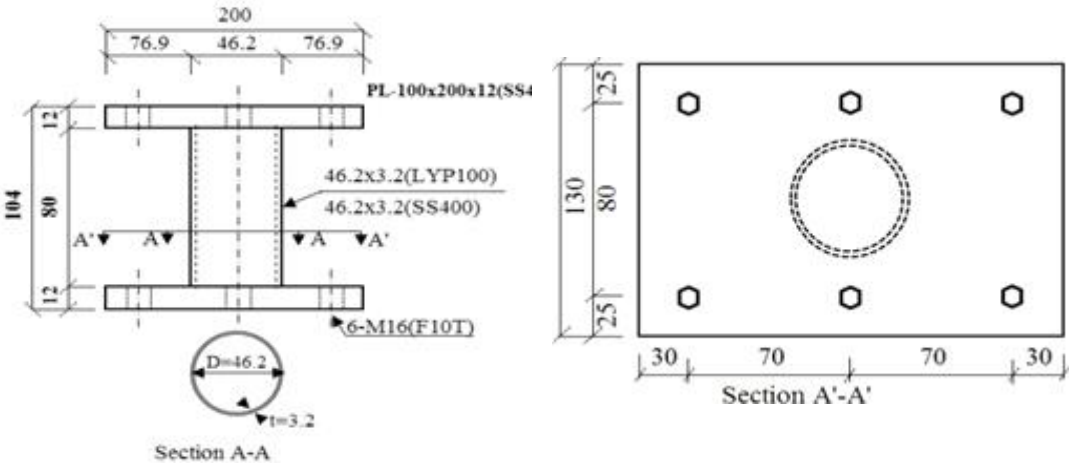

Fig. B.6 Detail dimension of specimen for K= $\sqrt{3}$ (K= H/D)

Table B.3. The physical property of specimen used in the analysis is presented as:

Property	Specimen (SS400)	Specimen (LYP100)	End plate (SS400)
Young's Modulus	205GPa	205GPa	205GPa
Poison's ratio	0.3	0.29	0.3
Density (kg/m3)	7860	7800	7860
Yield Strength (MPa)	369	202.6	369
Yield Strength (MPa)	369	202.6	369

B.4.2. Loading and Constraint Condition

The constrained condition of analysis is modeled to have a shear effect on the specimen; the lower end plate was constrained translation and rotation. Whereas the upper end plate was constrained rotation in all direction. Translation is allowed on the upper plate in the Y-axis (loading direction), constraint in other direction. The displacement control of loading system is shown in the fig. B.8 for both analysis and experimental simulation.

B.5. Experimental Process

To verify the analysis model, a serious of experiments has been carried out. Fig. 6 shows a loading experiment equipment system. In this system, to avoid rotation angle on the top of specimen pantograph was installed and counter weight installed using a principle of a pair of scale was arranged to protect axial force application to experiment specimen. Displacement meters for measuring displacement of circular pipe dampers were installed at the top end plate and the bottom end plate of the experiment specimen. Average value of the right and left side displacement devices was evaluated as displacement value of the experiment specimen. In addition, horizontal force on the experiment specimen was measured by installing load cell on the actuator.

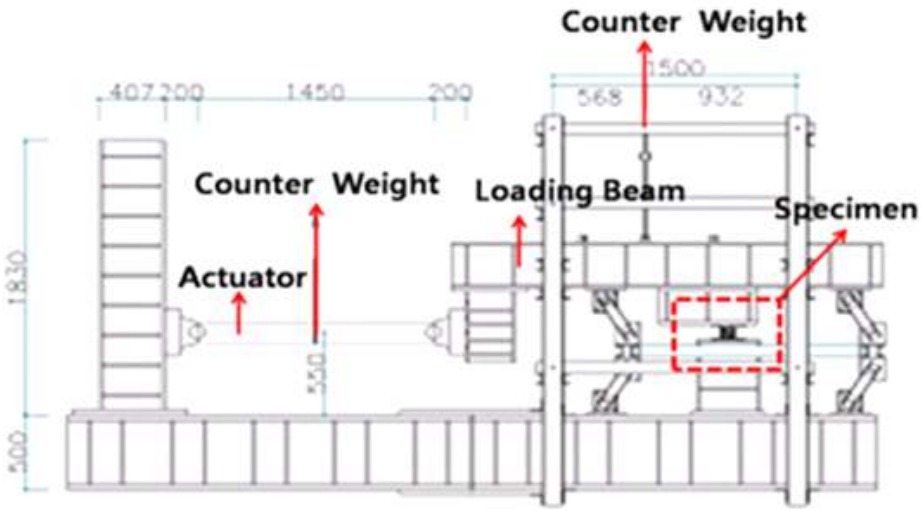

Fig. B.7. Schematic illustration of circular pipe steel damper tasting set up

For monotonic and cyclic loading during test two conditions are considered; type 1 and type 2 as shown in table 4 for all aspect ratios. In cyclic loading was carried out by controlling the displacement, shown in fig. 7, for all specimens.

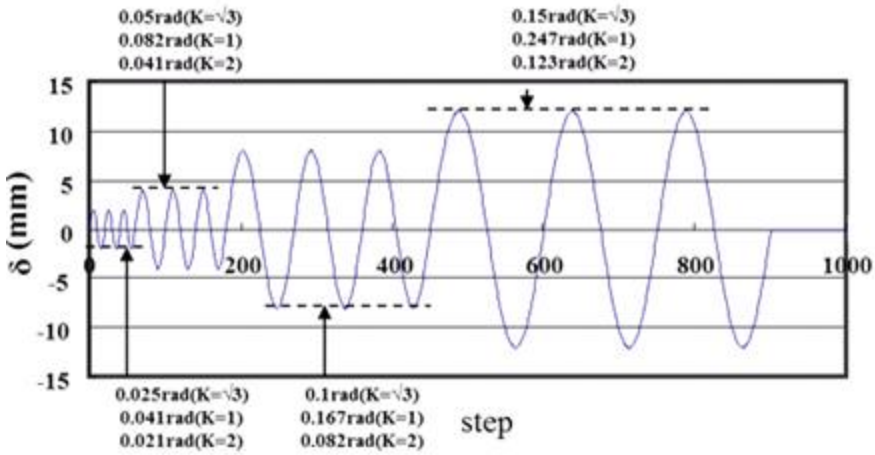

Fig. B.8. Displacement protocol

Table B.4 the two cases of experiment considered.

Type	Loading type	Test Code	Material type	Aspect ratio K(H/D)	Dimension (HxD) mm
1	Monotonic loading (loaded up to 35mm)	MSK-1	SS400	1	48.6x48.6
		MSK-2		$\sqrt{3}$	80x48.6
		MSK-3		2	97.2x48.6
		MSK-4	LYP100	$\sqrt{3}$	80x46.2
2	Cyclic loading (loaded up to 12mm)	CSK-1	SS400	1	48.6x48.6
		CSK-2		$\sqrt{3}$	80x48.6
		CSK-3		2	97.2x48.6
		CSK-4	LYP100	$\sqrt{3}$	80x46.2

Table B.5 Initial stiffness and plastic displacement of test result

Type 1	Steel grade	Aspect ratio K(=H/D)	Initial stiffness Test result k (kN/cm)	Plastic displacement δ_y (cm)oftestresult
	SS400	1	1765.7	0.04
	SS400	$\sqrt{3}$	1099.95	0.05
	SS400	2	901.6	0.06
	LYP100	$\sqrt{3}$	1822.2	0.0636

B.6. Results and Discussions

B.6.1 Deformation Shape

Monotonic loading and cyclic loading test result is shown in figure 8 and 9 respectively. The relationship between the applied shear force Q and strain ɣ at maximum resistant under monotonic loading is shown in table 6. As seen from the figures in both monotonic and cyclic loading though the best size and shape of the specimen determined theoretically was, the result shows K = 1 is more capability of resistance and deformation capacity. This is mainly because of the loading was pure shear and so that K = 1 is more effective for such loading style. However, it is expected in real situation that specimen with is the best as it is believed to resist both bending and shear stresses. The LYP100 has more plastic deformation capacity compared to conventional steel. As is observed in fig. 8 (d) the resisting capacity compared to the equivalent size specimen of SS400 steel but the deformation capacity higher and higher in case of LYP100 specimen.

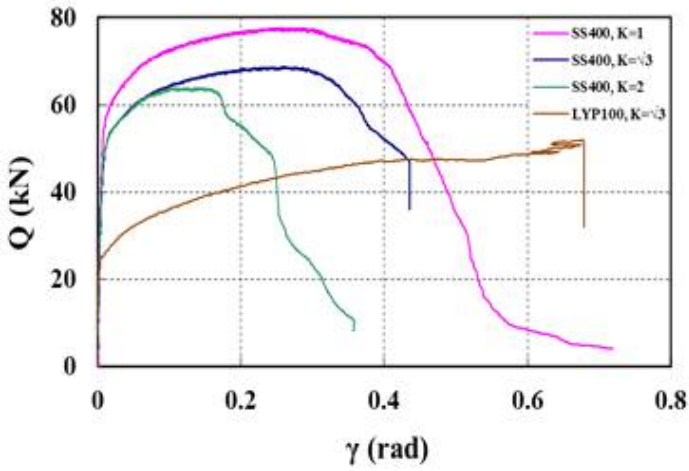

Fig. B.10. Test result for monotonic loading

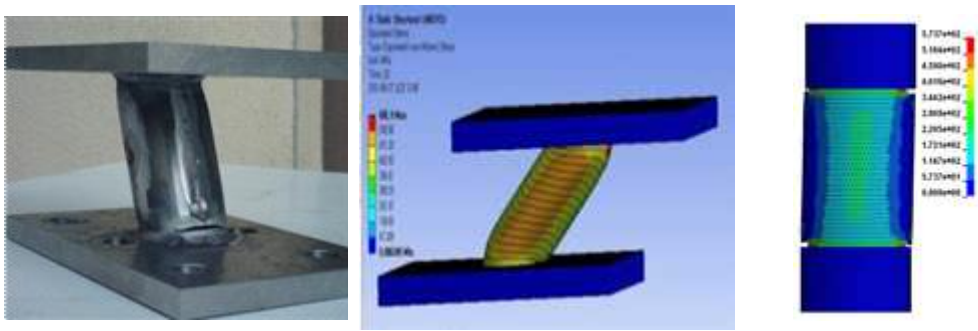

Test result Implicit Analysis Explicit Analysis

(a). Deformation Shape Result for K=1, SS400 steel

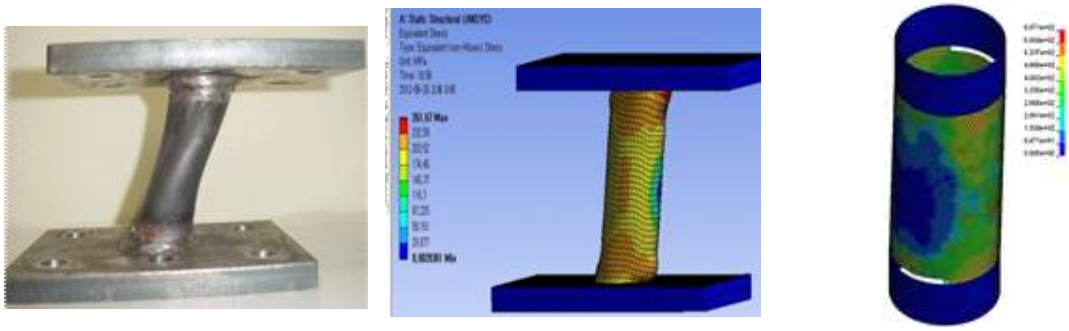

Test result Implicit Analysis Explicit Analysis

(b). Deformation Shape Result for K= $\sqrt{3}$, SS400 steel


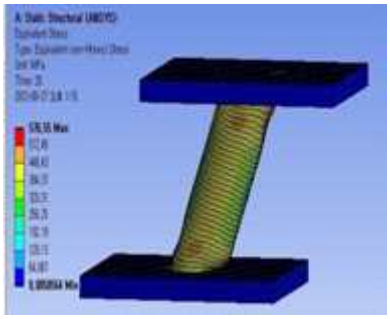
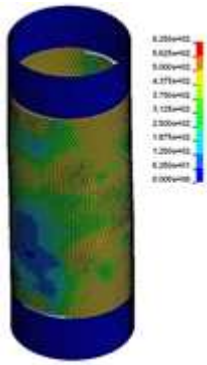

Test result Implicit Analysis Explicit Analysis

(c). Deformation Shape Result for K=2, SS400 steel

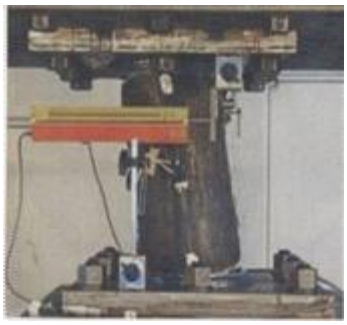
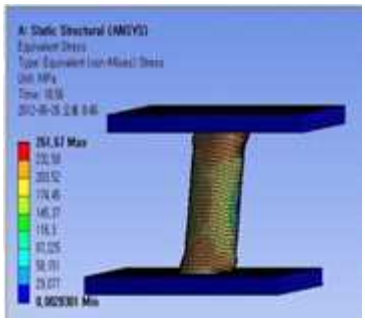
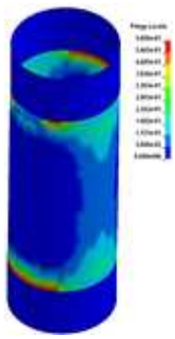

Test result Implicit Analysis Explicit Analysis

(d). Deformation Shape Result for K= $\sqrt{3}$, LYP100 Steel

Fig. B.11. Deformation Shape Results of Circular pipe damper

B.6.2 Hysteresis Curve

The hysteresis loops of all results have been compared. The explicit nonlinear analysis better to evaluate the hysteresis characteristics of circular pipe damper compared to implicit nonlinear analysis carried out by ANSYS workbench. This mainly because of the governing hardening behavior of steel material is the combined hardening model. ANSYS workbench lacks this option it has bilinear isotropic and kinematic and multi linear isotropic and kinematic hardening model. In

this study (Appendix A and B) is observed that low yield point steel has more isotropic behavior compared to that of common steel. For instance, in the analysis specimen of Appendix A, the hardening parameter for common steel is 0.25, whereas low yield point steel is 0.5, which is relatively close to 1.

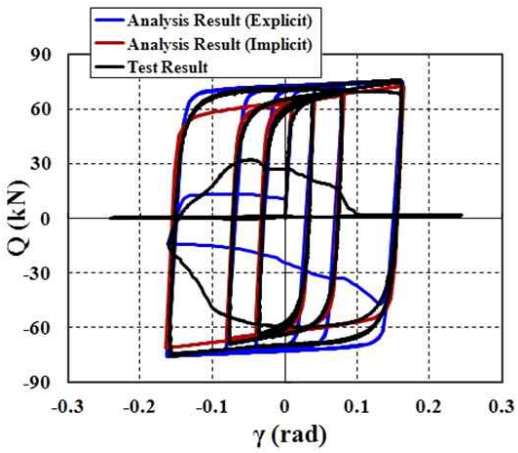

(a) Hysteresis loop result of K=1, SS400

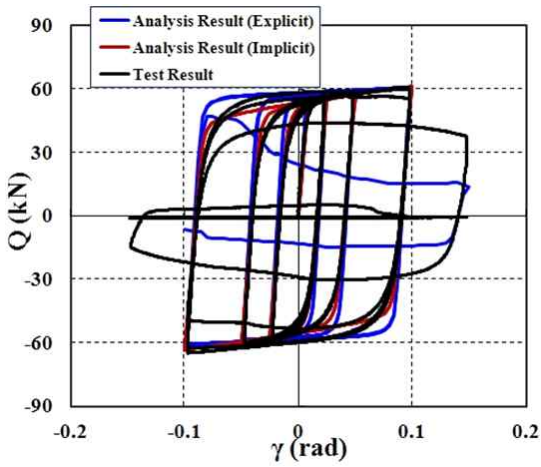

(b) Hysteresis loop result of K= $\sqrt{3}$, SS400

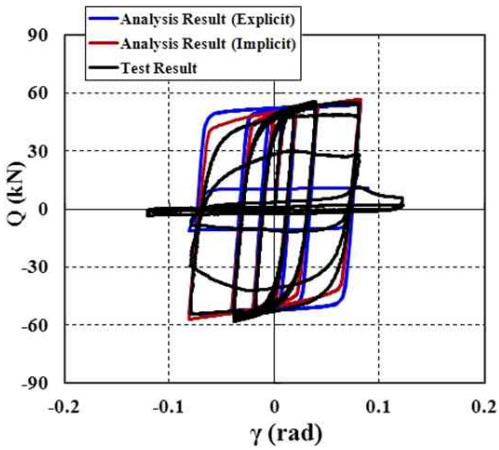

(c) Hysteresis loop result of K=2, SS400

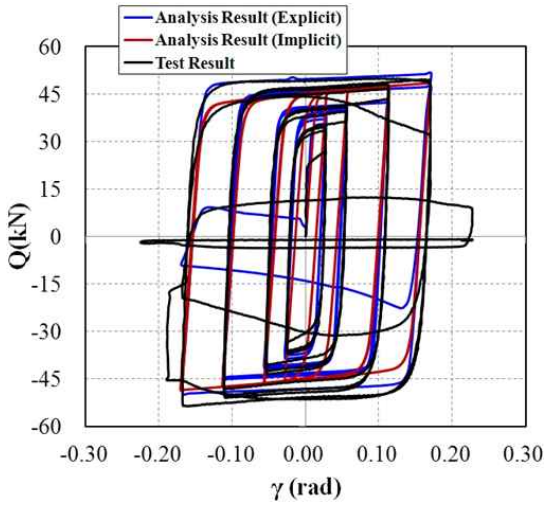

(d) Hysteresis loop result of K= $\sqrt{3}$, LYP100

Fig. B.12. Comparison of Test and Analysis (Explicit and Implicit) Hysteresis Loop Results

B.8 Summary

This paper attempts to evaluate the structural performance and hysteresis behavior of circular pipe steel damper with SS400 and LYP100 steel. The main conclusion is drawn as follows:

The most effective material use and optimum size of circular pipe steel damper though predicted equation is found to be for aspect ratio of.

The plastic deformation capacity and energy absorption capacity of the damper has been evaluated both experimentally and analytically. The lower the aspect ratio the higher the strength so energy absorption capacity but lower plastic deformation capacity.

The plasticity rate and plastic deformation capacity of LYP100 steel damper is higher than the corresponding equivalent SS400 steel damper. In addition to deformation capacity, the energy absorption capacity of LYP100 steel corresponding to SS400 steel is higher.

APPENDIX C
IMPERFECTION IN MODELLING STEEL MEMBERS

C.1. Introduction

Ideal solids does not exist. All contain various defects or imperfections. Several different imperfections: variance of dimensions of a structure or a member, lack of verticality of a structure and straightness or flatness of a member point defects, linear defects interfacial defects (boundaries).

Random geometrical imperfections are natural in structures. This imperfection is on both structural instability and geometrical imperfection. The initial imperfections used to be ignored in structure strength analysis and thus geometric-perfect models were used in most case of numerical simulation. However, collapse of axially compressed H-section is not such a case. Both initial geometrical imperfection and initial instability of column member is sensitive as we noticed from the result obtained. H-section column members tend to buckle in almost in the same mode with that of experimental compression test result.

C.2 Imperfection in Column Member

In column members initial stability considered by introducing an initial displacement of approximately $\delta = L/1000$ at critical part. For both end pinned condition the initial displacement is introduced at the central part as shown in the Fig. below.

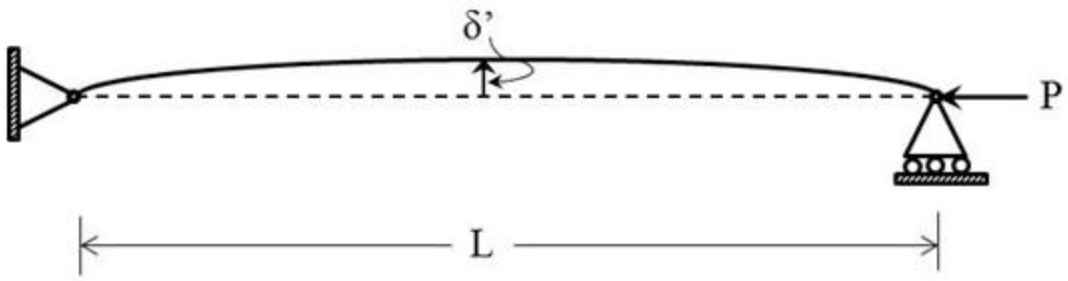

Fig. C.1 Initial instability in column under compression loading

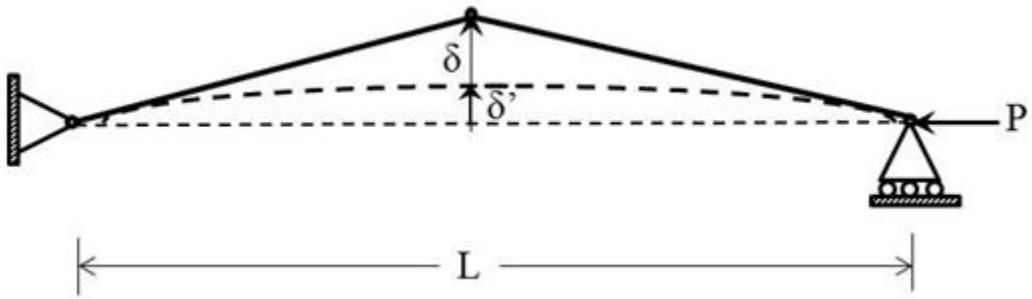

Fig. C.2. Buckling of a simply supported beam of length L with a plastic hinge at mid length.

The relationship between load and displacement is also expressed taking in to account the initial displacement.

$$P = \frac{2M_p}{\sqrt{(L-\delta')^2 - (L+\delta)^2}} \qquad \text{(C.1)}$$

where M_p is the plastic moment of the beam section (which depends on section shapes and material properties), δ' is the shortening of the beam length due to axial compression and bowing, δ is the prescribed displacement and P is the reaction force corresponding to δ. Eq. (2) can be derived from the simple conceptual model in Fig. C.2.

C.3. Non-linearity in FEA

From the finite element point of view, an element whose stiffness matrix is not constant is a nonlinear finite element. Equation 2.1 expresses a one degree of freedom13 representation of a nonlinear finite element model.

$$P = K(u)u \tag{C.2}$$

where u = displacement

P = external load

K(u) = stiffness which is a function of the displacement u

Cook et al. (1989) classified the nonlinearities in two main categories:

- Geometric nonlinearity due to large displacements.
- Material nonlinearity due to changes in the material properties.

Bathe (1995) divided geometric non linearities in two groups:

- Geometric non linearities with small strains: displacements and rotations may be large, but strains are small.
- Geometric non linearities with large strains: displacements, rotations, and strains may be large

The material law can be either linear or nonlinear in both cases. Figure 2.2 illustrates the two geometric nonlinearities.

As a direct consequence of geometrical non linearity, the stiffness matrix of the finite element model is not constant, it is a function of the residual displacements. Therefore, an iterative procedure is required to obtain the equilibrium state. For a given load there are two main formulations depending on the configuration to

which the variables involved in each step are referred: (1) the total Lagrangian formulation where all variables are referred to the initial configuration; and (2) the updated Lagrangian formulation where all the variables are referred to the configuration at the beginning of the load step considered.

The nonlinear finite element analysis consists of a series of linear analyses resulting in successive approximations of the equilibrium state. Hence, it is more time consuming than linear analysis. Although nonlinear analysis has become more feasible with the introduction of powerful computers, it still requires a considerable investment of computer time.

There are several approaches to perform a nonlinear finite element analysis. Most of them divide the total load in steps to track the equilibrium paths. The Newton-Raphson method is widely used in nonlinear analysis. The equilibrium point is approached by successive approximations to reduce the unbalanced load (difference between the applied and the internal nodal forces) in each iteration. The following expressions relate the displacement variation with the unbalanced load.

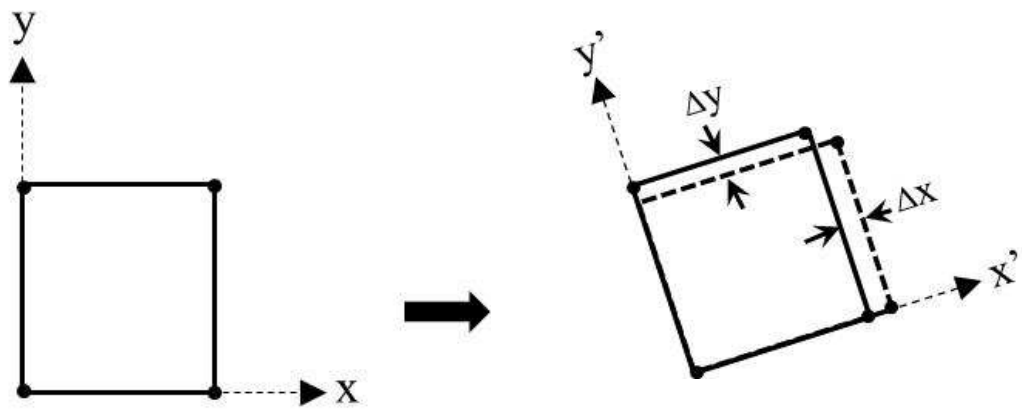

(a)

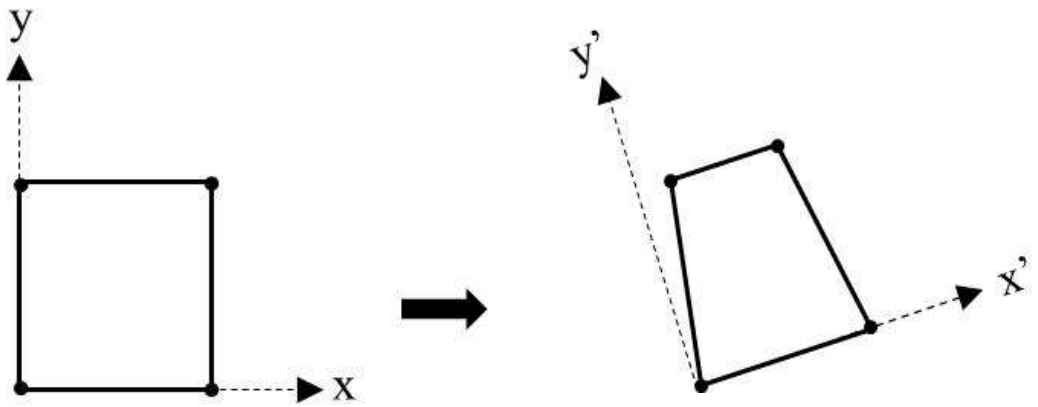

(b)

Fig. C.3. Geometric non linearities in a finite element: (a) large displacements, small strains; (b) large displacements, large strains.

$$k_t \triangle u_i = P_B - P_A \qquad \text{(C.3)}$$

where

k_t = tangent stiffness matrix

$\triangle u_i$ = displacementincrementoftheiteration“i”

P_B = applied load

P_A =nodal force

(P_A,u_A) = reference equilibrium state

Graphical representation of the Newton-Raphson is shown in Fig. C.3.

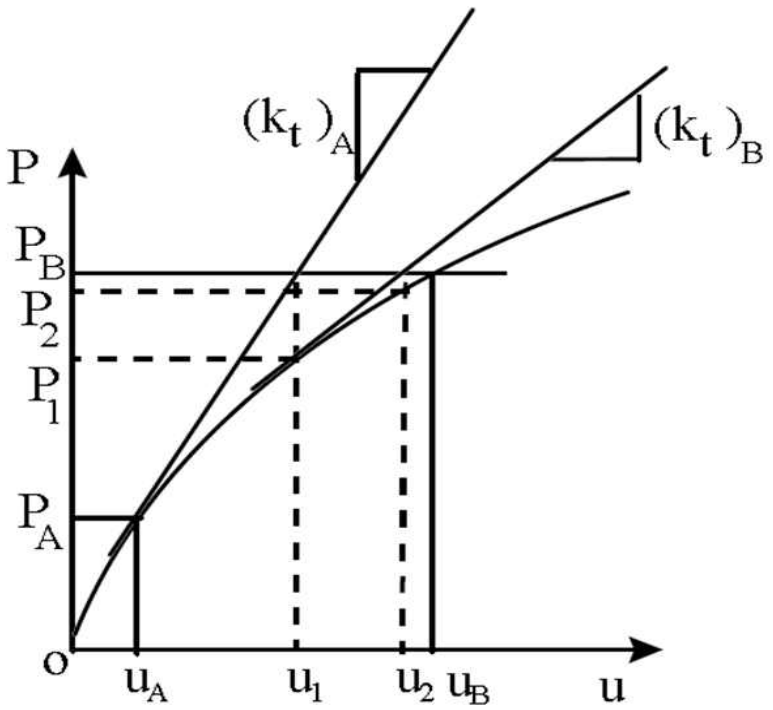

Fig. C.4. Graphical representation of the Newton-Raphson method.